Alma Mater Studiorum · University of Bologna

DEPARTMENT OF INDUSTRIAL ENGINEERING

SECOND CYCLE DEGREE IN ENERGY ENGINEERING

THESIS

in

Sustainable Technologies for Energy Resources

BOILING LIQUID EXPANDING VAPOR EXPLOSION FOR LIQUID HYDROGEN

Submitted by:
Leonardo Giannini

Supervisor:
Prof. Ernesto Salzano

Co-Supervisors:
Ing. Federico Ustolin
Ing. Gianmaria Pio
Prof. Nicola Paltrinieri

Academic Year 2021/2022
Session III

Contents

Chapter 1

Introduction

The transition towards a sustainable and clean energy production is one of the most discussed topics since the beginning of the 21st century. The implementation of renewable energy sources is thought to play an important role in the fight against global warming, climate change and environmental pollution. For example, the production of energy, especially electric, through solar panels and wind or hydroelectric turbines is absolutely one of the most important candidate to replace fossil fuels. In fact, due to their carbon neutrality, these solutions are widely spread and used today, but it appears clear that their intermittency is a problem for a constant energy production.
Today, the gap in the availability of renewable energy sources is currently filled with traditional energy production systems, such as *turbogas* or steam generators powered by fossil fuels. Is it possible that hydrogen might represent a solution to this problem? The International Energy Agency commented on this topic in June 2019, stating that: "the time is right to tap into hydrogen's potential to play a key role in a clean, secure and affordable energy future" in its report titled "The future of hydrogen" [1]. The increasing interest in the implementation of hydrogen fueled solutions is due to the fact that hydrogen is not only carbon neutral - so its combustion does not produce carbon dioxide - but it can also be renewable, meaning that both the production of the fuel and its utilisation do not have an impact on the environment.
However, there are some limitations which may represent a challenge to the diffusion of hydrogen as a fuel: it is in fact extremely flammable - minimum ignition energy of 0.017 mJ in a range of $4 - 75\%vol$ in air [2] - and it can also be aggressive towards some materials normally used in the fuel fields. Furthermore, the hydrogen molecule is the smallest in nature, meaning that it tends to escape through the smallest gapes of the containment devices where it is stored. Hence, these hydrogen properties may bring some concern in term of safety. Hydrogen has also a very low density, which makes it hard to transport in large quantities. A solution to this particular issue is thought to be the liquefaction of hydrogen, a process that increases its density about 800 times, from a value of 0.09 $kg\,m^{-3}$ to a virtual value of 70.9 $kg\,m^{-3}$ at atmospheric pressure [3]. The higher density of liquid hydrogen with respect to its gaseous form is the crucial aspect of this solution, but the absorbed energy and the required

ultra low temperature, around 20 K [3], are a difficult yet interesting challenge that needs to be overcome to make liquid hydrogen a viable and affordable solution to the climate change. Another issue is the necessity of particular containment systems to store liquid hydrogen. Cryogenic fuels storage is usually accomplished by means of double-walled vessels, which are characterized by strong insulation layers. As it will be explained in the following chapter (chapter 2), this kind of strong insulation may also be achieved by means of vacuum between the exterior and the interior vessel.

It is of overriding importance to underlined that the hydrogen demand is expected to grow in the next years [1] and it is also foreseen to be employed in new applications [1]. The growing interest towards hydrogen technologies is an aspect which makes its safety extremely relevant to study. Therefore, it is crucial to investigate and model hazardeous scenarios concerning liquid hydrogen. Furthermore, recent studies [4] have shown that a lack of knowledge concerning hydrogen behavior under cryogenic conditions still exists. Those are the reasons why the SH_2IFT Project (*Safe Hydrogen Fuel Handling and Use for Efficient Implementation)* and the safety tests conducted by BMW Car Manufacturer [5] focus on the consequences of liquid hydrogen catastrophic release. In particular, the analysed SH_2IFT Project experiment concerns a catastrophic explosion following the loss of integrity of a liquid hydrogen cryogenic container engulfed in propane flames. The "Bursting Tank Scenario" experiments conducted by BMW consisted in the analysis of the overpressure caused by nine different liquid hydrogen explosions, having inducted them with explosive charges attached to containers filled with different masses of hydrogen and pressurised at different pressure levels. More precisely, these kinds of explosions are usually referred as *BLEVEs (Boiling Liquid Expanding Vapor Explosions)*. A *BLEVE* is characterised by the rapid expansion of both the vapor and the liquid phase of a boiling fluid after the loss of its containment (LOC) [6]. Hence, a *Shock-wave* is most likely to occur after such event, along with the consequent overpressure, fragments projection and, if the expanding fluid is flammable like hydrogen, a potential fireball [7].
This work focuses on the modelling of such phenomena with the purpose to enhance the knowledge on the consequences of these explosions, using the data collected from the above mentioned experiments to validate the simulations. A *BLEVE* is an extreme and rare event and it is usually referred as *Atypical Accident Scenario* since its probability to happen is low. Hence, it is usually neglected by conventional risk assessment techniques [8], even if its consequences are often severe. The neglection of *Atypical Accident Scenarios* may lead to catastrophic accidents. The accidents occurred in Toulouse and Buncefield are unfortunate reminders [9]. As shown in the following chapter, severe accidents involving *BLEVEs* occurred in the past and this fact highlights how important it is not to neglect this particular accidental scenario, despite being atypical. The consequence analysis of the SH_2IFT Project and the "Bursting Tank Scenario" experimental *BLEVEs* is carried out simulating the explosions to verify the reliability of the implemented physical models. To complete the modeling of the catastrophic rupture of liquid hydrogen (LH_2) tanks, the combustion process is taken into account to describe the aftermath of the simulated accidents in terms of overpressure

and impulse. Furthermore, it is also discussed the possible involvement of the endothermic reaction of the hydrogen *para-isomer* converting into its *ortho-isomer* form.

In this way, a further validation and confrontation between the models currently used for classic liquid fuels like propane and liquefied petroleum gas (LPG) is possible, adopting and adapting them to the specific case of a liquid hydrogen catastrophic release. So, it is possible to consider this thesis as divided in three major steps: the first one is the analysis of the physical explosions with the proposed models, the second one is the adaptation of the models to take hydrogen combustion into consideration and the third and last one is an analysis of the *para-ortho* reaction which may follow the explosion [10]. At the end, a confrontation between the experimental data and the proposed calculations is carried out, underlining the aspects that still require further studies, experiments and documentation.

Chapter 2

State of the art

In this first chapter, a brief overview on hydrogen production and storage systems is proposed. Once these processes are identified, an extended discussion on a *Boiling Liquid Expanding Vapor Explosion* scenario is conducted. In the second section of this chapter, an overview on hydrogen combustion processes and their role in this types of explosions is presented, with particular emphasis on an accurate description of a hydrogen fireball.
In the end, a theoretical quantum-mechanical background is presented to understand the physics of the hydrogen isomers, along with the *para-hydrogen* to *ortho-hydrogen* reaction and its kinetics.

2.1 Hydrogen production and storage

Hydrogen is the most common molecule in the universe and the hydrogen molecule is the smallest and simplest in nature. It presents a very low density when in its gaseous form but it also contains a large amount of energy [11], that can be released and used in multiple applications when it is burned. It may be interesting to anticipate that one way to increase hydrogen density and therefore its storage capacity and portability is through the liquefaction process [12]. When liquefied, hydrogen presents a much higher density and so it becomes possible to transport more fuel mass in a given volume. The main drawbacks to this process are the extremely low temperature required to be liquefied (around 20 K) [3] and the energy consumption of the process itself. Before providing a more accurate description of LH_2 storage systems, it is relevant to present on overview on hydrogen production

2.1.1 Hydrogen Production and Liquefaction

Nowadays there is a tendency to classify hydrogen based on its production process. This is why it is very common to hear terms such as blue, green, gray or even purple when referring to hydrogen. These colors are used to identify different processes of hydrogen production, that can have a relevant, minimum or negligible impact on the environment. Here are some examples:

- Blue hydrogen is hydrogen produced with carbon capture facilities [13];
- Green hydrogen is produced directly with renewable energy (for example with electricity produced by hydrolysis of water powered by solar panels)[14];
- Grey hydrogen is produced with fossil fuels and it is considered to be the least interesting for an environmental point of view [15];
- Purple hydrogen is hydrogen produced with nuclear energy [16];

Once the hydrogen is produced, one way to store it and transport it is through the liquefaction process, which is similar to the process in use for other cryogenic fuels. The production of cryogenic fuels, such as *Liquefied Natural Gas* (LNG) [17] or LH_2, is a well known process. Several industrial plants exists for LH_2 production, but they are typically not efficient. In fact, their production rate is quite low, so LH_2 is now almost exclusively used in aerospace. Recent studies suggest that an upgrade in liquid hydrogen production could be made implementing a combined production of liquefied natural gas and LH_2 through advanced helium reverse Brayton cycles [18]. The tedious issue of LH_2 production represents an obstacle to the diffusion of this fuel and the research in terms of efficiency of the process and the used materials is still ongoing [19]. The goal is to reach a production system that does not require a tremendous amount of energy and the possibility of large-scale production, thus minimizing the costs.

2.1.2 Hydrogen and Liquid Hydrogen Storage

Another important challenge that needs to be faced when producing hydrogen in its gaseous or liquid form at extreme low temperatures is the storage system. In general, the storage processes may be performed by compression, liquefaction, physical storage in hydrides or chemical storage in hydrides [12]. As shown in figure 2.1 , these storage processes can be divided in physical and chemical process.

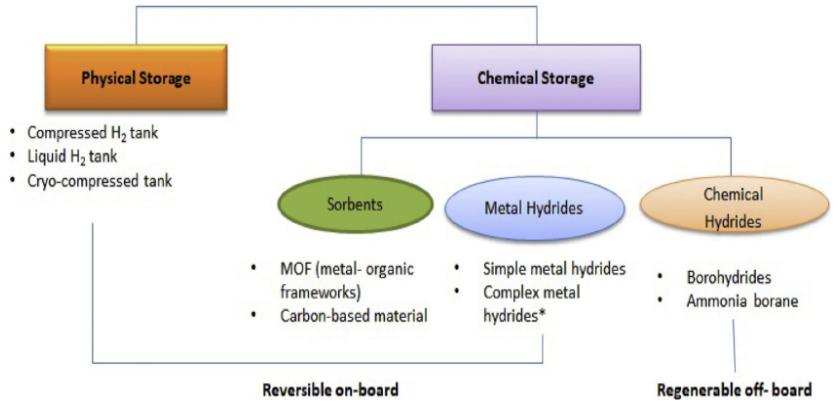

Figure 2.1: Hydrogen storage processes [12]

In this work, it was decided to describe the physical storage systems more accurately. Nowadays, the most common way to storage hydrogen is through compressed H_2 tanks, cryo-compressed tanks or, if liquefied, in LH_2 tanks. To do so, the utilization of double-walled vessels is the most reliable solution [20]. Double-walled vessels are in general composed by two different containment layers divided by an efficient insulating material and by vacuum. In the case of liquid hydrogen storage, this particular technique avoids excessive heat intrusions from the external atmosphere [21]. Doing so, double-walled vessels avoid the penetration of a high thermal heat flux that would vaporize part of the fluid inside the vessel. In fact, an excessive vaporisation may cause an increase in the pressure level that may lead to the activation of the pressure release valves venting the vapor phase or, in the worst case scenario, to the compromise of the containment structure [22].
Even with the most efficient thermal insulating material, it is not possible to reduce the heat flux to zero, but it is important to underline that there are other processes that helps keeping the cryogenic liquid in its more desirable state. In fact, when the liquid, due to the entering heat fluxes, vaporises, it absorbs its latent heat, thus contributing to keeping the temperature constant. The vapor that is formed is known as *Boil-off gas* (BOG). Another important reaction is the endothermic *para-isomer* to *ortho-isomer* transition. This process will be described in details in its dedicated paragraph. As mentioned above, the most common type of vessel in use for LH_2 storage is the double-walled vessel. It is also in use for other cryogenic fuels, such as LNG. More precisely, a further classification based on the required temperature, the pressure to maintain and the dormancy period is proposed.
With respect to hydrogen, four different inner vessel types can be identified [20]:

- Type I: all metal cylinders
- Type II: hoop-wrapped composite cylinders
- Type III: fully wrapped composite cylinders with metallic liners
- Type IV: fully wrapped composite cylinders with non-metallic liners

The first two types of vessels are the simplest and the least expensive. They are suitable for stationary applications since their weight is higher with respect to the other types that present a lower mean density.
Type III and IV vessels are more complex from a constructive point of view and they require particular materials. They are formed by an inner vessel made of a light-weight material and are wrapped in a fiber/epoxy matrix with an extreme low conductivity. On the external part they present a liner that contains the insulating material and thus play the role of the external vessel [21]. The wrapping is also important to help containing the pressure inside the inner vessel, if this one is pressurised at a level higher than the atmospheric pressure, but there are also composite support rings the helps out with the pressure containment. Those support rings need to be strong enough to support the inner vessel, but they can induct local vaporization near the joint with the inner vessel if their thermal conductivity is significantly

different, higher in particular, then the conductivity of the wrapping. The following picture is a scheme of a type III vessel used for cryo-compressed hydrogen: it is possible to notice the support rings for the inner vessel [21].

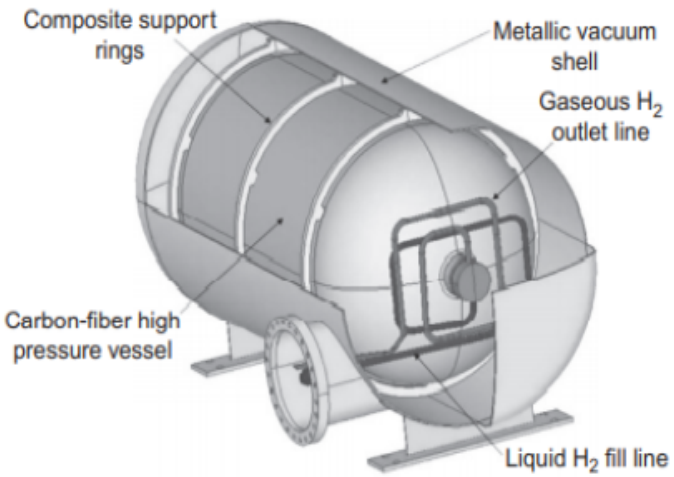

Figure 2.2: Example of type III vessel for cryo-compressed hydrogen [21]

It appears clear how the design of these supports is relevant and it requires particular attention. Furthermore, there are two other types of vessels designed for cryogenic fluids that deserve some discussion: the *non-vacuum-insulated vessels* and the *Dewars*.

2.1.3 Non-vacuum insulated vessels

A non-vacuum insulated vessel is a particular type of double-walled vessel. According with the European standard [23], the inner vessel is intended to contain a cryogenic fuel and it is separated from the outer one by a layer of porous means. The thickness of this insulating layer is a function of the target conductivity. In fact, insulating porous means, such as powders or foams, can reduce the entering heat flux by minimizing the conductive and convective heat exchange [24]. The first component of the heat exchange is dramatically reduced thanks to the aforementioned very low conductivity of the porous means. The convective heat exchange is avoided thanks to the small size of the pores inside the means that divides the inner from the outer layer. In fact, this type of heat transmission may take place if there is enough room to install a conductive cell [24]. The extremely small dimensions of the pores prevent the emerge of this phenomenon, thus minimizing the convective heat exchange. The inner layer is also held by supports made of stainless steel or polymers material [20] which need to be precisely designed to minimize the conductive heat exchange that may lead, as explained above, to a local formation of an excessive quantity of boil-off gas. Another characteristic of the non-vacuum insulated vessels is the resistance of the inner surface towards chemical action which may derive by the contact with cryogenic fuels [23].

2.1.4 Dewars

The last type of vessel that will be discussed is usually referred as *Dewar*, from the chemist and physicist inventor James Dewar. Dewars are characterised by the presence of a vacuum sealed layer that divides the inner vessel from the outer layer [25]. They are basically thermos and they are often used in laboratories for small-scale applications. Similarly to the non-vacuum insulated vessels, they are designed to minimize the heat exchange and the vacuum-sealed layer has the purpose to almost completely avoid the conductive and convective heat intrusions. To minimize the radiative exchange between the outer face of the inner vessel and the inner face of the outer one, the two surfaces are both covered with a thin layer of silver [20]. The silvering reduces the radiative heat exchange since it presents low values of emissivity and absorption coefficient [3].
Dewars are extremely efficient vessels for cryogenic fuels storage, they effectively maintain the extremely low temperatures required, minimising the boil-off production and maximizing the dormancy period of the contained liquid [25]. On the other hand, they can be fragile since the void layer can be problematic when, for example, the pressure inside the inner vessel rises. This can lead to the collapse of the outer or the inner layer on the other one, condition that will be discussed in the section dedicated to the *BLEVE* phenomenon. They may also be expensive, since the vacuum sealed layer is not easy to obtain and maintain [20]. In the end, Dewars present very important strengths and some drawbacks, but despite the last ones they are the most common container in use for cryogenic fuels [25].

2.2 *Boiling Liquid Expanding Vapor Explosions*

In this section, the description of the accidental scenarios of *Boiling Liquid Expanding Vapor Explosions* is presented. This phenomenon, referred as *BLEVE* is defined as a physical explosion which consists in the rapid expansion of both the vapor and the liquid phase of a boiling fluid when this loses its containment [26]. It can happen for both non-flammable or flammable substances: in fact about one-fifth of all *BLEVEs* occur with non-flammable pressure-liquefied gases [27]. If the substance which undergoes a *BLEVE* is non-flammable, the hazard will be primarily a shock-wave with almost certain vessel fragmentation [26]. In the other case, if the stored fluid is flammable, a fireball may occur, with radiative energy release and a pressure wave due to the explosively rapid vaporization of the liquid [26]. This event is well known and described for a series of fuels or other fluids, such as LNG, ammonia, gasoline and carbon dioxide [22]. When a *BLEVE* occurs, the consequences may be part of a severe accidents that leads to injuries or even casualties.
The following table is a list of accidents that happened in the period 1926-2004, as consequence of substances which underwent a *BLEVE* [22] [27].

Table 2.1: List of substances which underwent a *BLEVE* in the period 1926 - 2004 [22] [27]

Substance	Type	No. of accidents	Casualties	Injured
Propane	Flammable	24	121	7761
LPG	Flammable	17	12	35127
Chlorine	Toxic	7	139	-
Ammonia	Toxic	6	55	25
Butane	Flammable	5	394	7510
Gasoline	Flammable	3	10	2
Acrolein	Flammable	2	-	-
Carbon dioxide	Non-flammable, non-toxic	2	9	-
Ethylene oxide	Flammable	2	1	5
LNG	Flammable	2	14	76
Propylene	Flammable	2	213	-
Vinil chloride	Flammable and toxic	2	1	50
Borane tetrahydrofuran	Flammable and toxic	1	-	2
Butadiene	Flammable and toxic	1	57	-
Chloroubutadiene	Toxic	1	3	-
Ethyl ether	Flammable	1	209	-
Hydrogen	Flammable	1	7	-
Isobutene	Flammable	1	-	1
Maltodextrin	toxic	1	-	-
Methil bromide	Toxic	1	2	-
Nitrogen	Non-flammable non-toxic	1	2	-
Phosgene	Toxic	1	11	171
Steam	Non-flammable non-toxic	1	4	7
Water	Non-flammable non-toxic	1	7	-

2.2.1 The Super-heat Limit Temperature Theory

The *Super-heat limit Temperature* (T_{shl}) theory is usually adopted to determine the conditions under which a *BLEVE* may occur. For each pressure level it exists a value of T_{shl}, meaning that a locus of points of the different super-heat limit temperatures can be obtained as function of pressure. This curve is known as *Spinodal curve*. According to Reid [28], the liquid which undergoes the explosion must be significantly super heated to make the aftermath of the phenomenon as severe as a *BLEVE*. If the liquid exceeds the T_{shl}, the fluid reaches an unstable state and it could explode by undergoing homogeneous nucleation [28]. Furthermore, the super-heat limit temperature is the temperature value at which the adiabatic energy transfer between the liquid and vapor interface is maximized [29]. This aspect makes T_{shl} an important parameter to take into consideration when *Boiling Liquid Expanding Vapor Explosions* are studied. There is more then one way to determine the value of the super-heat limit temperature. Reid proposed an equation [28], which is still the simplest way to calculate T_{shl}:

$$T_{shl} = 0,895 T_c \tag{2.1}$$

where $T_c\,[K]$ is the critic temperature of the fluid, in the case of hydrogen: $T_c = 32,938\,K$ [3]. The equation proposed by Reid derives from bubble-column experiments conducted at different pressures for different chemical compounds, such as: di-chlorodifluoromethane, n-pentane, n-hexane, n-heptane, and cyclohexane.

There are also other ways to define and calculate the superheat limite temperature. One method suggests to estimate T_{shl} from the tangent to the saturation curve at critical point [30] and it results in one of the most conservative values [6]. In particular, the tangent line can be built graphically in order to avoid the significant error given by the Clausius-Clapeyron equation close to the critical point [6]. As showed in figure 2.3, joining the tangent identified with this method to the line at constant atmospheric pressure, a specific point is identified on the P-T chart. The coordinates of the point are the atmospheric pressure and the super-heat limit temperature.

A third and last method for the T_{shl} evaluation is through the energy balance equation [29]. As explained by Ustolin et al. [6], an adiabatic vaporisation process is considered to happen when the vessel depressurizes and, doing so, part of the liquid cools down to the boiling point at atmospheric pressure. When the liquid cools down, it releases a certain amount of heat, which can partially or totally be absorbed by an another liquid fraction which vaporises. In this case, the super-heat limit temperature is the temperature at which the heat released by 50% of the liquid is equal to the heat required by the other half of the liquid to vaporise.

The following images refer to the second and the third method explained for the T_{shl} calculation. [6].

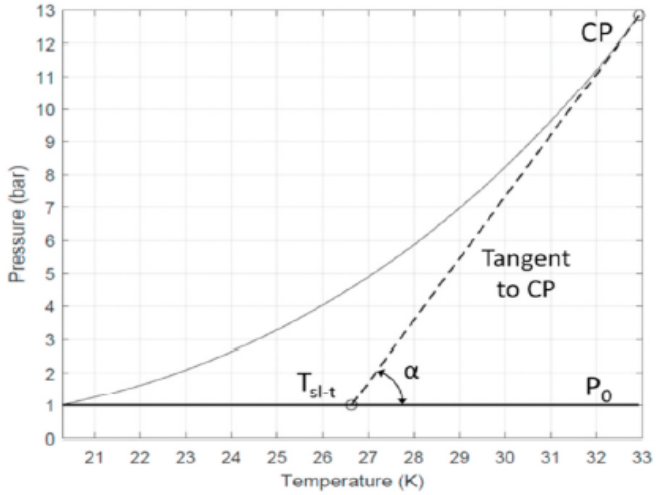

Figure 2.3: T_{shl} with the tangent to the saturation curve [6]

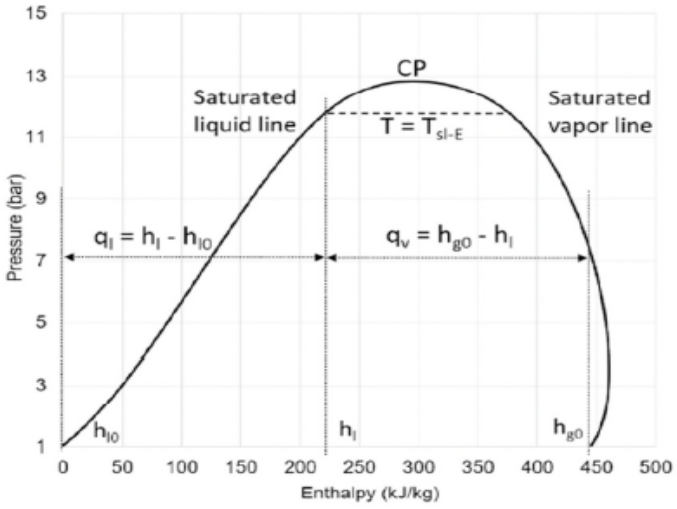

Figure 2.4: T_{shl} with the energy balance equation [6]

As previously mentioned, T_{shl} is an important parameter to take into consideration, since if the fluid which undergoes the explosion reaches this temperature, the yield of the explosion is maximized.
This affirmation does not exclude that explosions can happen even if the fluid does not reach the super-heat limit temperature. In this case [31], a liquid may explode if it is triggered, for example by a shock-wave, and a heterogeneous nucleation will take place, thus resulting in a lower yield of explosion. In the past, in fact, *BLEVEs* have also generated when the contained fluid was at a temperature below T_{shl} [31] [27].

2.2.2 Fired (Hot) *BLEVEs*

Along with the super-heat limit temperature, another parameter which characterises a *BLEVE* is how this phenomenon is triggered. It exists a distinction between a fired (hot) *BLEVE* and a un-fired (cold) one. The first phenomenon may happen if a tank containing a boiling liquid is engulfed in flames [22]. The generated heat leads to the vaporization of part of the liquid phase inside the vessel. The rising in the pressure level may lead to the catastrophic rupture of the vessel, whose consequences are usually the overpressure generated by the shock wave, fragments projection and, especially after hot *BLEVEs*, fireballs.

It is important to underline that the aforementioned phenomenon is exactly the aftermath of the SH_2IFT Project experiment that will be discussed in details in this thesis. In particular, this was the result of one out of three experiments. In one case the *Boiling Liquid Expanding Vapor Explosion* did not take place, as the hydrogen in the vessel was ejected from a pressure release valve, thus resulting in a phenomenon known as *Jet-fire* when the hydrogen started its combustion. In the other case, as previously mentioned, the collapse of the shell on the sealed vacuum layer took place as consequence of the embrittlement of the materials due to the strong heat caused by the propane flames. In this case there was no hydrogen release and the vessel maintained its integrity, although being damaged.

2.2.3 Un-fired (Cold) *BLEVEs*

An un-fired (cold) *BLEVE* happens when it is triggered not by a rising in pressure caused by heat fluxes but from other events such as shock-waves, explosive charges or violent impacts [6]. It is possible that the loss of containment necessary for the generation of the explosion is caused by the above mentioned causes. It is important to underline that a violent impact could happen, for example, after a road accident, when a truck or a car tank is filled with LNG or LH_2 [11].

This is the reason why BMW conducted experiments on cold *BLEVEs* for liquid hydrogen tanks in the 1990s, simulating violent impacts on these tanks triggering the explosions with explosive cutting charges [5]. In their dedicated section those experiments will be extensively discussed and analyzed and models to take into account the mechanical and the

chemical energy will be proposed.
In figure 2.5, an example of the fireball generated after the ignition of a cutting charge during one of the BMW Safety tests is proposed [5]. Despite being the case of a *"cold" BLEVE*, the fireball is generated due to the very low ignition energy of hydrogen (0,017 mJ [2])

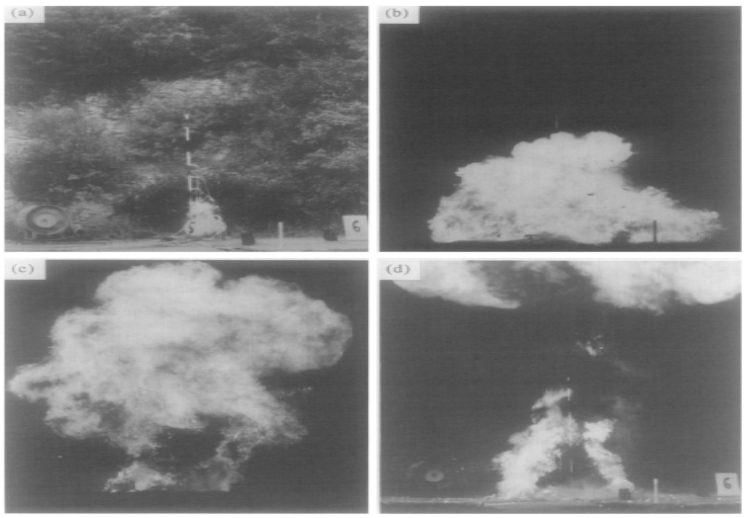

Figure 2.5: Development of a fireball. (a) Ignition; (b) 250 ms after ignition; (c) 1250 ms after ignition; and (d) 1800 ms after ignition; [5]

2.3 Combustion Phenomena

This section is dedicated to the identification of typical combustion processes and hazards that may need to be faced when an accidental scenario involving cryogenic fuels occurs. It can be noted that the hazard analysis adopted for LNG may be also applied to liquid hydrogen. Hence, an accurate description of fireballs in the specific case of liquid hydrogen is proposed, since this phenomenon occurred in the SH_2IFT Project experiment, whose description and analysis is the heart of this master thesis.

2.3.1 Jet-fire

A jet-fire may occur if a flammable fluid is ejected from a vessel or from a safety valve with significant momentum. If, for example, a pressure release valve opens, letting part of the fuel to exit a high pressure vessel, a jet composed by flammable liquid and vapor mixture has a certain probability to be formed.
In the presence of an ignition source, the result is a flame that propagates from the vessel towards the external ambient, causing hazards for the people they may be found in the proximity of the jet-fire. The flame is fed by the high-velocity fuel that is exiting the valve or the cracking in the vessel and it continues to burn as long as there is available fuel in its

proximity. Jet-fires are typically smaller than other similar hazardous event such as pool-fires or fireballs, but they can cause severe damage [32]. Moreover, jet-fires show an increasing trend in both number and magnitude since the applications of pressurised fuels vary from cooking to car engine power and industrial fuel or raw materials treatments [33].

Jet-fires can take place for both cryogenic or non-cryogenic fuels, and in figure 2.6, an example of a liquid hydrogen jet-fire is shown [20].

Figure 2.6: Example of a liquid hydrogen jet fire [20]

2.3.2 Pool-fire

Another hazard which may occur when handling liquid fuels, cryogenic or not, is the pool-fire. This kind of phenomenon can occur as consequence of leaks and spills, especially during transportation. If the spill of the fluid leads to the formation of a liquid pool that catches fire due to the presence of an ignition source, this phenomenon is called *Pool-fire*.

In the specific case of cryogenic fuels like LNG or LH_2, due to their low boiling temperatures, these fluids tend to evaporate quickly, spreading and dispersing without creating hazards or injuries after the dilution below their flammable limit [20]. On the other hand, if the ignition is started, the pool fire tends to burn the available fuel, especially if it is contained inside a trench. In figure 2.7 , it is possible to note examples of experimental LNG pool-fires.

Figure 2.7: Example of LNG pool-fires experiments conducted between 2005 and 2009 [34]

2.3.3 Fireballs

A serious hazard that may occur when handling liquid hydrogen, *LNG* or non cryogenic fuels is a fireball. A fireball is defined by Ustolin et al. as: "the combustion of the flammable cloud created after the fuel release and composed by the mixture of the latter and air." [35]. After the catastrophic rupture of a vessel, the most likely super-heated liquid flashes into two phases: saturated liquid (at its atmospheric boiling point) and vapor.
The expansion into the two phases, along with the expansion from the initial pressure to the atmospheric one, creates a pressure wave and projects fragments in the surroundings [26].

At this point, first the vapor phase and then the liquid one ignite quickly and produce a fireball that raises from the height of the vessel to many meters above the ground, due to the buoyancy forces. This description is particularly valid in the case of an immediate ignition, which is very probable in the specific case oh hydrogen since it presents a very low ignition energy: 0,017 mJ [2]. In other cases, if the ignition is not immediate, a flash fire or a vapor cloud explosion (VCE) are more likely to occur [26].
As previously mentioned, a fireball can be a consequence of a *BLEVE* and when the two phenomena are combined, the consequent hazard is greater. In fact, fireballs can often impose damaging thermal loads at greater distances than blast waves. It is possible to understand and estimate the entity of the radiation hazards from a *BLEVE* fireballs once the following fireball properties are known:

- The maximum diameter of the fireball, that is, fuel mass contributing to fireball generation;
- The surface-emissive power of the fireball;
- The total duration of the combustion;

It is relevant to specify that numerous correlations exists for the estimation of the above mentioned parameters, in table 2.2 some examples are reported:

Table 2.2: Empirical relationships for fireball durations and diameters [27] [26]

Source Empirical Correlations	Material	Diameter [m]	Duration [s]
Williamson and Mann 1981	Not provided	$5.88\,M^{0.333}$	$1.09\,M^{0.167}$
Lihou and Maund 1982	Rocket Fuel	$6.20\,M^{0.320}$	$0.49\,M^{0.320}$
Lihou and Maund 1982	Methane	$6.36\,M^{0.333}$	$2.57\,M^{0.167}$
Moorhouse and Pritchard 1982	F. L.	$5.33\,M^{0.327}$	$1.09\,M^{0.327}$
Duiser l985	F. L.	$5.45\,M^{1.3}$	$1.34\,M^{0.167}$
Gayle and Bransford 1965	F. L.	$6.14\,M^{0.325}$	$0.41\,M^{0.340}$
Prugh 1994 and TNO 1997	F. L.	$6.48\,M^{0.325}$	$0.852\,M^{0.260}$
Roberts 1982 and CCPS 1999*	F. L.	$5.80\,M^{0.333}$	$0.45\,M^{0.333}$
Roberts 1982 and CCPS 1999**	F. L.	$5.80\,M^{0.333}$	$2.60\,M^{0.167}$
Martinsen and Marx 1999***	F. L.	$8.66\,M^{0.25}\,t^{0.333}$	$0.9\,M^{0.25}$
Hardee and Lee 1973	LNG	$6.24\,M^{0.333}$	$1.11\,M^{0.167}$

Where:
*: valid for $(M < 3 \cdot 10^4)$
**: valid for $(M > 3 \cdot 10^4)$
***: valid for $(0 \leq t \leq t_b/3)$
M is the mass of fuel in fireball [kg];
t_b is the duration of the fireball [s];
t is the time since the explosion [s];
F.L. stands for "flammable liquid";

In the following subsection, a more detailed discussion on a hydrogen fireball is proposed, along with a consequence analysis.

2.3.4 Hydrogen fireball

As mentioned above, it is possible to estimate the diameter, the duration and the radiation of a fireball implementing numerical models and calculations. These models can be therefore implemented in the specific case of the fireball generated during the SH_2IFT experiment that will be discussed in this work. Before the experiment, a simulation of the expected fireball was proposed by Ustolin et al. [35].
In this subsection the main assumptions and models implemented for the simulation of the SH_2IFT hydrogen fireball are reported.

The fireball dynamic depends strongly on the release momentum which derives from the flash evaporation of liquefied gases during the *BLEVE*.
So, it is possible to categorize fireballs as [36]:

- Momentum-dominated fireballs
- Buoyancy-dominated fireballs

As indicated in table 2.2, the correlation proposed by the CCPS [26], which is similar to the one proposed by Gayle and Brasford [37] and High [38], can be implemented to estimate the duration of the fireball [35]:

$$t = 0.45\, M^{1/3} \tag{2.2}$$

While, for the buoyancy dominated fireballs, it is possible to estimate the duration as follows:

$$t = 2.6\, M^{1/6} \tag{2.3}$$

where M $[kg]$ is the mass of the fuel which takes part in the fireball.
It can be noted that the fuel concentration is higher in the centre of the fireball with respect to the outer layer, where the combustion takes place. As mentioned above, another important parameter necessary to define the hazard of a fireball is its diameter. This parameter can be calculated using the correlation proposed by Hord [39]:

$$D \approx 7.93\, M^{1/3} \tag{2.4}$$

where M $[kg]$ is again the mass of fuel that generates the fireball.
One last important geometrical parameter is the height reached by the flames. This distance depends on the fireball type - buoyancy or momentum dominated [40]. Nevertheless, the following equation can be implemented to estimate the maximum height of the center of the fireball [41]:

$$H = D_{max} \tag{2.5}$$

where D_{max} $[m]$ is the diameter of the fireball estimated with eq. (2.4).
One of the main hazards that can be faced when a fireball is formed is the radiation emitted by the flames. Once the duration of the fireball and the geometrical parameters are determined, it is possible to calculate the radiation emitted by the fireball in a scenario similar to the scenario described in figure 2.8.

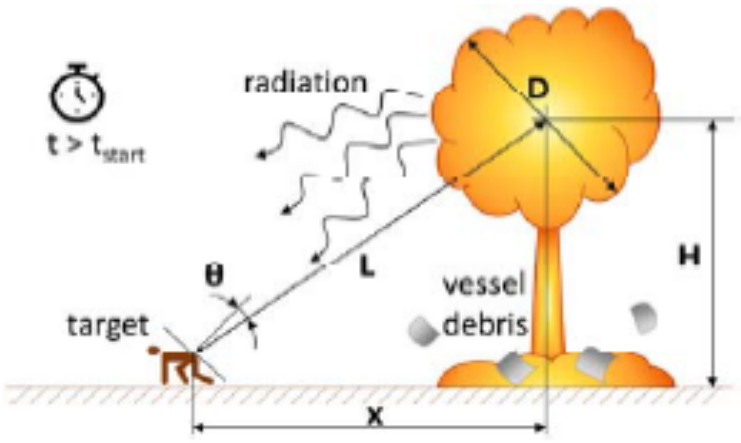

Figure 2.8: A fireball hazard scenario [35]

According to CCPS [26], it is possible to approximate the fire geometry with a geometrical shape, for example a sphere, and to assume the whole thermal radiation as diffused from the surface of the fireball. Following these assumptions, the radiation emitted from the fireball is:

$$q = \tau \, F \, E \tag{2.6}$$

Where τ $[-]$ is the transmissivity of the atmosphere, F $[-]$ is the view factor and E is the surface emissive power (SEP), expressed in $[W/m^2]$. The surface emissive power can be estimated with the Stefan-Boltzmann's law:

$$E = \epsilon \, \sigma \, T^4 \tag{2.7}$$

where:

- ϵ is the emissivity of the flames $[-]$;
- σ is the Stefan-Boltzmann constant: $\sigma = 5.67 * 10^{-8}$ $[Wm^{-2}K^{-4}]$;
- T is the temperature reached by the fire $[K]$;

To perform a conservative assumption of the value of SEP [35], it is possible to consider the fireball as a black body $\epsilon = 1$ and the temperature as the stoichiometric combustion

temperature of the burning fuel, in this case hydrogen [5].
The view factor takes into account the solid angle formed between the fireball and the receiver of the emitted radiation, and can be determined as follows:

$$F = \left(\frac{R}{L}\right)^2 cos\theta \tag{2.8}$$

where.

- R is the fireball radius $[m]$;
- L is the distance between the fireball centre and the target $[-]$;
- θ is the angle between the target surface normal and the fireball axis $[-]$

The transmissivity ($\tau\,[-]$) of the atmosphere is function of the air temperature, the humidity of the air and the path-length between the fire and the target. It can be determined as follows [41]:

$$\tau = 2.02 \cdot \left(p_w\,(L-R)\right)^{-0.09} = 2.02 \cdot \left(RH\,p_w^0\,(L-R)\right)^{-0.09} \tag{2.9}$$

where p_w is the pressure of vapor water in air $[Pa]$ and RH is the relative humidity expressed in kilograms of water per kilogram of air.
Finally, it is possible to determine the thermal dose of the fireball, as a function of the radiation emitted and the duration of the phenomenon [35]:

$$Thermal\ dose = q^{4/3} \cdot t \tag{2.10}$$

It is important to underline that the maximum tolerable thermal does which does not provoke injuries is 80 $kW^{4/3}\ m^{2/3}\ s$ [35]. With the determination of the thermal dose caused by a hydrogen fireball, such as the one generated during the SH_2IFT Project experiment in exam, the discussion regarding the combustion phenomena is concluded. The next section is dedicated to the phenomenon of the transition between the *para-hydrogen* and *ortho-hydrogen* isomers.

2.4 *Ortho-Para* and *Para-Ortho* reactions

This section focuses on the definition and the analysis of the two spin-isomers of the hydrogen molecule and the thermodynamic characteristics of the transition from one to the other.
In particular, a brief overview on the quantum-mechanic theory of the hydrogen molecule is proposed and an analysis of the production systems for the *para-hydrogen* molecule is conducted. At the end, the endothermic *para-hydrogen* to *ortho-hydrogen* transition is discussed more in details since it is deeply involved in the models implemented to conduct this study.

2.4.1 Theoretical background

Before discussing the specific case of the hydrogen molecule from a quantum-mechanical point of view, it is relevant to take a step back and analyse the $Schrödinger's$ equation. This famous equation can be obtained by the d'Alambert wave equation for the electromagnetic waves [42]:

$$\nabla^2\phi - \frac{1}{c^2}\frac{\partial^2\phi}{\partial t^2} = 0 \tag{2.11}$$

where $c\,[m\,s^{-1}]$ is the speed of light in the void, $t\,[s]$ is the time variable and ϕ is a function of space and time: $\phi = \phi\,(\vec{x}, t)$
The solution proposed by *Schrödinger* for the equation above is a sinusoidal function represented with complex numbers, with the quality of separating the time variable to the spacial variable:

$$\phi\,(\vec{x}, t) = e^{-i\omega t}\,\psi(x, y, z) \tag{2.12}$$

where $\omega = 2\pi f$ and $f\,[Hz]$ being the wave frequency.
Considering a one-dimensional system, it is therefore possible to rewrite the terms of the d'Alambert equation as follows:

$$\frac{\partial\,\phi}{\partial\,x} = e^{-i\omega t}\,\frac{\partial\,\psi\,(x, y, z)}{\partial\,x} \implies \frac{\partial^2\,\phi}{\partial\,x^2} = e^{-i\omega t}\,\frac{\partial^2\,\psi\,(x, y, z)}{\partial\,x^2} \tag{2.13}$$

$$\frac{\partial\,\phi}{\partial\,t} = -i\,\omega\,e^{-i\omega t}\,\psi\,(x, y, z) \implies \frac{\partial^2\,\phi}{\partial\,t^2} = -\omega^2\,e^{-i\omega t}\psi\,(x, y, z) \tag{2.14}$$

At this point, rewriting the d'Alambert equation using the function ψ and separating the variables, it can be obtained:

$$e^{-i\omega t}\,\nabla^2\,\psi = -\frac{\omega^2\,e^{-i\omega t}}{c^2}\,\psi(x, y, z) \tag{2.15}$$

which can be simplified in:

$$\nabla^2\,\psi = -\frac{\omega^2}{c^2}\,\psi\,(x, y, z) \tag{2.16}$$

Considering the definition of ω and the correlation between frequency and wave length ($f = \frac{c}{\lambda}$), another rearrangement of the terms of the last equation can be made:

$$\nabla^2\,\psi + \frac{4\pi^2}{\lambda^2}\,\psi\,(x, y, z) = 0 \tag{2.17}$$

This equation can be applied to electromagnetic waves but also to particles, using the particle

wave length identified with the De Broglie equation:

$$\lambda = \frac{h}{p} \implies \lambda = \frac{h}{m\,v} \implies \frac{1}{\lambda^2} = \frac{m^2\,v^2}{h^2} \tag{2.18}$$

where $p\,[kg\,m\,s^{-1}]$ is the momentum of the particle, $m\,[kg]$ and $v\,[m\,s^{-1}]$ are respectively its mass and its speed and h is the Planck constant ($h = 6,626 * 10^{-34} J\,s$).
The kinetic energy of a particle can be expressed as $K = m\,\frac{v^2}{2}\,[J]$, being again m the mass of the particle and v its velocity. So, combining eq (2.17) with equation (2.18) and using the definition of the kinetic energy, the *Schrödinger*'s equation for steady states can be obtained:

$$\nabla^2\psi + \frac{2Km}{\hbar^2}\psi = 0 \tag{2.19}$$

where $\hbar = \frac{h}{2\pi}$.
Another step can be made through the definition of energy as the sum of kinetic and potential energy: $E = K + U(x, y, z)$. By using this definition and by multiplying equation (2.19) by $-\frac{\hbar}{2m}$ the resulting equation is:

$$-\frac{\hbar}{2\,m}\nabla^2\,\psi + U\,\psi = E\,\psi \tag{2.20}$$

which is known as the *Schrödinger's equation for steady states in the presence of a potential U.*

The *Schrödinger's* equation solution is the ψ function and it is referred as *wave function.* In this particular case, equation (2.20) was found for a particle and it is valid for steady states with the presence of a potential U (there is not the time dependence). It is important to notice that the probability density function (i.e. the probability of finding the particle at any given location and time [4]) is defined as the product of the wave function ψ and its complex conjugate ψ^*. Once the probability density function is defined, it is possible to calculate the probability of finding the described particle between two points in the space: x_1 and x_2:

$$P\,(x_1 < x < x_2) = \int_{x_1}^{x_2} \psi\,(x,t)\,\psi^*\,(x,t)\,dx \tag{2.21}$$

with:

$$\int_{-\infty}^{+\infty} \psi\,(x,t)\,\psi^*\,(x,t)\,dx = 1 \tag{2.22}$$

which is a normalization condition necessary to define $\psi(x,t)\cdot\psi^*(x,t)$ as a density probability [42].

Coming back to the hydrogen molecule, it can be demonstrated that the complex wave function (ψ) for this particular molecule is the result of the product of five functions [43]:

$$\begin{aligned}\psi = (electronic\ orbital\ motion) \cdot (electronic\ spin) \cdot \\ (nuclear\ vibrational) \cdot (nuclear\ rotational) \cdot (nuclear\ spin)\end{aligned} \tag{2.23}$$

Experimental results have shown, in accordance with Pauli's exclusion principle, that the wave function - equation (2.23) - for the hydrogen molecule is antisymmetric in the proton coordinates (i.e. the wave function changes sign when the two protons are exchanged), while the product of the first three terms of equation (2.23) is symmetric in the proton coordinates. This conditions imply that the the last two terms of the equation (2.23) present opposite symmetries [44]. So, the existing possibilities are:

- *Para-hydrogen*: symmetric nuclear rotation and antisymmetric nuclear spin;
- *Ortho-hydrogen*: antisymmetric nuclear rotation and symmetric nuclear spin;

At room temperature the the hydrogen equilibrium composition is 75% ortho-hydrogen and 25% para-hydrogen: this mixture is referred as *normal-hydrogen*. This equilibrium is a consequence of the effect of the temperature on the rotational wave function of the hydrogen molecule, which affects the equilibrium concentration of the two isomers [4]. At low temperatures, the thermodynamic equilibrium shifts towards higher concentrations of para-hydrogen, in particular to a concentration of 99,8% [4]. The shift in the concentration, in function of the temperature can be noted in figure 2.9:

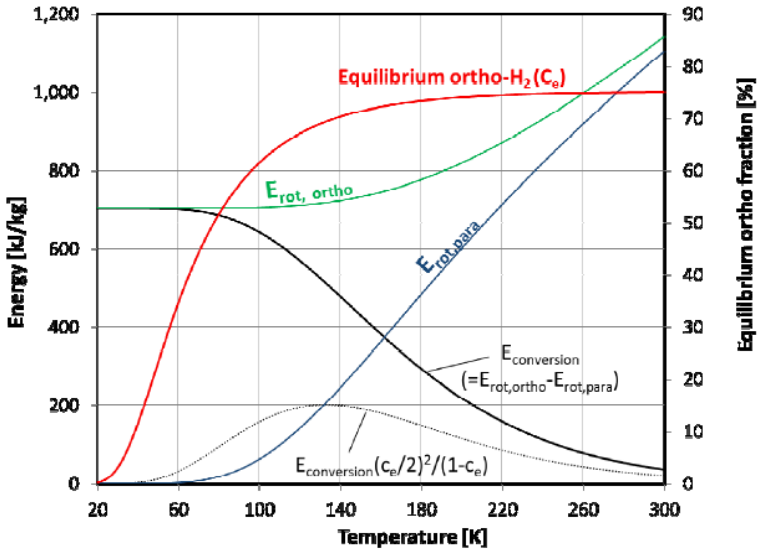

Figure 2.9: Concentration of para-hydrogen and ortho-hydrogen at different temperatures [4]

In figure 2.9 it is also shown the energy of the conversion from an isomer to the other. This energy is defined as:

$$E_{conversion} = |E_{rot\,ortho} - E_{rot\,para}| \tag{2.24}$$

Where $E_{rot\,ortho}\,[J]$ and $E_{rot\,para}\,[J]$, are respectively the energies of the ortho-hydrogen and para-hydrogen rotational nuclear states. The effect of the temperature on the energy of the conversion can be also highlighted by equation (2.25), where $K_b\,[J\,K^{-1}]$ is the Stefan-Boltzmann constant and Z is the previously mentioned wave function of the rotational states [4]:

$$E_{rot} = k_b\,T^2\,\frac{\partial\,ln(Z)}{\partial\,T} \tag{2.25}$$

The energy of the transition is the most important parameter to consider when conducting a study with a mainly thermodynamic footprint as the one proposed in this thesis. It can be treated similarly to the latent heat of vaporization [4], therefore simplifying the analysis of the para-hydrogen to ortho-hydrogen energy absorption in the specific case of a liquid hydrogen *Boiling Liquid Expanding Vapor Explosion.*
The next subsection is dedicated to the para-hydrogen production and its importance when storing LH_2.

2.4.2 *Para-hydrogen* production

As explained above, when hydrogen is brought to extremely low temperatures, the transition from the ortho-hydrogen molecule to the para-hydrogen one occurs. This transition generates a non-negligible amount of energy, which may vaporize part of the LH_2. This energy is comparable to the latent heat of vaporization of hydrogen, being the first between 100 and 708 $kJ\,kg^{-1}$ [4] and the second 445.4 $kJ\,kg^{-1}$ [3].
It is crucial to highlight that the conversion between the two isomers results from perturbations involving nuclear spins, which are small in magnitude. Therefore, it results in a slow process and it may occur many days to complete. This means that when normal-hydrogen is liquefied, the slow transition between $ortho - H_2$ and $para - H_2$ will liberate a significant amount of energy, enough to vaporize 65% of the LH_2, even with a perfect insulation [4]. To obtain an efficient liquefaction is therefore usually necessary a catalytic ortho to para H_2 conversion system.

There are many ways to increase the ortho to para conversion rate: for example the interaction with strong magnetic fields, electric discharges, metal catalysts or radiations are proved to increase the para-hydrogen production rate [4]. It is significant to underline that H_2 conversion kinetics has been well studied in the past few years, since it is crucial for an efficient liquefaction. However, kinetics conversion from para-hydrogen to ortho-hydrogen has until recently lacked practical interest.

Nowadays, this particular reaction is gaining interest, especially with the purpose of use its endothermic nature to reduce the boil-off gas production in long-term storage vessels, especially in the auto-motive field [45].

2.4.3 The endothermic *para-hydrogen* to *ortho-hydrogen* transition

When hydrogen is stored in its liquid phase around atmospheric pressure, it is usually in its para-hydrogen form. This prevents the cryogenic liquid from liberating energy avoiding the transition from the ortho-isomer to the para-isomer and it is also useful to reduce the boil-off gas production. In fact, in the presence of a entering heat flux, the para molecule will transform in its ortho form absorbing a considerable amount of energy, thus avoiding the vaporization of part of the stored liquid.
To understand the kinetics of the transition, it is possible to take into account the equation proposed by Milenko and Sibileva, eq. (2.26), which considers the reaction rates (k and k') of both ortho to para and para to ortho reactions.

$$\frac{d\,c}{d\,t} = -k \cdot c^2 + k' \cdot c \cdot (1 - c) \tag{2.26}$$

where:

- c is the concentration of the ortho-hydrogen isomere expressed in kilogram of ortho-isomer per kilogram of hydrogen;
- t is the time variable $[s]$;
- k is the kinetic constant of the ortho-para reaction $[10^{-3} \cdot h^{-1}]$;
- k' is the kinetic constant of the para-ortho reaction $[10^{-3} \cdot h^{-1}]$;

Equation (2.26) is valid in absence of an external catalyst and it explains the kinetics of the transition between the two isomers at any given temperature and pressure [46]. It is possible to understand the influence of temperature and pressure on the kinetics of the reaction through the following empirical correlation [46]:

$$k = (18.2 \pm 1.6)\, T^{0.56 \pm 0.02}\, \rho + 5 \cdot 10^4\, (0.77 \pm 0.03 + (921 \pm 94)\, T^{-2.5 \pm 0.2})\, \rho^{3.6} \tag{2.27}$$

Where T is the temperature of the system $[K]$, ρ is its density $[kg \cdot m^{-3}]$ and k is again expressed in $10^{-3}\, h^{-1}$.
The kinetic constant of the para to ortho reaction can be therefore defined by means of equilibrium constant:

$$K_{eq}(T) = \frac{k'}{k} = e^{\frac{-\Delta G^o}{R\,T}} \tag{2.28}$$

where:

- K_{eq} is the equilibrium constant $[-]$;
- R is the constant of gas for hydrogen ($4125.5\ J \cdot kg^{-1}K^{-1}$) ;
- T is again the temperature of the system $[K]$;
- ΔG^o is the Gibbs free energy $[J]$;

The Gibbs free energy is defined as:

$$\Delta G = \Delta H - T\,\Delta S = (H_{pH_2} - H_{oH_2}) - T\,(S_{pH_2} - S_{oH_2}) \tag{2.29}$$

where:

- H_{pH_2} is the enthalpy of the para-hydrogen $[kJ]$
- H_{oH_2} is the enthalpy of the ortho-hydrogen $[kJ]$
- S_{pH_2} is the entropy of the para-hydrogen $[kJ]$
- S_{oH_2} is the entropy of the ortho-hydrogen $[kJ]$
- T is the temperature of the system $[K]$

With equation (2.29) it is possible, at any given condition of temperature and pressure, to define the kinetic constant of the para-hydrogen to ortho-hydrogen transition, thus solving equation (2.26).

It is also possible to define the kinetic constant for the para to ortho transition (k') considering the variation of ortho-H_2 null at equilibrium. Under this condition, eq (2.26) can be rearranged as follows:

$$k' = \frac{k\,c_e}{1 - c_e} \tag{2.30}$$

where $c_e\,[-]$ is the concentration of ortho-hydrogen at the equilibrium.
Equation (2.30) allows one to rewrite equation (2.26) as follows:

$$\frac{d\,c}{d\,t} = -\frac{k\,c\,(c - c_e)}{1 - c_e} \tag{2.31}$$

which explains that the rate of change of the ortho-H_2 fraction is maximum for $c = \frac{c_e}{2}$, since the second derivative of concentration vs time is equal to zero [4]. It is also possible to analyse the energy of the conversion between the two isomers by means of the conservation

of the internal energy, in the specific case of a closed H_2 vessel with constant volume and an entering heat flux noted as Q.

$$m \frac{d\,E}{d\,t} = Q \tag{2.32}$$

where $m\,[kg]$ is the total mass of hydrogen contained in the vessel and the energy $E\,[J]$ can be expressed as $E = (1-c) \cdot E_{ortho} + c \cdot Epara$.
It is therefore possible to express the derivative of the energy vs time as:

$$\frac{d\,E}{d\,t} = -\frac{d\,c}{d\,t}\,E_{para} + (1-c)\,\frac{d\,E_{para}}{d\,t} + \frac{d\,c}{d\,t}\,E_{ortho} + c\,\frac{d\,E_{ortho}}{d\,t}$$

which means:

$$Q = -m\frac{d\,c}{d\,t}\,E_{para} + m\,(1-c)\frac{d\,E_{para}}{d\,t} + m\frac{d\,c}{d\,t}\,E_{ortho} + m\,c\frac{d\,E_{ortho}}{d\,t}$$

and so:

$$m\left[(1-c)\,\frac{d\,E_{para}}{d\,t} + c\frac{d\,E_{ortho}}{d\,t}\right] = Q - m\,\frac{d\,c}{d\,t}\left(E_{ortho} - E_{para}\right)$$

which can be combined with equation (2.24) and equation (2.31) to obtain:

$$m\left[(1-c)\,\frac{d\,E_{para}}{d\,t} + c\frac{d\,E_{ortho}}{d\,t}\right] = Q + m\,E_{conversion}\,\frac{k\,c\,(c-c_e)}{1-c_e} \tag{2.33}$$

Equation (2.33) predicts the rate of change in internal energy in the vessel, thus it governs its temperature and pressure rise. It is important to highlight that the right-hand side of this equation is known as *apparent heat transfer* and it gives an indication of the impact of the transition in the presence of an entering heat flux Q from the external environment [4].

The para to ortho transition energy absorption is considered in this study to analyse its effect on the shock-wave caused by the *Boiling Liquid Expanding Vapor Explosion* generated during the SH_2IFT Project.
Furthermore, an analysis of the time requested by the kinetics of the reaction to complete is conducted. Doing so, the reaction time is compared with the characteristic time of mechanical explosions, such as *BLEVEs*, to discuss the role of such transition in these kind of phenomena.

In the following chapter, an extensive discussion about the set-up of the simulated accidents is conducted, followed by an analysis of the models currently in use for similar scenarios for other fuels (i.e. propane and LNG). Particular focus is dedicated to the adaptation of such models to the specific case of liquid hydrogen and, as mentioned above, the role of its

combustion and the para-hydrogen to ortho-hydrogen transition.

Chapter 3

Material and methods

A description of the models implemented to analyse the the bursting tank scenario [5] and the SH_2IFT Project *BLEVE* is presented in this chapter. The boundary conditions of the experiments are defined and a more detailed discussion on the parameters involved in the generation of the *Boiling Liquid Expanding Vapor Explosions* is provided.
Hence, the first sections of this chapter are dedicated to the description of "ideal gas behavior" (IGB) and "real gas behavior" (RGB) models, while the following sections focus on the description of the case studies. These physical models, validated for conventional fuels like propane and liquefied petroleum gas (LPG) are implemented to study the mechanical energy of the explosions, the overpressure and the impulse generated by the shock-waves. This analysis is conducted according to the one presented by Ustolin et al. [6], based on the experiments conducted by BMW in the 1990s. In that previous work, a blind prediction of the SH_2IFT Project *BLEVE* was accomplished by applying the same conventional models. More precisely, the overpressure generated by the shock-wave was correlated with the mechanical energy through the TNT equivalent method, which will be discussed in its dedicated section.
In this study, along with the TNT equivalent method, the correlation between mechanical energy and overpressure is described through the method proposed by Baker [47], thus conducting a comparison between the two models.

Then, the combustion process is taken into account to describe the overpressure generated by the simulated accidents. To do so, the methodology proposed by Molkov et al. [11] is implemented, thus adding the contribution of the hydrogen combustion process to the mechanical energy of the explosions.
Finally, it is discussed and analysed the effect of the para-hydrogen to ortho-hydrogen transition on the overpressure generated by the shock-wave. In particular, the energy absorption of the endothermic reaction is compared with the gap, in terms of energy, between the experimental data and the calculations. In this way, the role of the transition between the two isomers is described by solving the reverse problem, thus proceeding with the same approach applied to the combustion process proposed by Molkov et al. in the first place [11].

Furthermore, the energy absorption of the reaction is correlated with the concentration of ortho-hydrogen through the utilisation of both para-hydrogen and ortho-hydrogen thermodynamic properties provided by the *CoolProp* package [48].

3.1 Mechanical energy models

This section is dedicated to the definition and the description of the implemented models to study the mechanical energy liberated with the LH_2 *Boiling Liquid Expanding Vapor Explosions* [49]. It is relevant to remind that the discussed models are already validated for common liquid fuels, such as propane and liquefied petroleum gas (LPG). Such models have been categorized in ideal gas behavior and real gas behavior models in the following subsections, in which they are described in details. Finally, the most conservative and the most accurate models will be discussed, along with the obtained results.

3.1.1 Ideal gas behavior models

The "ideal gas behavior" models (IGB) describe the mechanical energy of an explosion correlating it with the tank pressure and the volume of the expanding fluid. They also take into account the pressure ratio between the tank pressure and the atmospheric one and the specific heat ratio of the expanding fluid (hydrogen in this case). The volume of the expanding fluid is estimated through the equation proposed by Prugh [50]. In table 3.1 , the selected ideal models are shown:

Table 3.1: Ideal models: mechanical energy estimation

Proposed by	Assumption	Equation	
Brode (1959) [51]	Isochoric process	$E_{Brode} = \frac{P-P_0}{\gamma-1} V^*$	(3.1)
Smith and Van Ness (1996) [52]	Isothermal process	$E_{ie} = P\,V^* \cdot ln\frac{P}{P_0}$	(3.2)
Crowl (1991,1992) [53] [54]	Therm. availability	$E_{ta} = P\,V^* \left[ln\left(\frac{P}{P_0}\right) - \left(1 - \frac{P_0}{P}\right)\right]$	(3.3)
Prugh (1991) [50]	Adiabatic process	$E_{Prugh} = \frac{P\,V^*}{\gamma-1}\left(1 - \frac{P_0}{P}\right)$	(3.4)

Where:

- P is the pressure inside the tank at the moment of the explosion $[Pa]$;
- P_0 is the atmospheric pressure $[Pa]$;

- γ is the specific heat ratio (1.4 for hydrogen) $[-]$;
- V^* is the expanding volume of the fluid $[m^3]$;

The expanding volume of the fluid (V^*) is estimated with the following equation [50]:

$$V^* = V_T + m_l \left(\frac{f}{\rho_v} - \frac{1}{\rho_l} \right) \tag{3.5}$$

where V_T $[m^3]$ is the volume of the tank, m_l $[kg]$ is the mass of the liquid, ρ_v $[kg\, m^{-3}]$ and ρ_l $[kg\, m^{-3}]$ are respectively the density of the vapor and the liquid phase. f $[-]$ is referred as the "flashing fraction", which takes into account the fraction of the liquid phase that flashes at the moment of the explosion [6] and it is defined as follows:

$$f = 1 - exp \left\{ -2.63 \left[1 - \left(\frac{T_c - T_0}{T_c - T_b} \right)^{0.38} \right] \frac{c_{p_{L_0}}}{\Delta\, h_{v_0}} (T_c - T_b) \right\} \tag{3.6}$$

where:

- T_c is the critic temperature of hydrogen $[K]$ ($T_c = 32.8$ K [3]);
- T_0 is the temperature of the liquid phase inside the vessel at the moment of the explosion $[K]$;
- T_b is the boiling temperature of the liquid inside the vessel $[K]$ (around 20 K for hydrogen [3]);
- $c_{p_{L_0}}$ is the specific heat of the liquid at boiling temperature $[kJ\, kg^{-1}\, k^{-1}]$;
- $\Delta\, h_{v_0}$ is the latent heat of vaporisation at boiling point $[kJ\, kg^{-1}]$;

It can be noted that, in the case of $m_l = 0$, i.e. when the fluid inside the tank is completely super-critical, the expanding volume V^* is equal to the total volume of the tank V_T.

The peculiar characteristics of each model are well explained by Ustolin et al. in their comparative analysis [6], in which the models are described as follows:
the equation proposed by Brode [51] - eq. (3.1) - estimates the total energy generated by the detonation of a spherical charge of TNT considering it as an isochoric process [51]. Smith and Van Ness [52] assumed an isothermal expansion process - eq (3.2) - to develop their model.
The thermodynamic availability model - eq (3.3) - introduced by Crowl [53] [54] calculates the maximum mechanical energy extractable from a substance which reversibly reaches the equilibrium with the surrounding environment from the burst conditions.
The adiabatic process - eq. (3.4) - illustrated by Prugh [50] can be adapted to liquefied gas vessels by replacing the tank volume with the total volume of the expanding fluid in order to

determine the mechanical energy of a *BLEVE*. As previously mentioned, all the aforementioned models consider the expanding vapor (in this case hydrogen) as a ideal gas. In the next subsection, other models are described, which consider the expanding fluid as a real gas.

3.1.2 Real gas behavior models

To describe the mechanical energy of an explosion, models considering hydrogen as a real gas can be implemented (RGB). With respect to the previously described "ideal gas behavior" models, the following ones take into account not only pressure and temperature, but several more thermodynamic properties and variables. In table 3.2, the selected models are shown, along with their equations and the variables to take into consideration.

Table 3.2: Real models: mechanical energy estimation

Proposed by	Referred as	Equation	
v. d. Bosch and Weterings (2005) [41]	TNO	$E_{TNO} = m_v\,(u_v - u_{v_{is}}) + m_l\,(u_l - u_{l_{is}})$	(3.7)
Planas-Cuchi et al. (2004) [55]	Planas	$E_P = -[(u_{l_0} - u_{v_0})\,m_T\,X - m_T\,u_{l_0} + U_i]$	(3.8)
Casal and Salla (2006) [56]	Se	$E_{Se} = k\,m_l\,(h_l - h_{l_0})$	(3.9)
Genova et al. (2008) [57]	Genova	$E_{Genova} = \psi\,m_l\,c_{p_l}\,(T_l - T_{l_0})$	(3.10)
Birk et al. (2007) [58]	Birk	$E_{Birk} = m_v\,(u_v - u_{v_{is}})$	(3.11)

As shown in table 3.2, several thermophysical variables and parameters play a central role in the definition of the "real gas behavior" models. Assuming an isoentropic process, the "TNO" model takes into account the mass of both the vapor and the liquid phase ($m_v\,[kg]$ and $m_l\,[kg]$), along with their specific internal energy ($u_v\,[kJ\,kg^{-1}]$ and $u_l\,[kJ\,kg^{-1}]$).
The "Planas" model takes into account the mass of the tank $m_T\,[kg]$ and the specific internal energy of the vapor and the liquid phase under saturation conditions at atmospheric pressure, which are identified with the subscript 0 ($u_{v_0}\ [kJ\,kg^{-1}]$ and $u_{l_0}\ [kJ\,kg^{-1}]$).

The enthalpy difference of the liquid phase before and after the explosion ($h_l - h_{l_0}\,[kJ\,kg^{-1}]$) is considered in the "Se" model, while the temperature difference ($T_l - T_{l_0}\,[K]$) is taken into account by the "Genova" one, along with the mean specific heat of liquid hydrogen ($c_{p_l}\,[kJ\,kg^{-1}\,K^{-1}]$).
Along with these variables, in the "Se" and in the "Genova" models the fractions of the mechanical energy converted in overpressure are shown ($k\,[-]$ and $\psi\,[-]$).

It can be noted how the "Birk" model takes into account only the vapor phase, while the

"TNO" considers both the expansions of the vapor and the liquid. It is relevant to highlight that the other variables and coefficients that show up in the aforementioned equations may need a more accurate description, so they are collected in table 3.3, along with their equations.

Table 3.3: Real models: definition of the parameters

Equation	
$u_{v_{is}} = (1 - x_l)\, u_{l_0} + (x_l\, u_{v_0})$	(3.12)
$u_{l_{is}} = (1 - x_v)\, u_{l_0} + (x_v\, u_{v_0})$	(3.13)
$x_v = \frac{s_v - s_{l_0}}{s_{v_0} - s_{l_0}}$	(3.14)
$x_l = \frac{s_l - s_{l_0}}{s_{v_0} - s_{l_0}}$	(3.15)
$X = \frac{m_T\, P_a\, v_{l_0} - V_T\, P_a + m_T\, u_{l_0} - U_i}{[(u_{l_0} - u_{v_0}) - (v_{v_0} - v_{l_0})\, P_a]\, m_T}$	(3.16)

In particular:

- $u_{v_{is}}$ is the specific internal energy of the vapor phase after the isoentropic expansion $[kJ\ kg^{-1}]$;
- $u_{l_{is}}$ is the specific internal energy of the liquid phase after the isoentropic expansion $[kJ\ kg^{-1}]$;
- x_v and x_l are defined as entropy ratios of the vapor and the liquid phase $[-]$;
- X is the intersection point between the variation of internal energy and the adiabatic irreversible expansion work (Planas model) $[-]$;

As explained above, the "Se" and the "Genova" models directly consider the fraction of the mechanical energy converted into the pressure wave generation through the coefficients k and ψ. The other models consider different coefficients to identify this energy conversion fraction and they are collected in table 3.4:

Table 3.4: Real models: energy conversion fractions

Model	α	k	ψ
TNO	2.0	-	-
Planas	0.4 - 0.8	-	-
Se	1.0	0.14	-
Genova	1.0	-	0.07
Birk	2.0	-	-

As showed in table 3.4, real gas behavior models consider different coefficients to identity the fraction of the mechanical energy that is converted in the overpressure of the blast wave. In particular, the "TNO" and the "Birk" models consider a coefficient $\alpha = 2$, to take into account the reflection of the blast wave on the ground. In the model developed by Planas, a value between the 40% and 80% of the mechanical energy is considered to be involved in the shock-wave generation. More precisely, the models considers $\alpha = 0.8$ if the vessel ruptures in a fragile manner, while $\alpha = 0.4$ if the type of failure is ductile [59]. It is important to state that the α coefficient is considered equal to 1 in the case of the "ideal gas behavior" models.

The equations implemented in this work with the aim to estimate the mechanical energy of a *BLEVE* have now been defined. These models are applied to the different experiments described in the next sections. It may be anticipated that is possible to estimate the energy of the blast-waves generated during the different "bursting case scenario" tests [5] for each different tank pressure at the moment of the explosions. With regards to the SH_2IFT Project *BLEVE* analysis, by implementing the aforementioned models, it is possible to conduct a parametric analysis based on the liquid mass and temperature of the liquid phase inside the vessel at the moment of the explosion.
Furthermore, the overpressure generated after each experiment is estimated through the TNT equivalent mass and the Baker methods, which correlate the energy to the magnitude of the pressure wave, taking into account the conversion fraction (α) mentioned above. These methods are described in the following section.

3.2 Overpressure and impulse determination

This section is dedicated to the definition of the methods implemented in this work to correlate the mechanical energy of the aforementioned *Boiling Liquid Expanding Vapor Explosions* to overpressure estimations. In particular, both the TNT and the Baker method are be

discussed in details and a comparison between the two is carried out. The TNT equivalent mass method is selected in analogy with the analysis conducted by Ustolin et al. [6]. It is in fact a conservative method often implemented to estimate safety distances from hazardeous explosions. The Baker method [47] is selected considering its simplicity and adaptability to different types of explosions. It provides overpressure estimations for a large scale of pressure ratios and it allows one to conduct comparisons between high explosive blast-waves and pressurized tanks explosions [47]. Furthermore, by comparing the obtained results with the experimental data, it is possible to proceed with a discussion on the reliability of the two methods.

3.2.1 The TNT equivalent mass method

The TNT equivalent mass method (TNT method) is implemented to estimate both the overpressure and the impulse generated by the blast-wave. It is one of the most conservative methods [6] and it is often used to determine safety distances from such hazardeous events. In fact, it may provide extremely conservative results and to avoid this problem it is usually used to estimate overpressure and impulse in the *far field*: a region of space identified by a parameter referred as the Sachs scaled distance ($\bar{R}$). The Sachs scaled distance, as the name suggests, defines a dimensionless distance from the centre of the explosion in the following way:

$$\bar{R} = d \left(\frac{P_0}{\alpha \, E} \right)^{\frac{1}{3}} \tag{3.17}$$

where $d\,[m]$ is the dimensional distance from the explosion, $E\,[J]$ is the (mechanical) energy previously calculated, $P_0\,[Pa]$ is the atmospheric pressure and $\alpha\,[-]$, as previously mentioned, is the fraction of the mechanical energy which is converted into the pressure of the shock-wave. α depends by the model used to estimate the energy (i.e. $\alpha_{TNO} = 2$, $\alpha_{Planas} = 0.4 - 0.8$). The *far field* region is usually identified with values of $\bar{R} > 2$, and in this region the TNT method is often considered as mostly reliable. In the *near field* region ($\bar{R} < 2$), this method often provides extremely conservative estimations [58]. The distinction between far and near field is considered in this work and it is highlighted in the discussion of the obtained results.

The first step to calculate overpressure and impulse with the TNT equivalent mass method is to correlate the energy of the explosion - previously estimated with both ideal and real gas behavior models - with a parameter referred as *TNT equivalent mass*. This conversion can be obtained in an a useful and straight-forward way, considering 4,680 kJ (of explosion energy) equal to 1 kg of TNT [29]. Once the TNT equivalent mass is determined, it is possible to proceed with the definition of the *TNT scaled distance* ($Z\,[m\,kg^{-1/3}]$). This parameter takes into account the TNT equivalent mass and it correlates it with the overpressure and the impulse.

The TNT scaled distance is defined as follows:

$$Z = \frac{d}{(\alpha\, W_{TNT})^{\frac{1}{3}}} \tag{3.18}$$

where $W_{TNT}\,[kg]$ is the TNT equivalent mass. $d\,[m]$ and $\alpha\,[-]$ are again the distance from the centre of the explosion and the fraction of energy converted into the pressure of the blast-wave. Hence, it is possible to proceed with the overpressure calculation using the following equation [60], in accordance with the previously mentioned blind prediction by Ustolin et al. [6].

$$\frac{p_s}{P_0} = \frac{808\left[1+\left(\frac{Z}{4.5}\right)^2\right]}{\sqrt{1+\left(\frac{Z}{0.048}\right)^2}\sqrt{1+\left(\frac{Z}{0.32}\right)^2}\sqrt{1+\left(\frac{Z}{1.35}\right)^2}} \tag{3.19}$$

Equation (3.19) provides the values of the estimated overpressure ($p_s\,[Pa]$) normalized on the atmospheric pressure ($P_0\,[Pa]$) and it correlates their ratio with the TNT scaled distance by means of an empirical relation. It is also possible to estimate the impulse generated by the blast-wave with another empirical correlation [60], as showed below:

$$i_s = \frac{6.7\sqrt{1+\left(\frac{Z}{0.23}\right)^4}}{Z^2\sqrt[3]{1+\left(\frac{Z}{1.55}\right)^3}}\, W_{TNT}^{\frac{1}{3}} \tag{3.20}$$

where again $Z\,[m\;kg^{-1/3}]$ is the TNT scaled distance and $W_{TNT}\,[kg]$ is the TNT equivalent mass. Equations (3.19) and (3.20) allow one to estimate the values of overpressure and impulse at different distances from the centre of an explosion, with the only input of the energy liberated during the process. The determination of these two parameters is fundamental to validate the physical models for the estimation of the mechanical energy, since the experimental data are pressure measures. Furthermore, overpressure and impulse are crucial variables to take into account when it comes to define safety distances from explosions, with the purpose to avoid injuries on humans and damage on structures. It may be interesting to highlight that in this sense a conservative threshold can be set at 1.35 kPa of overpressure and 1 $Pa\;s$ of impulse [6].

By implementing the TNT equivalent method, it is possible to estimate the values of overpressure generated during the analysed *BLEVE* experiments and then to compare them with the provided experimental data. This process is then repeated using the Baker method to estimate the pressure of the blast-waves, which is described in the following subsection.

3.2.2 The Baker Method

The method proposed by Baker [47] to estimate blast-wave pressure is selected mainly for its reliability and for the possibility to compare the obtained results with those of high explosive charges and with the data obtained for a wide range of exploding vessels. In fact, the method was initially developed analysing experimental gas-filled vessel bursts [47].
In particular, the experimental data were obtained investigating bursting spheres pressurized at different pressure levels (from 5 to 37,000 atmospheres) and with temperature ratios ranging from 0.5 to 50 times the surrounding temperature.

The experiments were conducted on spheres filled with air, helium and sulphur hexafluoride to investigate the effect of different specific heat ratios (1.2, 1.4 and 1.667). All fluids were also assumed to obey equations of state for perfect gases. In table 3.5 and table 3.6, the conditions of pressure, temperature and specific heat ratios of the gases in the bursting spheres are collected.

Table 3.5: Experimental conditions used to build the method proposed by Baker [47]

Case	Pressure ratio: $\frac{p_1}{p_0}$	Temperature ratio: $\frac{\theta_1}{\theta_0}$	Specific heat ratio: γ_1
1	5.00	0.500	1.400
2	5.00	2.540	1.400
3	5.00	10.000	1.400
4	5.00	50.000	1.400
5	10.00	0.500	1.400
6	10.00	50.000	1.400
7	100.00	0.500	1.400
8	100.00	50.000	1.400
9	150.00	50.000	1.400
10	500.00	50.000	1.400

Table 3.6: Experimental conditions used to build the method proposed by Baker [47]

Case	Pressure ratio: $\frac{p_1}{p_0}$	Temperature ratio: $\frac{\theta_1}{\theta_0}$	Specific heat ratio: γ_1
A	94.49	1.000	1.400
B	94.49	1.000	1.200
C	94.49	1.167	1.200
11	37000.00	0.500	1.400
12	37000.00	5.000	1.400
13	37000.00	10.000	1.400
14	1000.00	1.000	1.400
15	1000.00	4.000	1.667
16	1000.00	0.500	1.400
17	5.00	5.000	1.400

In table 3.5 and 3.6, p_1 and θ_1 respectively indicate pressure and temperature inside the bursting spheres. p_0 and θ_0 are the atmospheric pressure and temperature and γ_1 is the specific heat ratio of the gas inside the exploding vessels.
An analysis of the estimated overpressure using the data provided in the above mentioned tables is also conducted in this work.

The first step to estimate the pressure of a blast-wave with this method consists in the definition of the energy-scaled radius of the bursting sphere ($\bar{R}_1$), as per the following equation:

$$\bar{R}_1 = \frac{r_1 \, p_0^{1/3}}{E^{1/3}} \tag{3.21}$$

where $r_1\,[m]$ is the distance from the explosion, $p_0\,[Pa]$ is the atmospheric pressure and $E\,[J]$ is the energy of the explosion.
It can be highlighted that the energy stored in a bursting sphere can be correlated with its volume, and therefore with the radius of the latter. Hence, the equation proposed by Brode [61] can be implemented:

$$E = \frac{(p_1 - p_0)\, V_1}{\gamma - 1} = \frac{4\,\pi}{3}\,\frac{p_1 - p_0}{\gamma_1 - 1}\, r_1^3 \tag{3.22}$$

where p_1 $[Pa]$ and p_0 $[Pa]$ are again the pressure inside and outside the vessel, V_1 $[m^3]$ and r_1 $[m]$ are respectively the volume and the radius of the sphere and γ_1 $[-]$ is the specific heat ratio of the contained gas.
Combining eq. (3.21) with eq. (3.22), eq. (3.23) is obtained, which is useful to correlate the dimensionless distance to the pressure inside the vessel:

$$\bar{R}_1 = \left[\frac{3\,(\gamma_1 - 1)}{4\,\pi\,(\frac{p_1}{p_0} - 1)} \right]^{1/3} \tag{3.23}$$

Once the dimensionless distance $\bar{R}_1$ is defined, the dimensionless overpressure calculation can be faced by means of the *Shock-tube equation* developed by Liepmann and Roshko [62], in which subscript 1 refers to the conditions inside the bursting spheres, while subscript 0 to the atmospheric conditions:

$$\frac{p_1}{p_0} = \frac{p_{so}}{p_0} \left\{ 1 - \frac{(\gamma_1 - 1)\,(a_0/a_1)\left(\frac{p_{so}}{p_0} - 1\right)}{\sqrt{2\,\gamma_0\left[2\,\gamma_0 + (\gamma_0 + 1)\left(\frac{p_{so}}{p_0} - 1\right)\right]}} \right\}^{(\frac{-2\,\gamma_1}{\gamma_1 - 1})} \tag{3.24}$$

where:

- $\frac{p_1}{p_0}$ is the pressure ratio $[-]$;
- a_0 and a_1 indicate the speed of sound outside and inside the vessels $[m\ s^{-1}]$;
- γ_1 and γ_0 are the specific heat ratios $[-]$;
- $\frac{p_{so}}{p_0}$ is the dimensionless overpressure $[-]$;

It is relevant to point that the dimensionless overpressure is usually the unknown in eq. (3.24). To solve such equation - thus to calculate p_{so}/p_0 under the experimental conditions collected in table 3.5 and table 3.6 - the VPA-solve feature of Matlab R2021b [63] is implemented.
Since the gases are supposed to obey the perfect gas low, the speed of sound $[m\ s^{-1}]$ inside and outside the bursting spheres is calculated using the following equations:

$$a_0 = \sqrt{\gamma_0\, R_{air}\, \theta_0} \tag{3.25}$$

$$a_1 = \sqrt{\gamma_1\, R_{H_2}\, \theta_1} \tag{3.26}$$

where R_{air} $[J\ kg^{-1}\ K^{-1}]$ and R_{H_2} $[J\ kg^{-1}\ K^{-1}]$ are the constants of gas respectively of air

and hydrogen. Considering the relations $R_{air} = \frac{R_0}{mm_{air}}$ and $R_{H_2} = \frac{R_0}{mm_{H_2}}$ the speed of sound ratio is therefore defined as follows:

$$\frac{a_0}{a_1} = \sqrt{\frac{\gamma_0}{\gamma_1}\,\frac{R_{air}}{R_{H_2}}\,\frac{\theta_0}{\theta_1}} \implies \sqrt{\frac{\gamma_0\,/\,\gamma_1}{\theta_1\,/\,\theta_0}\,\frac{R_0\,/\,mm_{air}}{R_0\,/\,mm_{H_2}}} \implies \sqrt{\frac{\gamma_0\,/\,\gamma_1}{\theta_1\,/\,\theta_0}\,\frac{mm_{H_2}}{mm_{air}}} \tag{3.27}$$

where R_0 is the universal gas constant ($R_0 = 8.314\,J\,mol^{-1}\,K^{-1}$ [3]) and mm_{air} and mm_{H_2} are the molar masses of air and hydrogen [$kg\,mol^{-1}$].

Once the dimensionless overpressure is found for each case of the aforementioned tables, the results are compared with the curves provided by Baker [47] to generalise his method.

In their study concerning hydrogen combustion role in shock-wave pressure generation, Molkov et al. [11] provide the same curves, which are shown in figure 3.1. Figure 3.1 also shows the curve corresponding to the high explosive charges, which is the one indicated by the arrow, and the curves identified by decreasing pressure ratios below it. Solving equation 3.24 for the cases illustrated in table 3.5 and 3.6, it is possible to identify the corresponding points ($\bar{R}_1\,,\,\bar{P}$) of the bursting spheres experiments on figure 3.1. Hence, the boundary conditions of the "bursting tank scenario" [5] and the SH_2IFT Projects experiment are used to calculate the dimensionless distance ($\bar{R}_1$) and therefore to find the estimated overpressure (p_{so}) of such explosions.

At the end, the overpressure results obtained with the TNT equivalent mass method and the Baker one are compared with the experimental results. In the next chapter (Results and Discussion) these results are shown and a extensive discussion regarding the obtained general underestimation is carried out. As explained above, only the mechanical energy of the analysed *BLEVEs* is considered up to this point.
In the following section, the contribution of the hydrogen combustion in the aftermath of the bursts is considered following the method suggested by Molkov et al. [11]. Therefore, the combustion energy is taken into account and, to do so, the TNT equivalent mass method and the Baker method were modified and adapted.

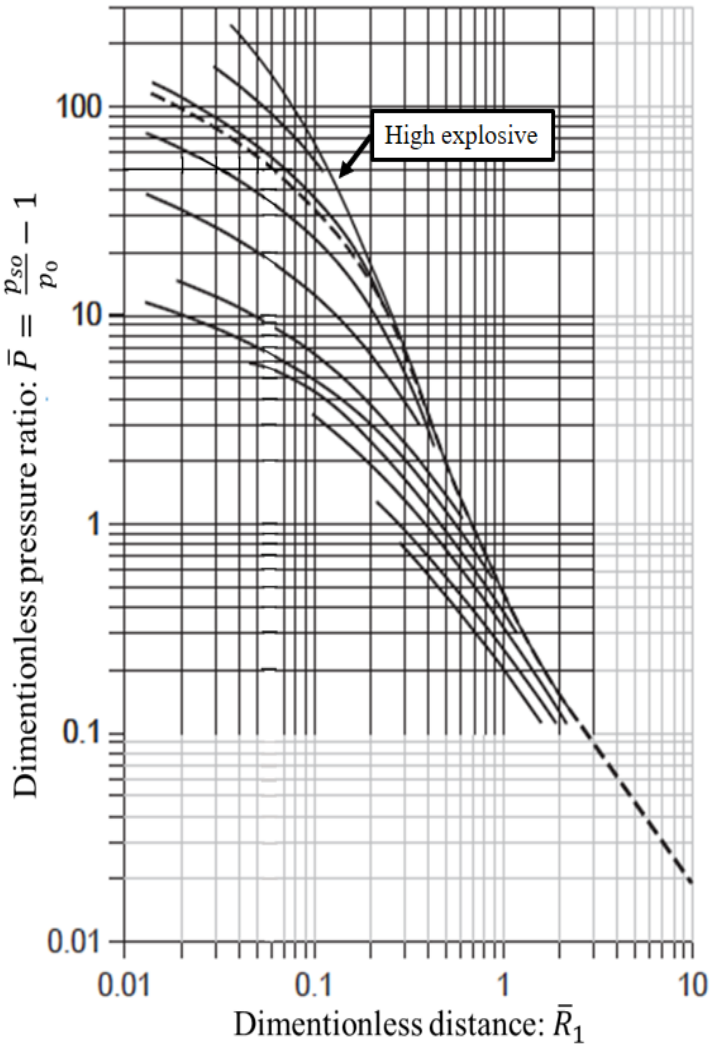

Figure 3.1: Dimensionless overpressure, $\bar{P}$, as a function of dimensionless distance, $\bar{R}_1$, [11]

3.3 Hydrogen Combustion

Hydrogen is a high flammable fuel. It presents a minimum ignition energy of 0.017 mJ [2], which makes it extremely likely to ignite during a violent process such as a *BLEVE*. In fact, after the explosions documented in the "bursting tank scenario" conducted by BMW [5] and in the SH_2IFT Project experiment, a fireball was immediately generated, which lifted many meters above the ground.
According to previously studies, it may be speculated that the combustion of hydrogen could play a role in the total overpressure generated by the shock-wave. In particular, in this work the methodology suggested by Molkov et al. [11] to take combustion into consideration is adopted. The method consists in the adaptation of the model proposed by Baker to take into account the fraction ($\beta\,[-]$) of the hydrogen lower heat value ($LHV\,[kJ\,kg^{-1}]$) which is converted in pressure-wave. To do so, Molkov et al. considered different fractions, depending on the presence of obstacles nearby the centre of the explosion.
These fractions are defined as follows:

- $\beta = 0.054$ if there is no obstruction near the centre of the explosion;
- $\beta = 0.09$ if there is an obstacle near the centre of explosion;

It may be interesting to highlight that the obstacle may consist in a car placed above a hydrogen tank after a road accident.

In the method proposed by Molkov et al., the definition of the parameter $\bar{R}_1$ (dimensionless distance in the Baker method) is modified to take into account this new fraction of energy. In analogy with this idea, it is also proposed a modification to the parameter TNT equivalent mass to take combustion into account when adopting the TNT method. These adaptations are explained and discussed in the following subsections.

3.3.1 Baker Method: Combustion

To take combustion into account when following the model proposed by Molkov et al. [11], the first step consists in the re-definition of the parameter $\bar{R}_1$.
In particular, the modification is explained in the following equation:

$$\bar{r}_p = r \left(\frac{p_s}{\alpha\, E_m + \beta \left(\frac{r_{sh}}{r_b} \right)^3 E_{ch}} \right)^{1/3} \tag{3.28}$$

where:

- $\bar{r}_p$ is the dimensionless distance from the explosion (it takes the role of $\bar{R}_1$ defined in the Baker method) $[-]$;
- r is the distance from the explosion $[m]$;

- p_s is the atmospheric pressure $[Pa]$;
- α is the fraction of the mechanical energy which is converted into overpressure (it is defined for each mechanical energy model) $[-]$;
- E_m is the total mechanical energy liberated by the *Bleve* $[J]$;
- β is the fraction of the combustion energy which is converted into the blast-wave pressure $[-]$;
- r_{sh} is the distance where the pressure is probed $[m]$;
- E_{ch} is the chemical energy contained in the tank $[J]$;
- r_b is defined as the radius of the hemisphere which could be occupied by combustion products $[m]$;

It can be noted that, although indicated with different symbols, most of the parameters that show up in equation (3.28) are the same used to define the dimensionless distance of the Baker method - eq. (3.21). The main difference is the presence of the combustion energy ($E_{ch}\,[J]$), which is multiplied by $\beta\,[-]$ (the fraction which is converted in overpressure) and by other coefficients, explained as follows.

$r_{sh}\,[m]$ is the distance where the pressure is probed. When the pressure is estimated at different distances, i.e. when the shock-wave is probed at different distances than r_{sh}, the model proposes to set $r_{sh} = r$.
$r_b\,[m]$ is the radius of the hemisphere which could be occupied by combustion products and it can be estimated following the next steps.
The total amount of hydrogen moles which undergo the combustion process can be find as:

$$n_{H_2} = m_T \cdot mm_{H_2} \tag{3.29}$$

where $m_T\,[kg]$ is the total mass of hydrogen and $mm_{H_2}\,[mol\,kg^{-1}]$ is molar mass of hydrogen. It can be highlighted that this number is the maximum possible number of moles which can be burned. Considering normal conditions 1 mole occupies 22.4 liters, so it is possible to calculate the total volume of the un-burned hydrogen as follows:

$$V_{u_{H_2}} = n_{H_2} \cdot \frac{22.4}{1000} \tag{3.30}$$

Where $V_{u_{H_2}}$ is expressed in m^3.
At this point, the hydrogen combustion reaction is considered to estimate the total volume of air needed for the complete stoichiometric combustion.

$$2\,H_2 + (\,O_2 + 3.76\,N_2\,) \implies 2\,H_2O + 3.76\,N_2 \tag{3.31}$$

Therefore, 1 mole of hydrogen reacts with 2.38 moles of air ($n_{air} = \frac{1+3.76}{2}$). Hence, the total volume occupied by an un-burned stoichiometric mixture of air with the released hydrogen be estimated by adding the volume of hydrogen to the volume of air as follows:

$$V_u = V_{u_{H_2}} + n_{air} \cdot \frac{22.4}{1000} \tag{3.32}$$

To estimate the volume the hemisphere occupied by combustion products formed after hydrogen complete combustion, the relation $V_b = V_u \cdot E_i$ can be used, where $E_i\,[-]$ is an expansion coefficient of combustion products (i.e. $E_i = 6.85$ for 30% hydrogen-air mixture [64]).
Finally, the radius of the hemisphere occupied by the combustion products of stoichiometric combustion can be calculated by definition:

$$r_b = \left(\frac{3\,V_b}{2\,\pi}\right)^{1/3} \tag{3.33}$$

Once the ratio of the radii ($\frac{r_{sh}}{r_b}$) is defined, it has to be noted that this ratio is monotonically increasing with the distance traveled by the shock-wave. When this ratio reaches is maximum value of 1 ($r_{sh} = r_b$) than the model suggests to consider it to remain constant and equal to 1.
It can also be underlined that this ratio could be re-written as $[(r_{sh} - r_v)/r_b]^3$, being $r_v\,[m]$ the radius of the vessel, since the shock and thus the release of chemical energy are not possible for distances less than or equal to the vessel radius. Following the model [11], this distinction is not considered due to small effect of this change on the overall predictive capability of the model itself.

The only parameter of eq. (3.28) which needs more discussion is the total combustion energy - i.e. the chemical energy contained in the hydrogen. To estimate this value, the lower heat value ($LHV\,[J\,kg^{-1}]$) of hydrogen is considered. Hence, the chemical energy E_{ch} is calculated as follows:

$$E_{ch} = m_T \cdot LHV \tag{3.34}$$

where LHV is the lower heat value for the hydrogen $[kJ\ kg^{-1}]$ and m_T is again the total mass of hydrogen contained in the vessel $[kg]$.

A comparison between the obtained values of $\bar{r}_p$ and $\bar{R}_1$ highlights the difference between this method and the method proposed by Baker. As it will be shown in the next chapter, the values of $\bar{r}_p$ are always smaller then the the values of $\bar{R}_1$. This difference implies that when placing these values on figure 3.1, the overpressure results are always higher with the

method proposed by Molkov et al. This fact appears particularly clear in the region of the above mentioned graphics including dimensionless distances between 0.5 and 10.
In fact, in this region the pressure ratio curves are almost completely parallel and similar to lines, meaning that an almost inverse proportionality relationship exists between the dimensionless distance and the dimensionless overpressure.

3.3.2 TNT Method adaptation

In the previous subsection, the adaptation of the Baker method following the model proposed by Molkov et al. was shown. In this work, it was decided to apply a similar modification to the TNT method to take into account the combustion energy of the explosion along with the mechanical one. To do so, the parameter TNT equivalent mass (W_{TNT} $[kg]$) was modified as follows:

$$W_{TNT} = \frac{\alpha\, E_m + \beta \left(\frac{r_{sh}}{r_b}\right)^3 E_{ch}}{4680} \tag{3.35}$$

where α $[-]$ is again the fraction of the mechanical energy which is converted into the pressure of the shock-wave (it depends from the mechanical energy model). E_m $[kJ]$ is again the mechanical energy of the explosion, β $[-]$ is the fraction of the chemical energy which is converted into the overpressure and E_{ch} $[kJ]$ is the total chemical energy of the hydrogen in the vessel. The ratio $\frac{r_{sh}}{r_b}$ is once again the ratio between the distance traveled by the shock-wave (r_{sh} $[m]$) and the radius of the hemisphere which could be occupied by the products of complete combustion (r_b $[m]$).
It can be noted that eq. (3.35) takes into account the fraction of the mechanical energy α in the definition of the TNT equivalent mass, while this parameter originally showed up in the definition of the TNT scaled distance (Z) in eq. (3.18). Hence, eq. (3.35) takes into account both the fractions of the chemical and the mechanical energy that are converted into the pressure of the shock-wave, thus simplifying the definition of the TNT scaled distance (Z $[m\, kg^{-1/3}]$) as follows:

$$Z = \frac{d}{(W_{TNT})^{1/3}} \tag{3.36}$$

With this adaptation, it is possible to take combustion into account to estimate the total overpressure generated by the shock-wave.

It is relevant to consider the general overestimation that the TNT equivalent method usually lead to. As mentioned before, this method is often adopted in a region of space referred as *far field*, identified by values of the Sachs scaled distance ($\bar{R} > 2$). In the region usually referred as the *near field* ($\bar{R} < 2$) the TNT equivalent method often provides extremely conservative estimations. The Sachs scaled distance was previously defined in the section dedicated to the definition of the TNT equivalent method - eq. (3.17).

To be able to investigate the results obtained with the TNT equivalent method when combustion is taken into account, the Sachs scaled distance definition is modified in a similar way to the TNT equivalent mass, thus providing a different distinction between *near field* and *far field* regions. In this way, it is possible to exclude the results obtained within a certain range into the *near field*, which presented an extreme overestimation of the experimental data.
This new Sachs scaled distance is defined as follows:

$$\bar{R}_s = d \left(\frac{P_0}{\alpha\, E_m + \beta \left(\frac{r_{sh}}{r_b} \right)^3 E_{ch}} \right)^{1/3} \tag{3.37}$$

where again $d\ [m]$ is the distance from the explosion, $P_0\ [Pa]$ is the atmospheric pressure and the other parameters are the same as explained previously.
It can be noted that once the TNT scaled distance is calculated by means of the latter definition, the impulse and the overpressure of the shock-wave can be calculated using again the empirical correlation proposed in eq. (3.20) and eq. (3.19), since they depend only by the TNT scaled distance (Z) and the TNT equivalent mass (W_{TNT}). To provide continuity, these equations are reported below:

$$\frac{p_s}{P_0} = \frac{808 \left[1 + \left(\frac{Z}{4.5} \right)^2 \right]}{\sqrt{1 + \left(\frac{Z}{0.048} \right)^2} \sqrt{1 + \left(\frac{Z}{0.32} \right)^2} \sqrt{1 + \left(\frac{Z}{1.35} \right)^2}} \tag{3.38}$$

$$i_s = \frac{6.7 \sqrt{1 + \left(\frac{Z}{0.23} \right)^4}}{Z^2 \sqrt[3]{1 + \left(\frac{Z}{1.55} \right)^3}} W_{TNT}^{\frac{1}{3}} \tag{3.39}$$

The overpressure generated by the analysed *Boiling Liquid Expanding Vapor Explosions* is, after these considerations, estimated by taking into account both the chemical and the mechanical energy of the vessel bursts. These estimations are conducted implementing the previously described mechanical energy models and following the method proposed by Molkov et al. [11]. A new model to take combustion into account when adopting the TNT equivalent method was then proposed, with the idea of comparing the obtained results to the experimental data.
At this point, an extensive discussion about the role of the para-hydrogen to ortho-hydrogen transition during the process is carried out. As explained in the following subsection, an estimation of the time required by the complete reaction to occur is proposed by means of the kinetics of the transition. Then, an analysis of the absorbed energy is carried out with

respect to the estimated reaction time.

3.4 The *Ortho-Para* transition's role

As discussed in the previous chapter, the transition from the para-isomer to the ortho-isomer of the hydrogen molecule is an aspect which needs to be investigated when approaching a liquid hydrogen *BLEVE* or *RPT* [10]. In this study, the analysis of this transition is focused on two main aspects.
The first one is the determination of the time requested by the endothermic reaction to complete itself and the second one regards the energy absorption of this process. More precisely, it was decided to calculate the reaction time by means of the kinetics of the reaction, which could allow one to conduct a comparison between the latter and experimental data regarding *BLEVEs* and fireballs. Doing so, it is possible to discuss the role of this chemical reaction into the development of the blast-wave, conducting an analysis on the compatibility of the characteristic times.
As regards the thermodynamic of the reaction, it is estimated the total energy which can be absorbed by the hydrogen molecule when it is converted from para-hydrogen to ortho-hydrogen. In accordance with literature [4], the hydrogen contained in the vessels is considered to be 99.8% para-hydrogen and 0.2% ortho-hydrogen.
After the explosion, these fractions are believed to change to values around 25% para-hydrogen and 75% ortho-hydrogen. These concentrations are usually found in hydrogen at room temperature and pressure, therefore this mixture is often referred as normal-hydrogen $(n - H_2)$.

Once the energy absorption of the complete transition is defined, a model to take this phenomenon into account is proposed. In particular, the experimental data of the SH_2IFT Project experiment are compared with the estimations obtained implementing both the modified TNT equivalent mass and the Baker method. In this sense, the reverse problem is solved with the purpose to track back the energy difference which could be assigned to the para to ortho reaction. Hence, the obtained values are compared with the maximum possible energy absorption of the reaction, which was calculated previously. Finally, a discussion on the compatibility of these energies (in terms of order of magnitude) is carried out, which is proposed in its dedicated subsection.

3.4.1 Reaction time

As explained in the previous chapter, the time required by the complete reaction to complete is calculated by means of the kinetics of the reaction, thus implementing the equation proposed by Milenko and Sibileva [46]. For the sake of simplicity, the equation is recalled below:

$$\frac{d\,c}{d\,t} = -k \cdot c^2 + k' \cdot c \cdot (1 - c) \tag{3.40}$$

where:

- c is the concentration of the ortho-isomer ($o - H_2$);
- t is the time variable;
- k is the kinetic constant of the ortho-para reaction;
- k' is the kinetic constant of the para-ortho reaction;

This equation is solved by imposing the initial and final concentrations of ortho-hydrogen in the mixture. It is possible to re-write the equation as follows:

$$\frac{d\,t}{d\,c} = \frac{1}{-k \cdot c^2 + k' \cdot c \cdot (1-c)} \implies d\,t = \frac{d\,c}{-k \cdot c^2 + k' \cdot c \cdot (1-c)} \tag{3.41}$$

From a mathematical point of view, eq. (3.41) is a simple differential equation with separable variables. It is possible to solve eq. (3.41) analytically knowing the initial and final concentrations of the ortho-isomer, thus calculating the required time to reach a particular $o - H_2$ concentration. In this study, it was decided to calculate the time to reach an ortho-hydrogen concentration of 70%, which is a value near to the one found in normal conditions (75% of ortho-isomer in $n - H_2$). To do so, the first and the second members of the equation are integrated imposing the following boundary conditions:

- $t = t_0 = 0 \implies c = c_0 = 0.2\%$;
- $t = t_1 \implies c = c_1 = 70\%$

Hence, eq. (3.41) can be re-arranged as follows:

$$\int_{t_0}^{t_1} d\,t = \int_{c_0}^{c_1} \frac{d\,c}{-k \cdot c^2 + k' \cdot c \cdot (1-c)} \tag{3.42}$$

The equation above can be solved analytically by means of the simple fractions method. The salient steps to solve the integral at the second member are highlighted below. The first one consists in the explication of the second member of eq (3.42):

$$\frac{d\,c}{-k \cdot c^2 + k' \cdot c \cdot (1-c)} = \frac{1}{-c^2 \cdot (k + k') + k' \cdot c}\, d\,c$$

As regards the fraction above, it appears clear that the degree of the numerator is 0 while the degree of the denominator is equal to 2:

$$deg[\,N(c)\,] = 0$$

$$deg[\,D(c)\,] = 2$$

which means that, by imposing $-(k+k') = \beta$ and $k' = \gamma$ and using the scomposition in simple fractions it is possible to rewrite the fraction as follows:

$$\frac{1}{c \cdot \beta \cdot (c + \frac{\gamma}{\beta})} = \frac{1}{\beta}\left(\frac{A_1}{c} + \frac{A_2}{c + \frac{\gamma}{\beta}}\right)$$

from which it follows:

$$A_1 = \frac{\beta}{\gamma} \quad A_2 = -\frac{\beta}{\gamma}$$

Once the coefficients A_1 and A_2 are defined, the equation can be integrated easily using the property of the integral of the sum:

$$\frac{1}{\beta}\int \frac{d\,c}{c \cdot (c + \frac{\gamma}{\beta})} = \frac{1}{\beta}\int \left(\frac{\beta/\gamma}{c} + \frac{-\beta/\gamma}{c + \frac{\gamma}{\beta}}\right) d\,c$$

Finally, replacing the definitions of $\gamma = k'$ and $\beta = -(k+k')$, the solution of eq. (3.42) can be found as follows:

$$\Delta\, t = \left[\frac{ln(c) - ln(k\,c + k'\,(c-1)}{k'} - \frac{ln(k+k')}{k'}\right]_{c_0}^{c_1} \tag{3.43}$$

where $\Delta\, t = t_1 - t_0$.
By imposing the initial and final concentration of ortho-hydrogen: $c_0 = 0.2\%$ and $c_1 = 70\%$, the reaction time $\Delta\, t$ results in a function of only the kinetic constants k (ortho to para) and k' (para to ortho).
In particular:

$$\Delta\, t = \frac{1}{k'}\left[ln\left(\frac{c_1}{c_0}\right) - ln\left(\frac{k\,c_1 + k'\,(c_1 - 1)}{k\,c_0 + k'\,(c_0 - 1)}\right)\right] \tag{3.44}$$

As mentioned in the previous chapter, the kinetic constants of the reaction from ortho-hydrogen to para-hydrogen (k) and from para-hydrogen to ortho-hydrogen (k') can be estimated by means of the empirical correlation shown in eq. (2.27) and with the help of the Gibbs free energy. In fact, the constants can be calculated as follows:

$$k = (18.2 \pm 1.6)\, T^{0.56 \pm 0.02}\, \rho + 5 \cdot 10^4\, (0.77 \pm 0.03 + (921 \pm 94)\, T^{-2.5 \pm 0.2})\, \rho^{3.6} \tag{3.45}$$

which is the empirical correlation proposed by Milenko [46] to estimate the kinetic constant of the ortho-para transition (expressed in $10^{-3} \cdot h^{-1}$) as a function of temperature $T\,[K]$ and

density $\rho\,[kg\,m^{-3}]$. The kinetic constant of the para to ortho reaction is defined as follows:

$$k' = k \cdot e^{\frac{-\Delta G^o}{R\,T}} \tag{3.46}$$

where R is the constant of gas for hydrogen ($4125.5 J kg^{-1} K^{-1}$ [3]), T is again the temperature, expressed in kelvin and k' is expressed in $10^{-3} \cdot h^{-1}$. $\Delta\,G^o\,[J]$ is the Gibbs free energy and it is defined as a function of the enthalpy and entropy of both the isomers of the hydrogen molecule.

$$\Delta G = \Delta H - T\,\Delta S = (H_{pH_2} - H_{oH_2}) - T\,(S_{pH_2} - S_{oH_2}) \tag{3.47}$$

Eq. (3.46) is obtained, as explained in the previous chapter, considering the equilibrium of the reaction [4].

Under these conditions, it appears clear that it is possible to estimate the reaction time ($\Delta\,t$) considering different conditions of temperature and density of hydrogen. In this study, to estimate the reaction time, hydrogen is considered to be found instantaneously at atmospheric pressure as saturated vapor after the explosion. This consideration allow one to set just the temperature to calculate the kinetic constants and therefore the reaction time. In fact, setting the hydrogen temperature and by imposing the hydrogen to be at atmospheric pressure, it is possible to calculate density, enthalpy and entropy of both para and ortho isomers by means of the Cool-Prop package [48].

The temperature of the cryogenic fuel a moment after the *Boiling Liquid Expanding Vapor Explosion* is currently unknown. Nevertheless, keeping in mind the immediate ignition of the expanding fluid obtained during the experiment, it is not unreasonable to consider hydrogen temperature to range between values from few hundreds kelvins up to almost the hydrogen adiabatic temperature of flame. Hence, it was decided to considered various temperatures and investigate the dependency of the reaction time from the latter.
As previously mentioned, the reaction time is a crucial parameter to take into account to investigate the possible involvement of the para to ortho transition in the magnitude of the shock-wave. Once the reaction time is calculated, it was decided to proceed with the estimation of the energy which could be absorbed by the reaction. This aspect is discussed more in details in the following subsection.

3.4.2 Energy absorption

As mentioned above, the energy absorption of the endothermic para-ortho reaction is studied to carry out a discussion about the role of such transition in the blast-wave generated after the SH_2IFT Project *BLEVE*. The maximum amount of energy absorption which can be associated with the reaction is estimated considering the para-hydrogen ($p - H_2$) and ortho-hydrogen ($o - H_2$) thermodynamic properties provided by the Cool-prop package [48]. It may be useful to remind that the initial concentration of $o - H_2$ is considered to be around 0.2%

in accordance to literature [4], while its final concentration around 75%. The latter is the concentration of the hydrogen ortho-isomer in conditions of room pressure and temperature. The total enthaply difference between the initial and final condition is estimated as follows:

$$\Delta\, h_{p \Longrightarrow o} = (H_p + H_o)_{final} - (H_p + H_o)_{initial} \tag{3.48}$$

where:

- $\Delta\, h_{p \Longrightarrow o}$ is the enthalpy difference between the initial and final conditions $[J\ kg^{-1}]$;
- H_p and H_o are respectively the hentalpy of the para and the ortho isomers $[J\ kg^{-1}]$;
- the subscripts $final$ and $initial$ indicate the conditions at which the concentrations are defined;

To calculate the total enthalpy the initial and final concentrations are considered as follows:

$$(H_p + H_o)_{final} - (H_p + H_o)_{initial} = (c_p \cdot h_p + c_o \cdot h_o)_{final} - (c_p \cdot h_p + c_o \cdot h_o)_{initial} \tag{3.49}$$

where:

- c_p and c_o are the concentrations of the para and the ortho isomer expressed in kilograms of para or ortho isomer per kilogram of hydrogen $[-]$;
- h_p and h_o are respectively the specific enthaplies of $p - H_2$ and $o - H_2$ $[J\ kg^{-1}]$;

The maximum enthalpy difference $\Delta\, h_{p \Longrightarrow o}$ is obtained considering the above mentioned initial and final concentrations of ortho-hydrogen. Hence, the maximum value of enthaply absorbed by the reaction is estimated considering the total mass of hydrogen contained in the tank to undergo the transition, as shown in the following equation:

$$\Delta\, H_{p \Longrightarrow o} = m_T \cdot \Delta\, h_{p \Longrightarrow o} \tag{3.50}$$

where m_T $[kg]$ is the total mass of hydrogen contained in the exploding tank.
As explained above, the difference between the experimental data and the estimations obtained with both the modified TNT equivalent mass and Baker methods is calculated to identify the error (and therefore the accuracy) of the implemented models. The results will be shown in the following chapter, but it may result interesting to underline that a general over-prediction of the experimental data was obtained for the SH_2IFT Project experiment. The difference between the experimental overpressure and the estimated one is also used to track back the energy which could be associated with the reaction. To do so, the TNT equivalent method and the Baker method are again modified, as explained in the following subsection.

3.4.3 TNT equivalent mass method: para-ortho contribution

With the purpose of investigating the role of the reaction in the aftermath of the explosion, the experimental data and the estimations are used to associate the difference in terms of measured and expected pressure to a difference in terms of energy. Therefore, the TNT equivalent method is used to solve the reverse problem, which means that parameters such as TNT scaled distance and TNT equivalent mass are calculated from the overpressure difference between the experimental data and the estimations. The following equation highlights this aspect:

$$\frac{\Delta\, p_{p \Longrightarrow o}}{P_0} = \frac{808\left[1+\left(\frac{Z}{4.5}\right)^2\right]}{\sqrt{1+\left(\frac{Z}{0.048}\right)^2}\sqrt{1+\left(\frac{Z}{0.32}\right)^2}\sqrt{1+\left(\frac{Z}{1.35}\right)^2}} \tag{3.51}$$

where $\Delta\, p_{p \Longrightarrow o}\,[Pa]$ is the difference between the measured overpressure and the estimated one, $P_0\,[Pa]$ is the atmospheric pressure and $Z\ [m\ kg^{-1/3}]$ is the TNT scaled distance associated with the pressure difference. It is important to underline that the unknown of eq (3.51) is Z. Hence, the TNT equivalent mass associated with the error (i.e. the difference between the experimental data and the expected ones) can be defined as follows:

$$W_{TNT_{p \Longrightarrow o}} = \left(\frac{d}{Z}\right)^3 \tag{3.52}$$

where $d\,[m]$ is the distance at which the ovepressure is probed and W_{TNT} is expressed in kilograms. In this way, it is possible to associate the error made by the model to an equivalent difference in TNT mass. A new definition of TNT equivalent mass is now proposed, in which the enthalpy difference associated with the para to ortho reaction shows up:

$$W_{TNT} = \frac{1}{4680}\cdot\left[\alpha\, E + \beta\left(\frac{r_{sh}}{r_b}\right)^3 E_{ch} - \gamma\, \Delta\, H_{p \Longrightarrow o}\right] \tag{3.53}$$

where:

- α is the fraction of the mechanical energy which is converted into overpressure (it depends by the model used to estimate the mechanical energy) $[-]$;
- E is the mechanical energy liberated by the explosion $[kJ]$;
- β is the fraction of the combustion energy which is converted into ovepressure ($\beta = 0.054$ [11]) $[-]$;
- r_{sh} is the distance where the pressure of the shock-wave is probed $[m]$;
- r_b is the radius of the hemisphere which could be occupied by products of complete stoichiometric combustion $[m]$;

- E_{ch} is the chemical energy liberated by hydrogen combustion ($E_{ch} = m_T \cdot LHV$) $[kJ]$;
- $\Delta H_{p \Longrightarrow o}$ is the enthalpy difference associated with a transition from a concentration of 0.2 % $o - H_2$ to 75% $o - H_2$ of the total mass of the fuel in the vessel $[kJ]$;
- γ is a coefficient which identifies the fraction of the above mentioned hentalpy which can be neglected from the generation of the shock-wave $[-]$;

With this new definition, it is possible to associate the TNT equivalent mass ($W_{TNT_{p \Longrightarrow o}}$) calculated using the error made by the model with the enthalpy of the $p - H_2$ to $o - H_2$ transition. In particular, the coefficient γ can be calculated with the following equation:

$$W_{TNT_{p \Longrightarrow o}} = \frac{1}{4,680} \gamma \Delta H_{p \Longrightarrow o} \tag{3.54}$$

The coefficient γ identifies the fraction of the transition enthalpy ($\Delta H_{p \Longrightarrow o}$) which is associated with the overpressure generated by the explosion. In particular, a reasonable value of γ means that the enthalpy difference ($\Delta H_{p \Longrightarrow o}$), is compatible with the difference between the experimental data and the expected ones. More precisely, three different ranges of γ can be identified:

- $\gamma < 0$ means that the measured overpressure is higher than the one calculate with this method. In this case it is not possible to justify this difference with the para to ortho reaction following the proposed model.
- $\gamma > 1$ means that the energy absorption of the complete transition from 0.2% $o - H_2$ to 75% $o - H_2$ is not enough to entirely justify the difference between the experimental data and the estimations.
- $0 < \gamma < 1$ means that the error made by the model in terms of overpressure could be justified by the para-ortho transition. Hence, this value of γ could be a hint to understand the role of this chemical reaction in the generation of the shock-wave.

The same approach is adopted with the Baker method to estimate the fraction of the absorbed energy associated with the transition which could be involved in the shock-wave magnitude. In this way, the fraction γ is calculated after a re-definition of the Baker method, as explained in the following subsection.

3.4.4 Baker method: para-ortho contribution

The Baker method was initially defined to associate the overpressure generated by the explosion to the mechanical energy of the latter. Then, the combustion process was taken into account following the model proposed by Molkov et al. [11]. Now, the method is once again modified to take into account the fraction of the energy associated with the para to ortho

transition. In particular, a modification of the dimensionless distance ($\bar{R}_1$) is proposed to take this fraction into account:

$$\bar{R}_1 = r \left[\frac{p_0}{\alpha\, E + \beta \left(\frac{r_{sh}}{r_b} \right)^3 E_{ch} - \gamma\, \Delta\, H_{p \Longrightarrow o}} \right]^{1/3} \tag{3.55}$$

where $r\ [m]$ is the distance where the overpressure is probed, $p_0\ [Pa]$ is the atmospheric pressure and the other coefficients are the same explained in the previous subsection. The unknown of eq. (3.55) is γ (the fraction of the energy absorbed by the reaction which could have a role in the generation of the shock-wave). To calculate this fraction, the only parameter which needs to be set is the dimensionless distance $\bar{R}_1$.

To be able to calculate the dimensionless distance, the reverse problem is once again solved starting with the difference between the experimental data and the estimated overpressure, defining the dimensionless pressure ratio as follows:

$$\bar{P}_{p \Longrightarrow o} = \frac{p_{so_{p \Longrightarrow o}}}{p_0} - 1 \tag{3.56}$$

where $p_{so_{p \Longrightarrow o}}\ [Pa]$ is the pressure difference and $p_0\ [Pa]$ is again the atmospheric pressure. The dimensionless distance is then estimated using the graphics shown in figure 3.1. which is reported in the following page:
Once the dimensionless distance $\bar{R}_1$ is calculated, the coefficient can be calculated from eq. (3.55) as follows:

$$\gamma = \frac{1}{\Delta\, H_{p \Longrightarrow o}} \left[\alpha\, E + \beta\, E_{ch} \left(\frac{r_{sh}}{r_b} \right)^3 - p_0 \left(\frac{r}{\bar{R}_1} \right)^3 \right] \tag{3.57}$$

The same considerations explained in the previous subsection about the coefficient γ remain valid in this case. Therefore, a reasonable value of γ could be a hint about the role of the para-hydrogen to ortho-hydrogen transition in the generation of the shock-wave. In particular, in the case of $0 < \gamma < 1$, a fraction of the absorbed energy could be enough to justify the difference between the measured overpressure and the expected one.
It is relevant to underline that the energy associated with the transition from the para-isomer to the ortho one is calculated as the enthalpy of the "complete" reaction. The term "complete" reaction indicates that the hydrogen in the exploding vessel has a ortho-isomer concentration of 0.2% before the explosion and 75% after the vessel rupture. Hence, the coefficient γ identifies the fraction of this enthalpy which could be associated with the overpressure generation. Nevertheless, it is not unreasonable to approach the problem in a different way, considering what it will be referred as an "incomplete transition".

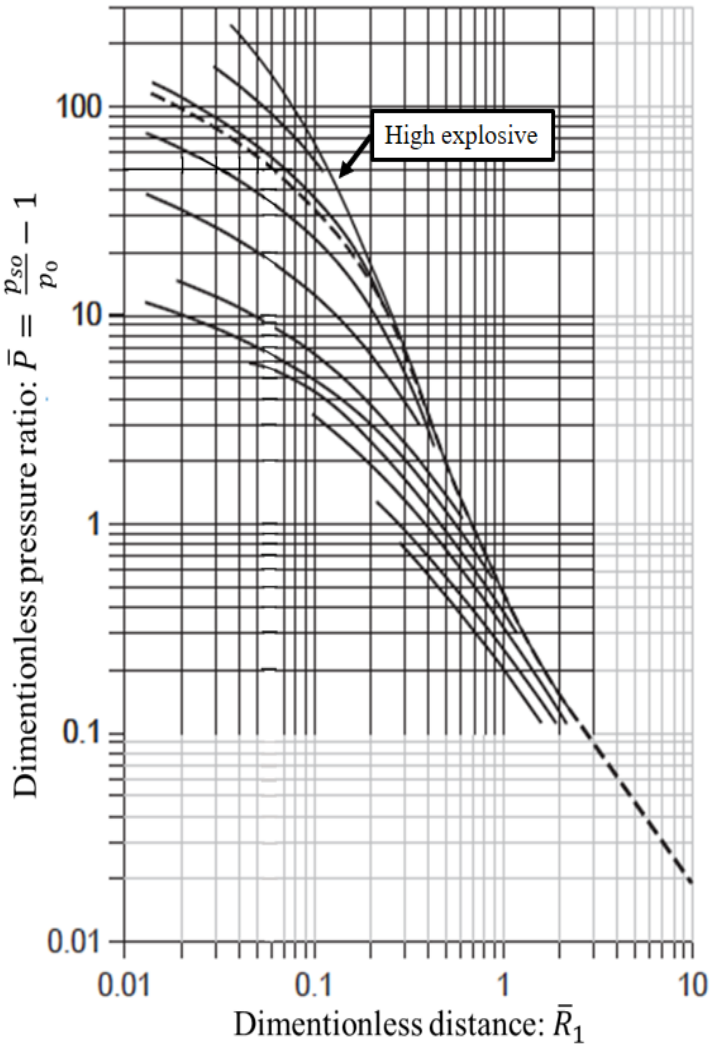

Figure 3.2: Smooth version of the Baker's curves [47] [11]

3.4.5 Incomplete transition: reaction time

The term "incomplete transition" indicates that the reaction from para-hydrogen to ortho-hydrogen does not reach the ortho-isomer typical concentration of normal-hydrogen (75% [4]). In the hypothesis that the reaction can influence the generation of the shock-wave, it is interesting to correlate the error made by the model (i.e. the difference between the experimental data and the simulated ones) to a particular concentration of ortho-hydrogen after the explosion. To do so, the same reverse problem explained in the previous subsection is again solved, with a particular difference, explained below. The following list has the purpose to summarize the steps of the process:

- Step 1) The error made by the model is used to set the reverse problem for the TNT equivalent and the Baker method;
- Step 2) The TNT equivalent mass $W_{TNT_{p \Longrightarrow o}}$ and the dimensionless distance $\bar{R}_1$ are defined following the same procedure identified in the previous subsections;
- Step 3) The enthalpy fraction of the reaction associated with the overpressure (γ) is once again defined;
- Step 4) The enthalpy difference of the incomplete reaction is defined;
- Step 5) The ortho-hydrogen final concentration associated with the above mentioned enthalpy difference is calculated;
- Step 6) The time requested to reach this particular ortho-hydrogen concentration is calculated;

It appears clear that the steps from one to three are not different from the ones explained in the previous subsection, therefore they will not be discussed any further. Step four to six are new considerations which need further discussion and they are explained as follows, starting from the enthalpy difference of the incomplete reaction.

$$\Delta H'_{p \Longrightarrow o} = \gamma \, \Delta H_{p \Longrightarrow o} \qquad [0 < \gamma < 1] \tag{3.58}$$

This new enthalpy difference $\Delta H'_{p \Longrightarrow o}$ $[J]$ is defined as the product between the fraction γ and the enthalpy difference of the complete transition (i.e. from 0.2 % ortho to 75 % ortho). It is useful to defined this new enthalpy difference because it allows one to calculate the ortho-hydrogen final concentration indicated in step 5 on the list above. More precisely, this new ortho-hydrogen final concentration is the concentration which could justify the difference between the experimental data and the expectations in terms of pressure, since the transition from 0.2% ortho to this new concentration is associated with the enthaply difference $\Delta H'_{p \Longrightarrow o}$. The new ortho-hydrogen final concentration can be estimated considering the

following enthalpy balance:

$$\Delta H'_{p \Longrightarrow o} = \Big[(c'_p \cdot h_p + c'_o \cdot h_o)_{final} - (c_p \cdot h_p + c_o \cdot h_o)_{initial} \Big] \cdot m_T \tag{3.59}$$

where $c'_p\,[-]$ and $c'_o\,[-]$ are respectively the new $p-H_2$ and $o-H_2$ concentrations expressed in kg of isomer per kg of hydrogen. $h_p\,[J\,kg^{-1}]$ and $h_o\,[J\,kg^{-1}]$ are the specific enthapies of para-hydrogen and ortho-hydrogen (calculated considering the two isomers to be found in saturated vapor conditions at atmospheric pressure immediately after the explosion). $m_T\,[kg]$ is the total mass of hydrogen in the vessel and subscripts $final$ and $initial$ indicate the conditions before and after the reaction.
From eq. (3.59) it is possible to calculate the final concentration of ortho-hydrogen considering the relation: $c'_p = 100 - c'_o$. Therefore, this concentration results:

$$c'_o = \frac{\frac{1}{m_T} \cdot \Delta H'_{p \Longrightarrow o} + c_p \cdot h_p + c_o \cdot h_o - h_p}{h_o - h_p} \tag{3.60}$$

The new final ortho-hydrogen concentration (c'_o) is now defined. The next and last step of this work is to estimate the time necessary to reach this particular concentration. The reaction time is again an important parameter since it allows one to conduct a comparison between this time and the typical duration of *BLEVEs*. The reaction time was calculated before for the "complete" reaction (i.e. from 0.2% ortho to 75% ortho) and now it is estimated for the "incomplete" reaction (i.e. from 0.2% ortho to c'_o). It is not unreasonable to expect this new reaction time to be lower then the previous one, since the final concentration of ortho-hydrogen is lower in the latter case (γ between 0 and 1 ensures this).

To estimate this new transition time the same equation derived from the Milenko and Sibileva equation [46] is once again implemented. This equation is recalled below:

$$\Delta t' = \frac{1}{k'} \left[ln\left(\frac{c'_o}{c_o}\right) - ln\left(\frac{k\,c'_o + k'\,(c'_o - 1)}{k\,c_o + k'\,(c_o - 1)}\right) \right] \tag{3.61}$$

where $c_o\,[-]$ and $c'_o\,[-]$ are the concentrations of ortho-hydrogen before and after the reaction. k and k' are again respectively the kinetic constants of the ortho to para and para to ortho reactions. It may be relevant to remind that these constants are calculated using the empirical correlation previously explained and by means of the equilibrium constant.
Therefore, applying the same considerations and hypothesis explained in the previous sections, the reaction time is estimated considering different hydrogen temperatures after the explosion. The obtained results are shown in the next chapter, which is dedicated to an extensive discussion about all the obtained results. Starting from the mechanical energy estimations obtained with the aforementioned models, the analysis of the data provided by the

SH_2IFT Project experiment and the BMW experiments is carried out. The role of hydrogen combustion and the para-ortho transition is highlighted through the analysis of experimental data and the simulations. Before presenting the obtained results, it is crucial to discuss in details the analysed experiments. The following sections focus on the definition of the setup, the boundary conditions and the thermophysical variables involved in such experiments.

3.5 BMW: Bursting tank scenario

The "Bursting tank scenario" tests are a series of nine experiments conducted on liquid para-hydrogen tank systems designed for passengers cars. In particular, the aim of the experiments was to analyse the safety of the vessels in the unfortunate scenario of a road accident involving liquid hydrogen fueled cars [5]. As previously mentioned, to study the behavior of the tank systems, un-fired (cold) *BLEVEs* were inducted by means of high explosive cutting charges detonated in proximity of the vessels. The overpressure generated by the blast-waves was measured from a distance of 3 meters.
Different conditions where applied to the cryo-vessels: the mass of liquid hydrogen varied from a minimum value of 1.8 kg to a maximum of 5.4 kg. Along with the different fillings of the tank systems, different pressures where reached before inducting the explosions. More precisely, the pressure of the vessels was set between values of 2 bar and 11 bar in the case of a sub-critical *BLEVEs*, while a value of almost 15 bar was set to analyse the behavior of the tanks in super-critical conditions (it is important to clarify that the critic pressure of hydrogen is 12.98 bar [3]). For the sake of simplicity, only the sub-critical experiments are analysed in this study (8 out of 9 tests). In table 3.7, the measured overpressure is reported in function of different values of tank pressures.

Table 3.7: Tank pressure vs measured overpressure

Tank Pressure [*bar*]	Min. Overpressure [*mbar*]	Max Overpressure [*mbar*]
2	30	170
4	50	110
11	150	450

As shown in table 3.7, the measured overpressure tends to increase with the pressure in the tanks before the explosions. As explained above, several models are implemented to describe the mechanical energy of the *Boiling Liquid Expanding Vapor Explosions* and their resulting shock-waves. Before discussing the obtained results, it is relevant to describe more in details the setup of the experiments. Particular attention is given to the different values of liquid mass, vapor mass, pressure and temperature of the cryogenic fluid contained in the tanks.

3.5.1 Setup and hypothesis

The liquid phase is initially considered as saturated liquid at ambient pressure. For each value of tank pressure, both the liquid and the vapor phase are considered as saturated at that pressure, hence it is possible to determine the temperature inside the tanks. Therefore, the estimation of the total mass of hydrogen contained is carried out.
The total mass of hydrogen (M_T) is a fundamental parameter to take into account to describe the catastrophic phenomenon, since the chemical energy released with the combustion is a function of this parameter. To explain these steps in a more compact way, figure 3.3 and figure 3.4 show the stages of the experiment: tank filling, pressurization and burst.

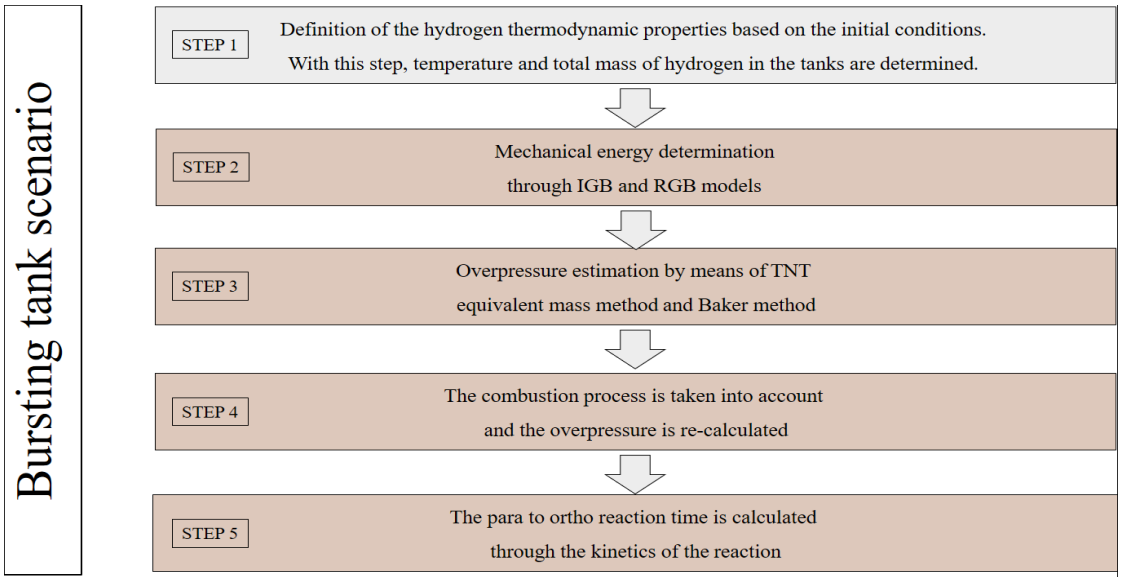

Figure 3.3: Bursting tank scenario - stages of the experiment

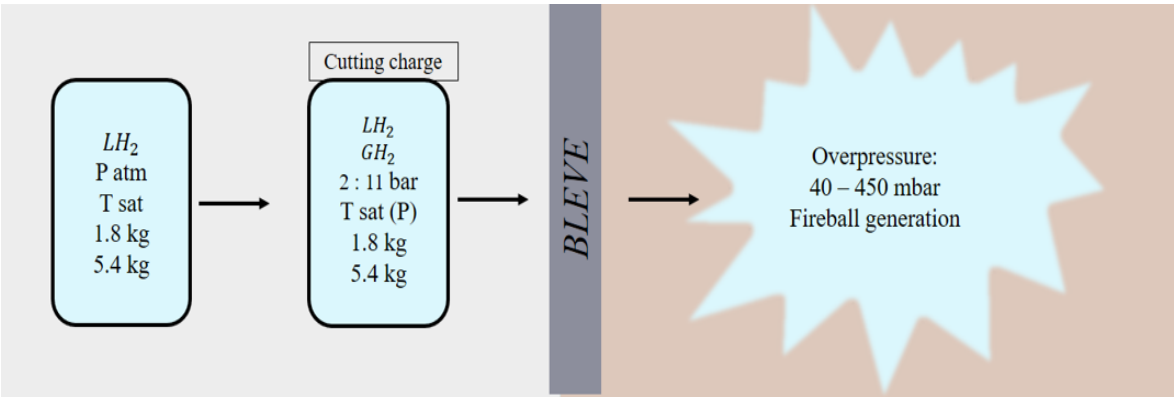

Figure 3.4: Bursting tank scenario - experiment description

Before the description of the obtained results in terms of mechanical energy, chemical energy and overpressure, it is crucial to explain the setup of the SH_2IFT Project experiment as well. After that, the description of the experiment is concluded with the next section, an extensive discussion regarding the estimations carried out by the physical models is carried out.

3.6 SH_2IFT Project Experiment

In this section, the setup of the SH_2IFT Project *BLEVE* experiment and the thermodynamic variables involved are described. It is relevant to remind that, unlike the BMW "bursting case scenario", this experiment was conducted on a fired (hot) *BLEVE*, so a liquid hydrogen tank was engulfed in propane flames to induct the explosion. The pressure release valves were forcibly closed to simulate their malfunction. Once the external fire was started, the entering heat flux caused the vaporization of part of the liquid hydrogen. The increase of the title of the gaseous phase caused the pressure inside the vessel to rise. According to the experimental data, the catastrophic rupture of the tank system happened when the pressure reached 50 bar.
After the tremendous explosion, the hydrogen immediately ignited and a fireball rose many meters above the ground, thanks to the buoyancy forces. According to the experimental data, in the moment of the explosion not all the mass of the hydrogen was under super-critical conditions. In fact, part of the cryo-fuel was still in its liquid phase.
In the blind prediction proposed by Ustolin et al. [6], the total amount of hydrogen was considered as super-critical, so a first distinction between the two analysis and the obtained results can be justified by this consideration. In the following subsection, a more detailed description of the hypothesis and the boundary conditions set to describe the experiments is proposed. Hence, it was decided to proceed in analogy with the approach adopted for the previously explained LH_2 experiments.

3.6.1 Setup and hypothesis

To conduct the experiment on the *Boiling Liquid Expanding Vapor Explosion* simulated accident, the necessary liquid para-hydrogen was transported in loco with a truck. The hydrogen was stored as a saturated liquid at ambient pressure, so its temperature was around 20 K [3]. From the truck, the cryogenic liquid was used to fill the tank system object of the experiment. To do so, part of the hydrogen was vaporized, thus rising the pressure of the system. Once a value of 9.5 bar was reached, the valve between the container on the truck and the double-walled vessel was opened. In this way, it was possible to fill the vessel without the help of a cryogenic pump, since the pressure difference was enough to push the LH_2 inside the insulated tank. To describe the thermodynamic conditions of the fluid, some assumption regarding the thermophysical variables are needed:

- The liquid phase is considered as saturated liquid at ambient pressure;

- The vapor phase is considered as saturated vapor at 9.5 bar;
- The temperature of both the vapor and the liquid phase is therefore unambiguously determined;
- The density of both the vapor and the liquid phase is therefore unambiguously determined;

Other important parameters necessary to describe the two phases are the total mass contained in the vessel and its volume:

- Total mass in the vessel: $M_T = 25\,kg$;
- Total volume of the vessel: $V_T = 1\,m^3$;

Having set the aforementioned variables, it is possible to determine the mass of the liquid and the vapor phase through an iterative process. This process is explained as follows:

1) a "first try" liquid mass is set:

$$liquid\,mass = M_l^{ft}\,[kg]$$

2) Through the known density of the liquid phase (ρ_l), it is possible to determine its volume:

$$liquid\,volume = V_l^{ft} = \frac{M_l^{ft}}{\rho_l}\,[m^3]$$

3) Using the total volume of the vessel, the determination of the volume of the vapor can be done phase by subtraction:

$$vapor\,volume = V_v^{ft} = V_T - V_l^{ft}\,[m^3]$$

4) Through the known density of the vapor phase (ρ_v), the "first try" mass of the vapor is therefore defined:

$$vapor\,mass = M_v^{ft} = V_l^{ft} \cdot \rho_v\,[kg]$$

5) A "second try" value of liquid mass is defined by subtraction, using the total mass of hydrogen in the vessel:

$$liquid\,mass = M_l^{st} = M_T - M_v^{ft}\,[kg]$$

6) the iterative process is repeated until the difference between the values of M_l^{ft} and M_l^{st} is under the 0.01 %. To do so, an "error variable" is set:

$err = |M_l^{ft} - M_l^{st}|$

At the end of the process, all the necessary thermophysical variables are known. To sum up, the liquid phase is considered as a subcooled liquid, since its temperature is around 20 kelvin at 9.5 bar. The mass of the liquid phase, its density and volume are unambiguously determined. The vapor phase is considered as saturated vapor at 9.5 bar, its mass is determined by difference and its density and volume are calculated.

At this point in the experiment, the external fire was started and the double-walled vessel was engulfed in propane flames. As previously mentioned, the pressure inside the vessel reached 50 bar at moment of the explosion and, according to the experimental data, part of the hydrogen was still in liquid phase when the *BLEVE* was generated. The temperature of this phase was therefore under the critical point ($T_c = 32.8\,K$ [3]).
The exact values of temperature of the liquid phase and its mass at the moment of the explosion are currently unknown, so it was decided to conduct a parametric analysis of the mechanical energy of the explosion by considering temperature and mass of the liquid phase as independent variables. As explained above, the models implemented to calculate the mechanical energy (both ideal and real gas behavior models) show a relevant dependency from the two variables, which underlines their importance and their role in the cryogenic fuel expansion process.

The temperature of the liquid phase is considered to range between the boiling temperature at atmospheric pressure (T_b), which is also the value considered before the fire was started, and the critical temperature (T_c), which is the highest possible temperature that LH_2 can reach remaining in its liquid phase above the critic pressure.
The mass of the liquid phase is considered to range between the value calculated before starting the propane burners (at 9.5 bar) and a value of zero kg. In the latter case, the total mass of the liquid fuel is therefore considered as super-critical (with its temperature defined by pressure and density), thus resulting in a similar scenario to the one proposed by Ustolin et al. in their blind prediction [6]. To sum up, before the explosion the liquid temperature is considered to range between T_b and T_c while the liquid mass between 0 and its initial value. As it will be shown in the following chapter, the combination of these two variables has a crucial role in the estimation of the mechanical energy of the explosions.
In figure 3.5 and 3.6, a flow-chart describing all the aforementioned hypothesis and the experiment steps is shown. As illustrated in both figure 3.3 and figure 3.5, the aftermath of the explosion is described through the implementation of both ideal and real gas behavior models, with the purpose to estimate the mechanical energy of the *BLEVEs*.
As explained in the previous sections, once the mechanical energy is simulated, the overpressure generated by the shock-wave is analysed through the TNT equivalent mass method and the Baker method. Hence, a first comparison with the experimental data is carried out.

It may be relevant to remind that a second comparison between the calculated overpressure and the experimental data is proposed after taking into account the energy of the combustion process, following the method proposed by Molkov et al. in 2015 [11]. Figure 3.3 and 3.5 also show another step, which consists in the determination of the reaction time required by the complete transition of the para-hydrogen stored in the vessels to reach the normal concentration of ortho-hydrogen (normal-hydrogen composition: 25% para-hydrogen - 75% ortho-hydrogen at ambient temperature and pressure [4]). Doing so, a comparison between these results and the typical duration of this kind of mechanical explosions is possible, thus allowing a further discussion on the involvement of the para-to-ortho transition on *BLEVEs* shock-wave. All the considerations concerning the reaction involvement in the shock-wave generation are collected in the following chapter.

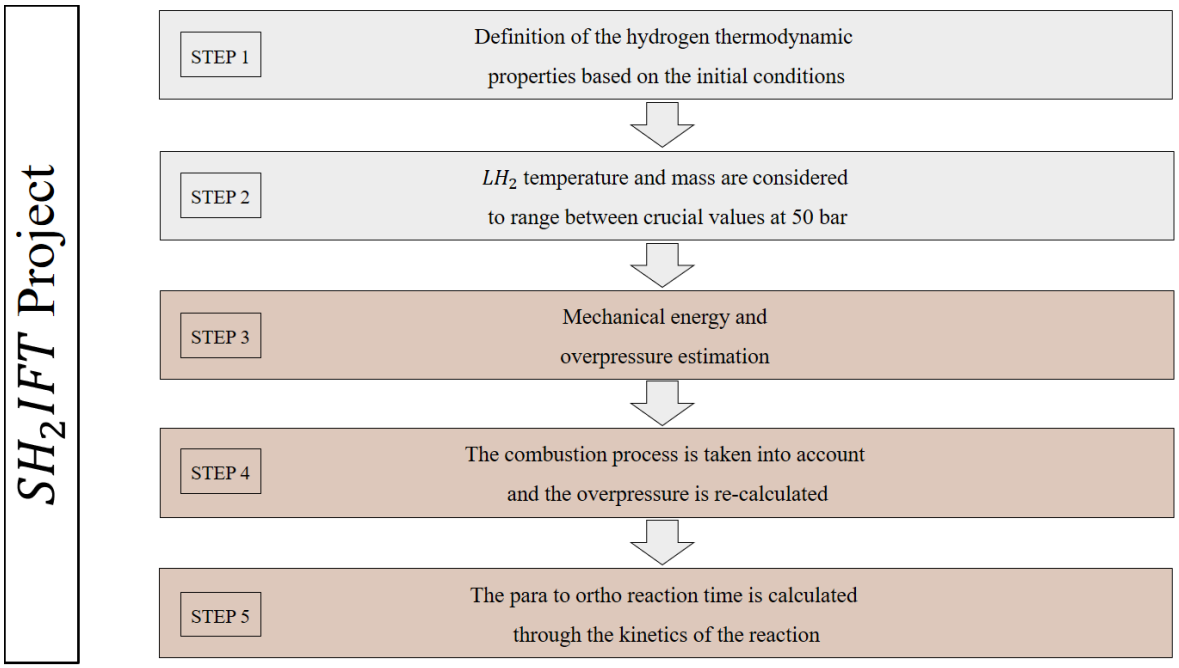

Figure 3.5: SH_2IFT Project - steps made to analyse the experimental data

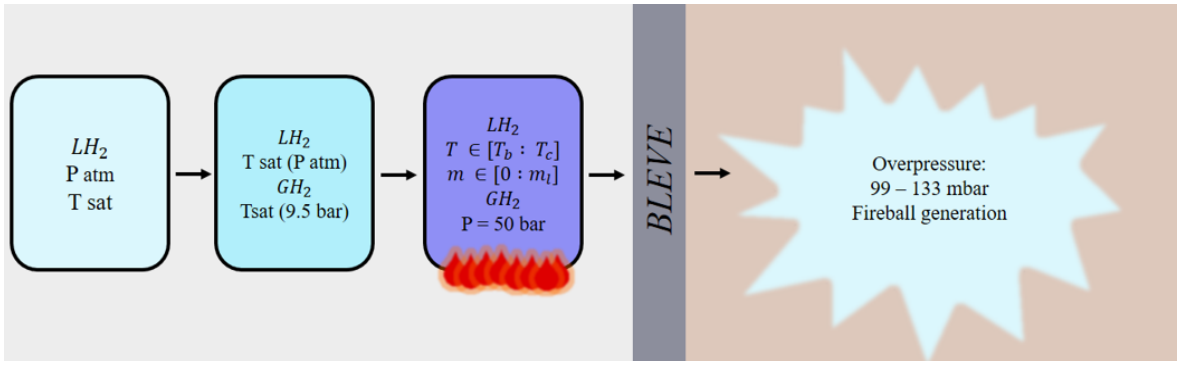

Figure 3.6: SH_2IFT Project - experiment description

Chapter 4

Results and discussion

This chapter focuses on the analysis of the results obtained with the models discussed in the previous paragraphs. The results obtained modeling the "Bursting tank scenario" experiments and the SH_2IFT Project one are discussed in their dedicated sections. As previously mentioned, the estimation of the mechanical energy and the generated overpressure are reported in analogy with the work proposed by Ustolin et al. [6]. The role of hydrogen combustion process is discussed in this chapter through the analysis of the obtained results. The para-isomer to ortho-isomer transition is also analysed through the estimations obtained with the implemented models. Finally, a comparative description of the experimental data is carried out.

4.1 "Bursting tank scenario": discussion of the results

This section is dedicated to the analysis of the results obtained for the "Bursting tests scenario" experiments conducted by BMW [5]. As explained previously, the mechanical energy of the *BLEVEs* is estimated through "ideal gas behavior" and "real gas behavior" models. The obtained results are collected in the following subsection. Hence, the data obtained taking into account the combustion process are discussed in subsection (4.1.2). Before presenting the results, it is important to remind that the 8 analysed BMW experiments can be divided in two different categories. These categories are based on the liquid mass of hydrogen in the exploding tanks at the beginning of the experiments. This aspect is highlighted in the following table.

Table 4.1: Total mass in the "Bursting tank scenario" vessels at different pressures

Tank pressure $[bar]$	2	3	4	5	6	7	8	9	10	11
$LH_2\ mass:\ 1.8\,kg$	2.03	2.13	2.24	2.35	2.46	2.58	2.71	2.84	2.99	3.17
$LH_2\ mass:\ 5.4\,kg$	5.50	5.53	5.56	5.59	5.60	5.61	5.61	5.60	5.56	5.47

As shown in table 4.1, the total hydrogen mass (liquid + vapor) inside the exploding tanks is a function of the pressure of the tanks and the initial liquid mass (1.8 and 5.4 kg). This dependence is a consequence of the method considered to fill the tanks. In fact, it is assumed that the vessels were initially filled with liquid hydrogen and then the pressure was raised injecting gaseous hydrogen inside. In this way, it was possible to analyse the results for different pressure levels keeping constant the mass of the liquid phase inside. More precisely, the total hydrogen mass also depends by the initial filling of the liquid phase. The following graphics highlights this aspect:

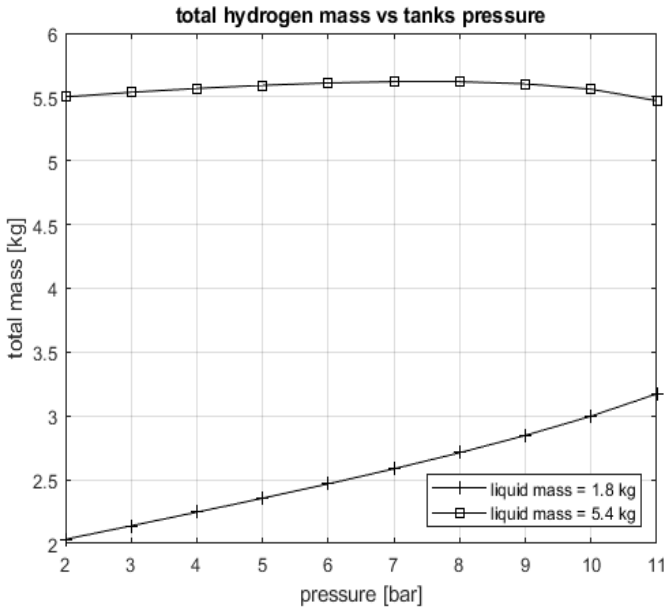

Figure 4.1: Total hydrogen mass vs tank pressure

It is interesting to point out that in the case of a filling with 1.8 kg of LH_2, the total mass in almost directly proportional to the tank pressure. In the case of a filling of 5.4 kg of LH_2 this aspect is different: the total mass of hydrogen is in fact almost constant, with a maximum around a pressure of 7 bar. To understand this behavior it is necessary to remind that the liquid phase is considered as saturated liquid at the pressure inside the vessel. This means that the specific volume of the liquid phase increases with the pressure. Being the volume of tanks a constant ($V_T = 0.12m^3$), it means that the vapor phase has less available volume when the pressure increases. Hence, in the case of an initial filling of 5.4 kg of LH_2, the vapor phase mass necessary to reach the target pressure is lesser the higher the target pressure. This consideration explains the behavior of the total hydrogen mass in the case of a liquid mass equal to 5.4 kg of LH_2. Once the total mass of hydrogen is determined, it is possible to proceed with the analysis of the mechanical energy of the explosion, as shown in the following subsection.

4.1.1 Mechanical energy estimation

The mechanical energy of the explosion is calculated, as mentioned above, through several physical models. It is relevant to underline that the obtained results are divided according to the initial filling of liquid mass. The following charts show the estimations in function of the pressure inside the vessels. The "ideal gas behavior" models are identified with the red color, while the black color is used for the "real gas behavior" models.

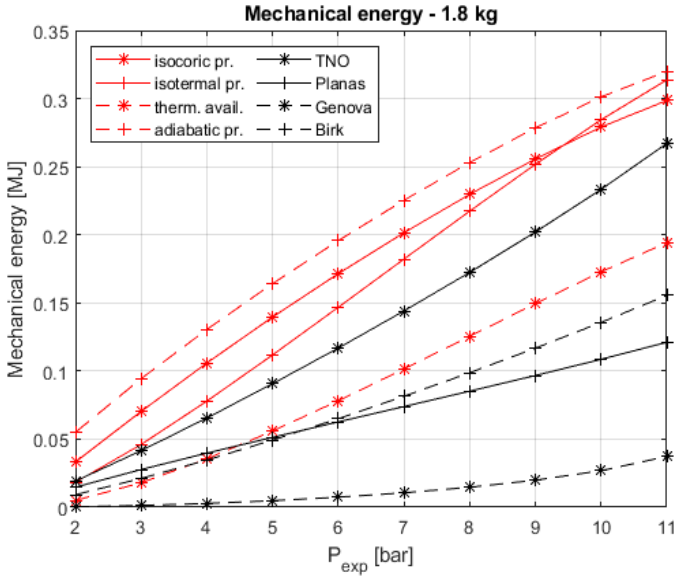

Figure 4.2: Bursting tank scenario: Mechanical energy

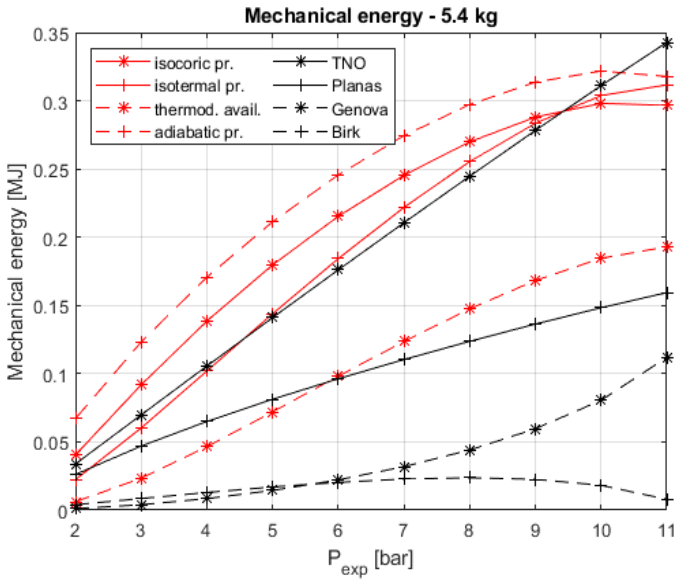

Figure 4.3: Bursting tank scenario: Mechanical energy

Figure 4.2 shows the mechanical energy of the *BLEVEs* in function of the pressure inside the

vessels for a 1.8 kg LH_2 filling. It can be noted how the "ideal gas behavior (IGB)" models tend to be more conservative with respect to the "real gas behavior (RGB)" ones. The most conservative result is obtained considering the adiabatic process proposed by Prugh [50]. It is also possible to note how all the models estimate the energy as monotonically increasing with the pressure in the tanks. This fact is not found in the case of a 5.4 LH_2 filling (figure 4.3). In fact, both the IGB and the RGB models proved a different behavior of the estimated energy when the pressure rises. Each IGB model shows a *plateau* in proximity of the critical pressure. The RBG models provide complete different estimations of the mechanical energy: there is in fact a 0.3 MJ gap between the TNO and the Birk models at 11 bar.

It may be interesting to point out that the most conservative model is the TNO, which predicts a maximum energy of almost 0.35 MJ in the case of 5.4 kg of liquid hydrogen at 11 bar. The obtained results agree with the estimations of Ustolin et al. in their previous work [6].
Once the mechanical energy of the "Bursting tank scenario" *BLEVEs* is defined, it is possible to proceed with the analysis of the pressure generated by the shock-wave. Hence, the overpressure prediction is accomplished to validate the implemented models, since the experimental data are pressure measurements probed at 3 meters from the centre of the *BLEVEs*.

4.1.2 Overpressure and impulse analysis

As mentioned in the previous chapters, the pressure wave generated by the *BLEVEs* is described through the TNT equivalent mass and the Baker method. More precisely, the overpressure which follows the explosion is estimated through the two methods, while the impulse is estimated with the TNT equivalent mass one. For the sake of simplicity, it was decided to show the results of one IGB and one RGB model. In particular, the following charts show the TNO and the isothermal models results obtained applying the TNT equivalent mass method. Furthermore, the overpressure and the impulse are calculated for a pressure of 11 bar at 3 meters from the explosion.

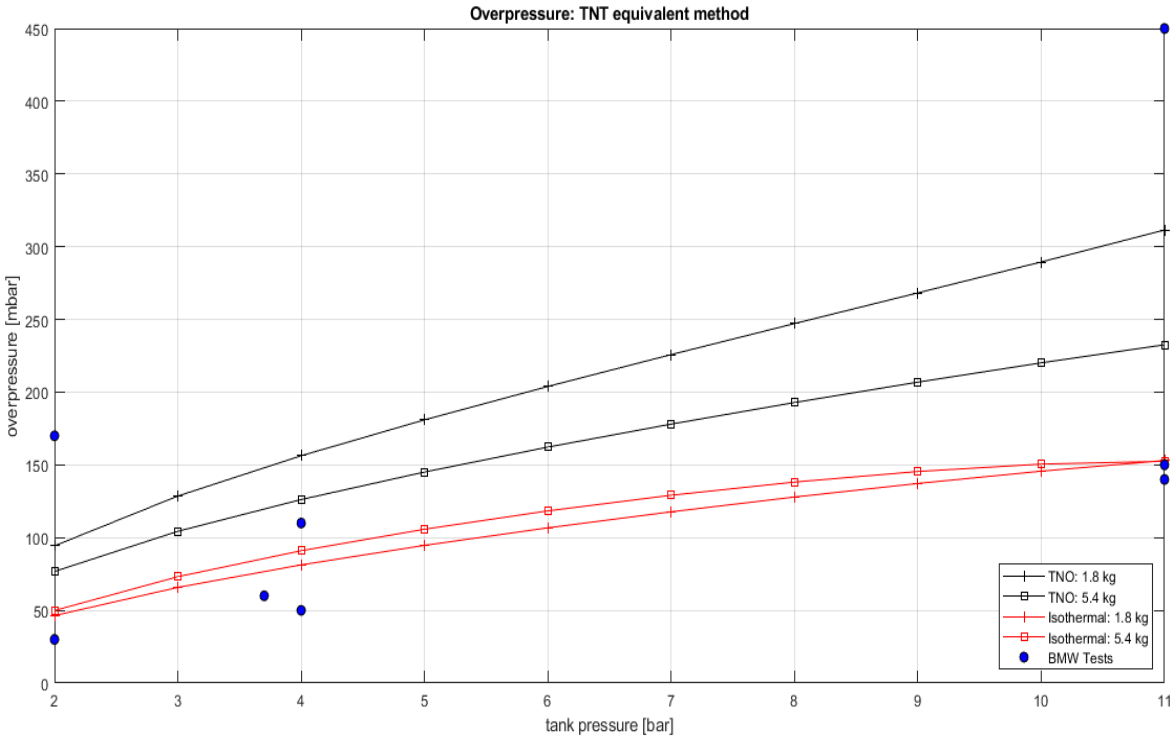

Figure 4.4: Overpressure: calculations vs experimental data

The blue dots in figure 4.4 represent the experimental data of the eight analysed "Bursting tank scenario" *BLEVEs*. The red and the black lines show the estimations of respectively the isothermal model (IGB) and the TNO one (RGB).
It appears clear the maximum measured overpressure (450 mbar at 11 bar) is well above the estimations. Nevertheless, 6 out of 8 experiments resulted in an overpressure measurement within or under the expectations of the models.
It is also relevant to show the results for distances above 3 meters. There are no experimental data available for these distances, but it is important to show the effect of distance on the overpressure. In fact, this correlation is useful to define a safety distance from the explosion. More precisely, figure 4.5 shows the effect of distance and tank pressure on the estimated overpressure:

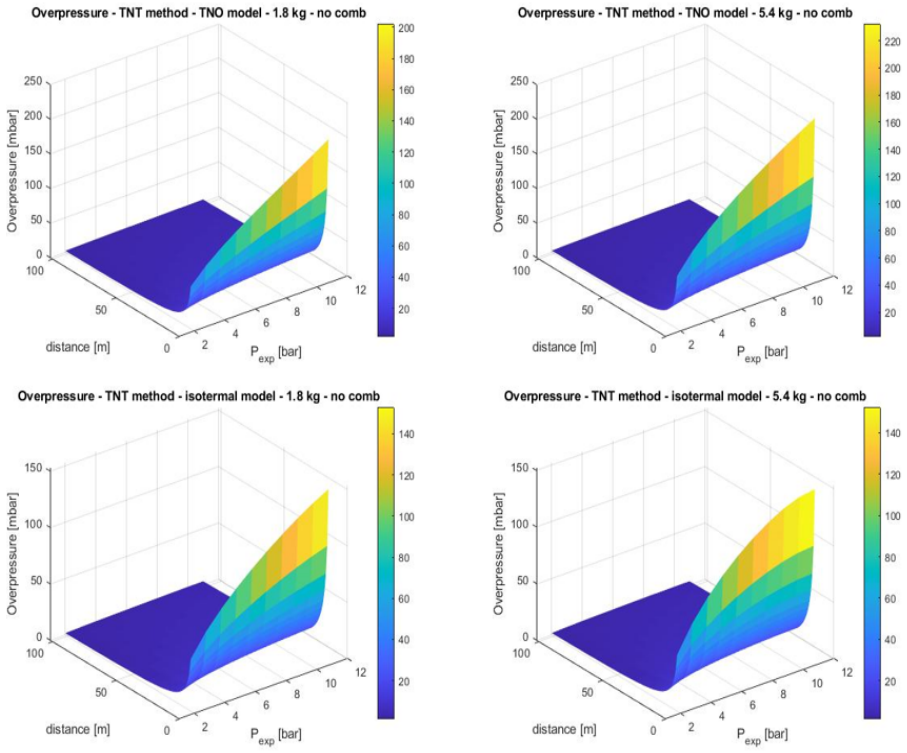

Figure 4.5: Overpressure: the effect of distance and tank pressure

Figure 4.5 collects the overpressure estimations for the above mentioned cases through the TNT equivalent mass method. The results are similar: the maximum pressure is obtained for a combination of distance and pressure of 3 meters and 11 bar. The effect of the liquid mass is different if considering an ideal or real gas behavior. The isothermal model provides the same overpressure values at 11 bar for both the LH_2 fillings (1.8 and 5.4 kg). In fact, it estimates 153 mbar in both of the cases.
Unlike the isothermal model, the TNO model foresees around 30 mbar gap between the two fillings at 11 bar (respectively 202 mbar and 233 mbar for 1.8 kg and 5.4 kg of LH_2). The exact values are reported in tables 4.2 and 4.3, which also collect the estimations achieved with the Baker method.

Table 4.2: Overpressure results with TNO and Isothermal models by considering only the mechanical energy generated by the physical explosion. LH_2 mass in the tanks: 1.8 kg. (Abbrevations: RGB real gas behavior, IGB = ideal gas behavior)

Pressure [bar]	Overpressure at 3 m from the explosion [mbar]				
	TNT Method		Baker Method		Exp data
	RGB - TNO	IGB - Isothermal	RGB - TNO	IGB - Isothermal	
2	61	47	46	51	30 - 170
4	102	81	71	91	50 - 110
11	202	153	91	152	150 - 450

Table 4.3: Overpressure results with TNO and Isothermal models by considering only the mechanical energy generated by the physical explosion. LH_2 mass in the tanks: 5.4 kg. (Abbrevations: RGB real gas behavior, IGB = ideal gas behavior)

Pressure [bar]	Overpressure at 3 m from the explosion [mbar]				
	TNT Method		Baker Method		Exp data
	RGB - TNO	IGB - Isothermal	RGB - TNO	IGB - Isothermal	
2	77	50	61	61	30 - 170
4	126	91	91	112	50 - 110
11	233	153	152	152	150 - 450

The tables above also show a general accordance between the Baker and the TNT method. As indicated in tables 4.2 and 4.3, up to this point only the mechanical energy of the *BLEVEs* is considered to estimate overpressure and impulse. The following charts show the impulse estimation obtained with the TNT equivalent mass method, for each analysed model and at different distances from the explosion centre.

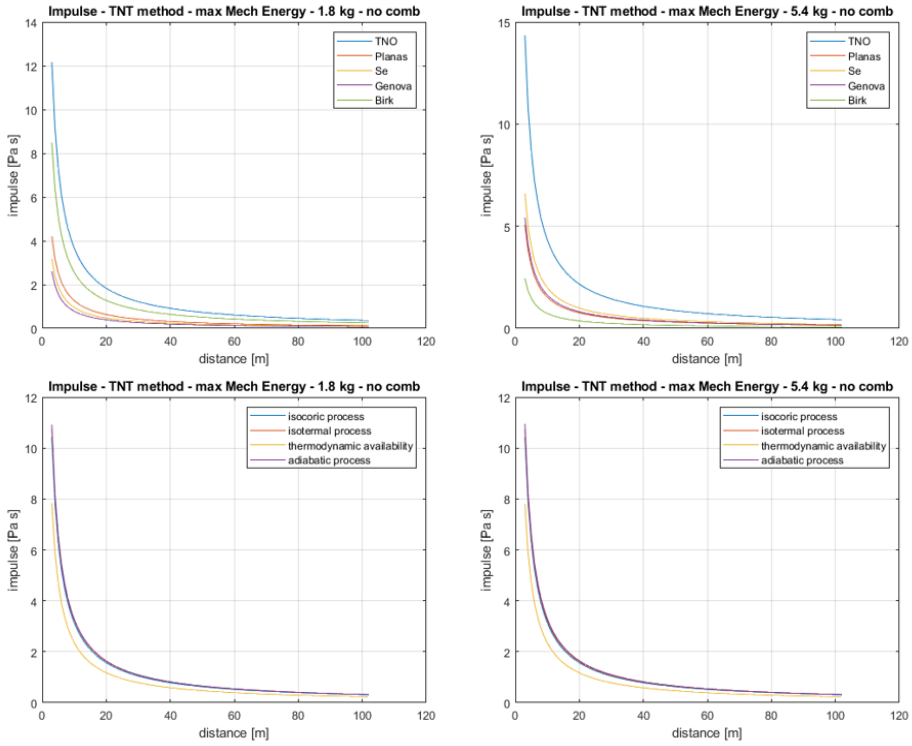

Figure 4.6: Estimated impulse at different distances from the *BLEVEs*

According to figure 4.6, the TNO model provides the most conservative results. Regarding the "ideal gas behavior" models, the adiabatic, isocoric and isothermal models provide close estimations of the generated impulse. In the following subsection (4.1.3), the results obtained considering the combustion process are collected. The estimated overpressure is once again confronted with the experimental data.

4.1.3 Combustion process results

The estimations obtained by adding the combustion process to the models to calculate the overpressure generated by the shock-wave resulted in a general overestimation of the experimental data. Nevertheless, a good agreement is found between the prediction obtained with the TNO model and the maximum shock-wave overpressure (450 mbar) measured in one of the BMW tests. This agreement may indicate that the combustion process takes part to the generation of the shock-wave. It is possible to notice the overpressure predictions considering hydrogen combustion in the following chart:

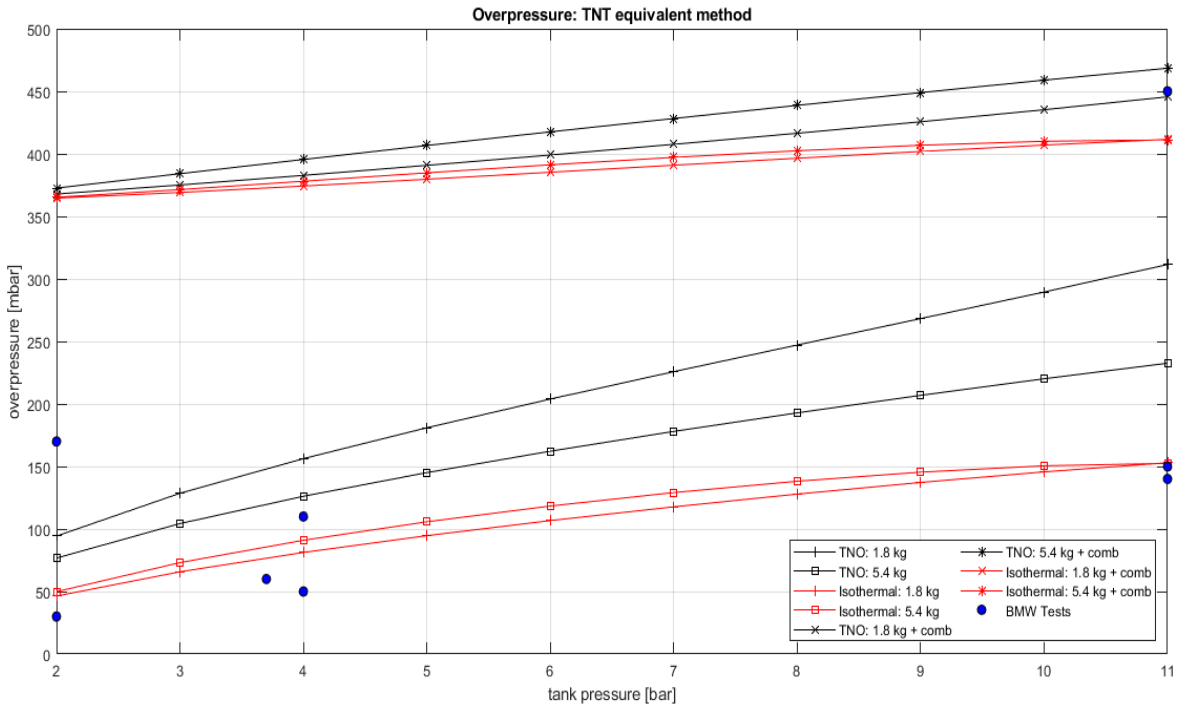

Figure 4.7: Overpressure estimations considering combustion vs experimental data

Figure 4.7 compares the results obtained considering only the mechanical energy (as already depicted in figure 4.4) with the results obtained adding the combustion energy. It is relevant to remind that the TNT equivalent mass method usually provides conservative estimations if applied close to the explosion source - i.e., the *near field*. As explained in section 3.2.1, the parameter used to determine *far field* and *near field* is the Sachs scaled distance. When only the mechanical energy is considered, the Sachs scaled distance defined for each model suggests that the distance from the *BLEVE* where the TNT method is applied is close to the *far field*. When adding the combustion energy, the Sachs scaled distance always identifies the distance where the overpressure is probed as *near field*. It may be speculated that in the latter case the TNT equivalent mass method might provide extremely conservative estimations. This consideration may be applied to 7 out of the 8 investigated experiments, while the maximum measured overpressure (450 mbar at 11 bar and probed at 3 meters) is well within the estimations of the models when combustion is considered.
Table 4.4 shows the Sachs scaled distances calculated with and without the energy of hydrogen combustion, in the case of a tank pressure equal to 11 bar.

Table 4.4: Sachs scaled distances

Sachs scaled distances [-]			
Mechanical energy only			
LH_2 mass: 1.8 kg		LH_2 mass: 5.4 kg	
RGB - TNO	IGB - Isothermal	RGB - TNO	IGB - Isothermal
1.72	2.05	1.58	2.06
Mechanical energy + Chemical energy			
LH_2 mass: 1.8 kg		LH_2 mass: 5.4 kg	
RGB - TNO	IGB - Isothermal	RGB - TNO	IGB - Isothermal
1.23	1.23	1.22	1.16

As shown in table 4.4, if the combustion process is neglected, the Sachs scaled distance if above 1.5. When considering the combustion process this value drops under 1.3. Therefore, it is crucial to compare these results with the estimations obtained with the Baker method when combustion is considered, as shown in the following tables:

Table 4.5: Overpressure results with TNO and Isothermal models by considering both mechanical and chemical (combustion) energy generated by the explosion. (Abbrevations: RGB real gas behavior, IGB = ideal gas behavior)

Pressure [*bar*]	Overpressure at 3 m from the explosion [mbar] - LH_2 mass: 1.8 kg				
	TNT Method		Baker method		Exp data
	RGB - TNO	IGB - Isothermal	RGB - TNO	IGB - Isothermal	
2	368	365	213	203	30 - 170
4	383	374	223	203	50 - 110
11	446	412	403	404	150 - 450

Table 4.6: Overpressure results with TNO and Isothermal models by considering both mechanical and chemical (combustion) energy generated by the explosion. (Abbrevations: RGB real gas behavior, IGB = ideal gas behavior)

Pressure [bar]	Overpressure at 3 m from the explosion [mbar] - LH_2 mass: 5.4 kg				
	TNT Method		Baker method		Exp data
	RGB - TNO	IGB - Isothermal	RGB - TNO	IGB - Isothermal	
2	373	365	223	203	30 - 170
4	396	378	273	203	50 - 110
11	468	411	405	405	150 - 450

The data collected in table 4.5 and 4.6 indicate a better agreement between the estimations of the Baker method and the TNT equivalent mass one at 11 bar. In particular, the results obtained with the TNO model at 11 bar are good predictions of the experimental data for both the implemented methods.
The role of combustion was taken into account to describe primarily the overpressure generated by the *BLEVEs* shock-waves. The analysis of the "Bursting tank scenario" has shown a good agreement with the experimental data for one explosion at 11 bar. In the other cases, a general over-prediction was obtained. Section 4.2 is dedicated to the analysis of the results obtained for the SH_2IFT Project *BLEVE*. The same approach, in terms of mechanical energy and combustion process, is adopted. Hence, a confrontation between the experimental data and the expectations is provided in analogy with the "Bursting tank scenario" experiments.

4.2 SH_2IFT Project: discussion of the results

The first step of the discussion of the SH_2IFT Project experiment, as explained in the previous chapter, consists in the parametric analysis of the mechanical energy of the *BLEVE*. Then, the combustion process is taken into account with the same assumptions of the BMW experiments. Finally, the para to ortho transition is discussed: the obtained results in terms of reaction time and energy absorption are collected in their dedicated subsection.

4.2.1 Mechanical energy estimation

The parametric variables on which the analysis is based are the temperature of the liquid phase and the LH_2 mass at the moment of the explosion. The isothermal model proved once again to be the most conservative one. So, it is relevant to show the estimation of the mechanical energy using this model, in function of LH_2 temperature and mass.

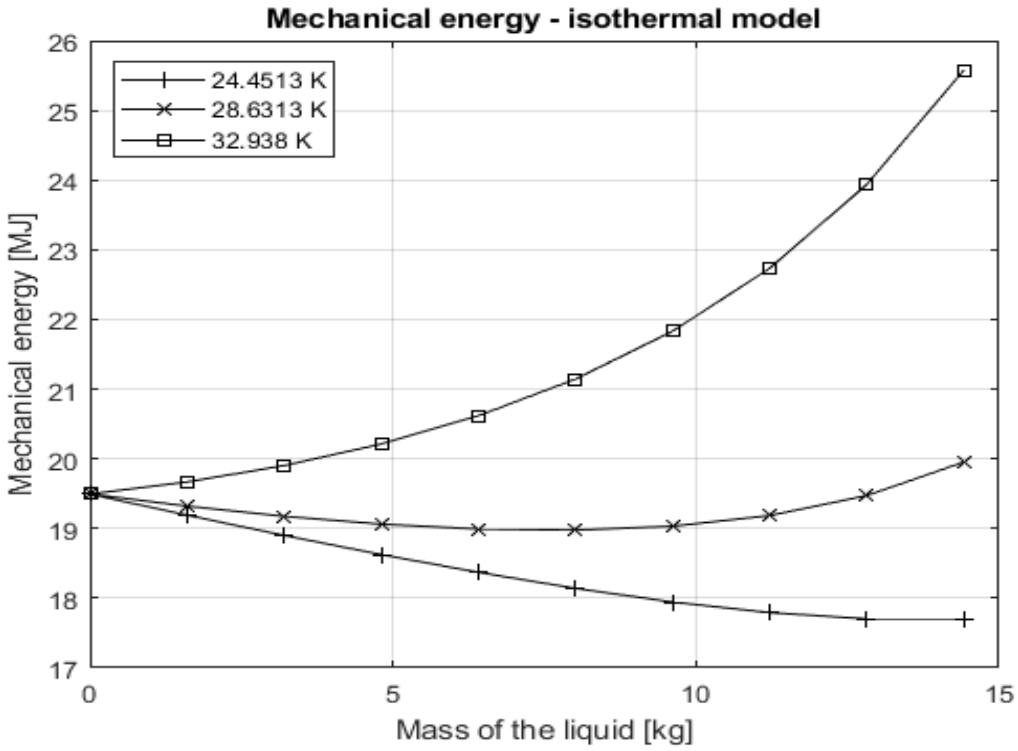

Figure 4.8: Mechanical energy: parametric analysis considering ideal gas behavior

Figure 4.8 shows the dependency of the mechanical energy from the liquid mass and the LH_2 temperature. It is interesting to note the great energy difference at different temperatures when the mass of the liquid phase increases. As mentioned above, the exact values of mass and temperature are unknown. According with the experimental data, there was still liquid inside the vessel at the moment of the explosion. If the liquid mass remains constant and equal to its initial value (almost 15 kg) the yield of the explosion is maximized if its temperature is near the critic temperature. It is not unreasonable to consider the temperature of the liquid phase to increase during the experiment, since the external propane flames provide a significant heat flux. Moreover, another consequence of the external fire was the reduction of the efficiency of the insulating layer. Nevertheless, the double-walled vessel proved to be extremely efficient in insulating the internal fluid even if the vacuum between the external and the internal layers was lost before the explosion. Therefore, more experimental data are required to be able to provide a better estimation of the mechanical energy liberated after the *BLEVE*.

It is relevant to underline that the difference between the estimated energy in figure 4.8 at different temperatures can be explained considering its dependency from the parameter f ($flashing\,fraction$). This coefficient identifies the fraction of the liquid phase which flashes in the moment of the explosion and it is a function of the difference between the LH_2 temperature inside the vessel and the LH_2 boiling temperature (at atmospheric pressure). This difference is maximized in the case of $T_{LH_2} = T_c$, which explains the maximum estimated

energy of almost 26 MJ.

As it concerns the mechanical energy estimation carried out with RGB models, the TNO model proved once again to be the most conservative one. In particular, if the total mass inside the vessel is considered to be in vapor phase, the TNO and the Birk models coincide. As mentioned above, there was still liquid hydrogen inside the vessel at the moment of the explosion, and the TNO model takes into account the energy of the liquid phase along with the vapor. Hence, it provided the most conservative estimations, which are collected in figure 4.9.

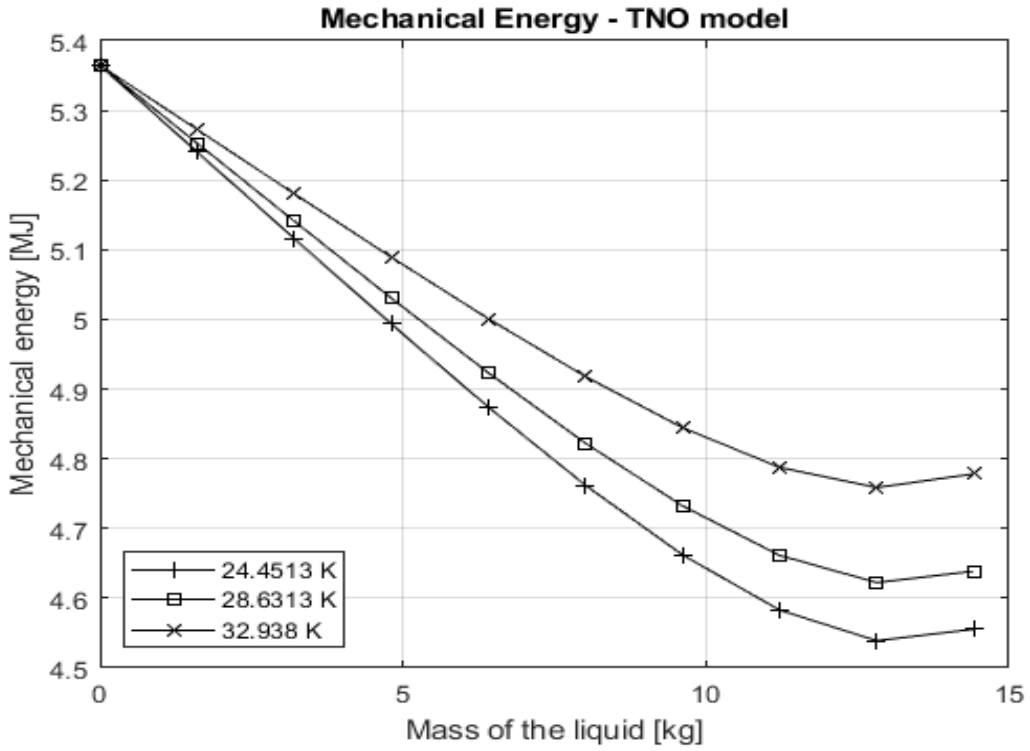

Figure 4.9: Mechanical energy: parametric analysis considering real gas behavior

Figure 4.9 shows the mechanical energy in function of LH_2 mass and temperature. It can be noted that an opposite behavior is obtained with respect to the IGB estimations (figure 4.8). If the LH_2 mass increases, the estimated energy decreases. Given the boundary condition and being the tank volume constant ($V_T = 1m^3$), if the mass of the liquid increases, the mass, and therefore the volume, of the vapor phase decreases. Hence, more liquid in the vessel means less vapor able to expand when the vessel bursts. As per the TNO model definition, the specific internal energy of the vapor phase, along with the specific internal energy of the liquid phase, is a crucial parameter to define the yield of the explosion.
It is fundamental to notice that, despite the enormous difference in terms of mechanical energy between the IGB and RGB models, the calculated overpressure is not fully affected by this

gap. In fact, the TNO model takes into account the reflection of the shock-wave on the ground through the coefficient $\alpha = 2$, which is neglected in the IGB models. The consequences of this consideration and the calculated ovepressure are collected in the following subsection (4.2.2), along with a comparison with the experimental data.

4.2.2 Overpressure and impulse analysis

To estimate the overpressure and the impulse of the *BLEVE*, it was decided to consider the maximum mechanical energy calculated for each model. Doing so, the estimations are the most conservative for each model. In figure 4.10, the overpressure calculated with the TNT equivalent mass method considering the maximum mechanical energy is proposed. Then, the overpressure is also calculated with the Baker method.

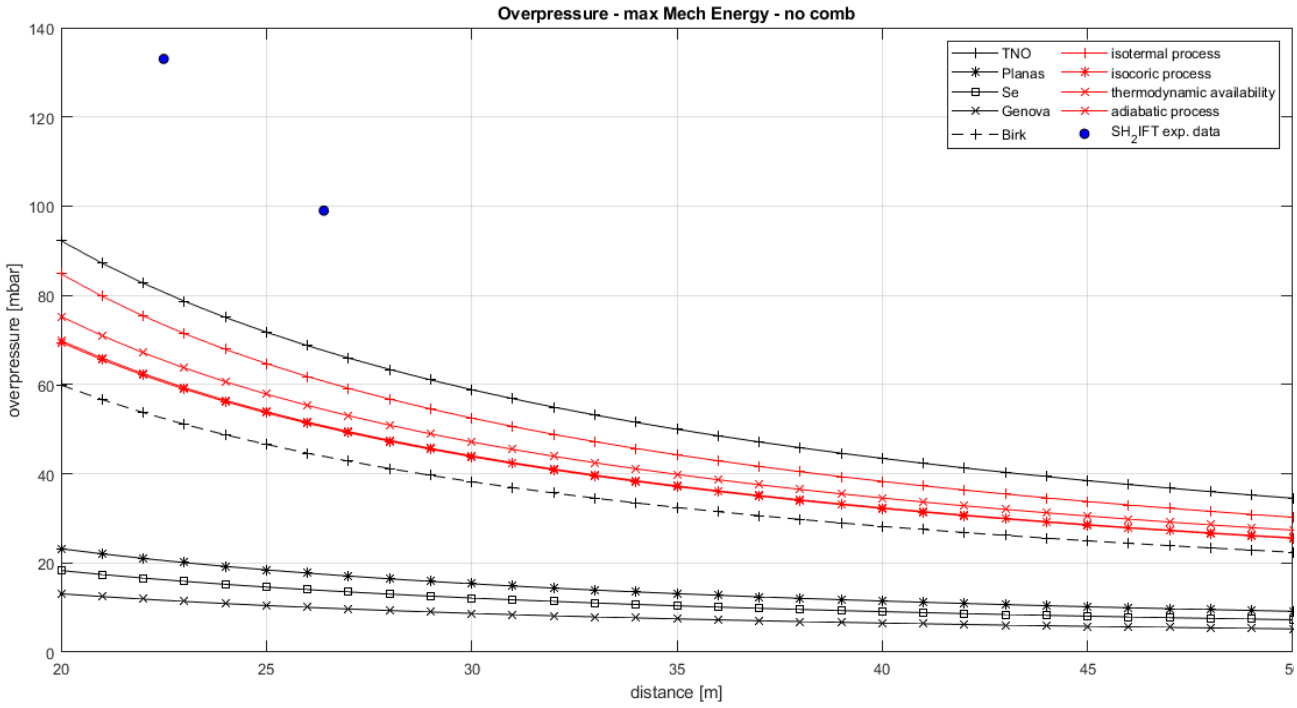

Figure 4.10: Overpressure estimations vs experimental data

Figure 4.10 shows that the maximum estimated overpressure calculated with each model at different distances. It can be noted how the estimations are far below the experimental data (blue dots), even with the most conservative models. The TNO and the isothermal are respectively the most conservative of the RGB and IGB models. Nevertheless, an underestimation between 50 and 60 mbar was obtained at 22.5 meters from the explosion, while a gap of around 30 mbar was found at 26.4 meters.
As previously mentioned, only the mechanical energy is considered up to this point. Table 4.7 shows the exact results obtained with the the TNT equivalent mass and the Baker method, applying them to the isothermal and the TNO models.

Table 4.7: SH_2IFT Project - Overpressure results with TNO and Isothermal models by considering only the mechanical energy generated by the physical explosion at different distances. (Abbrevations: RGB real gas behavior, IGB = ideal gas behavior, d = distance from the explosion)

d = 22.5 m	RGB - TNO	IGB -Isothermal	Exp data
TNT method	81	73	133
Baker method	51	81	133
d = 26.4 m	RGB - TNO	IGB -Isothermal	Exp data
TNT method	69	61	99
Baker method	41	56	99

As shown in table 4.7, the estimations of the overpressure do not provide a good agreement with the experimental data. In fact, both RGB and IGB models underestimate the overpressure of the explosion when the latter is calculated using both TNT equivalent mass and the Baker method to correlate the mechanical energy with the pressure of the shock-wave.
Figure 4.11 shows the difference in terms of impulse estimated with all the proposed models. As mentioned above, the impulse generated by the *BLEVE* is a crucial parameter to take into account to define if, at a given distance, people might be exposed to a certain injury risk. In fact, to estimate a safety distance from the burst, a conservative threshold can be set at 1 $Pa \cdot s$.

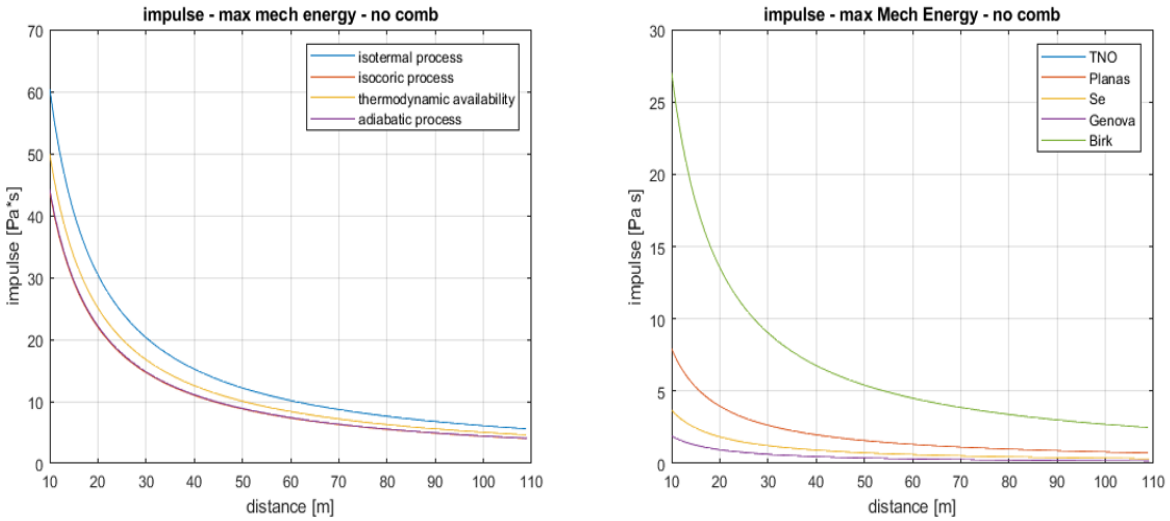

Figure 4.11: Estimated impulse: comparison between models

In figure 4.11, it is possible to notice that the isothermal model and the TNO one provide once again the most conservative estimations. It may be relevant to point out that the Birk model provide the same estimations of the TNO when considering the maximum release of mechanical energy. This is a consequence of the fact that the two models coincide if the liquid mass inside the exploding vessel is equal to zero.

In subsection 4.2.3, the combustion process is taken into account to describe overpressure and impulse of the explosion. In this way, a new comparison with the experimental data is conducted, highlighting the possible involvement of hydrogen combustion in the shock-wave generation.

4.2.3 Combustion process results

The fuel combustion is taken into account following the same procedure explained for the "bursting tank scenario" experiments. A comparison between the estimations and the experimental data is proposed in figure 4.12. The results obtained considering only the mechanical energy are reported in the same chart to highlight the resulting difference when hydrogen combustion is added to the models. For the sake of simplicity, only the most conservative models are reported. Hence, the TNO and the isothermal models estimations are collected in figure 4.12.

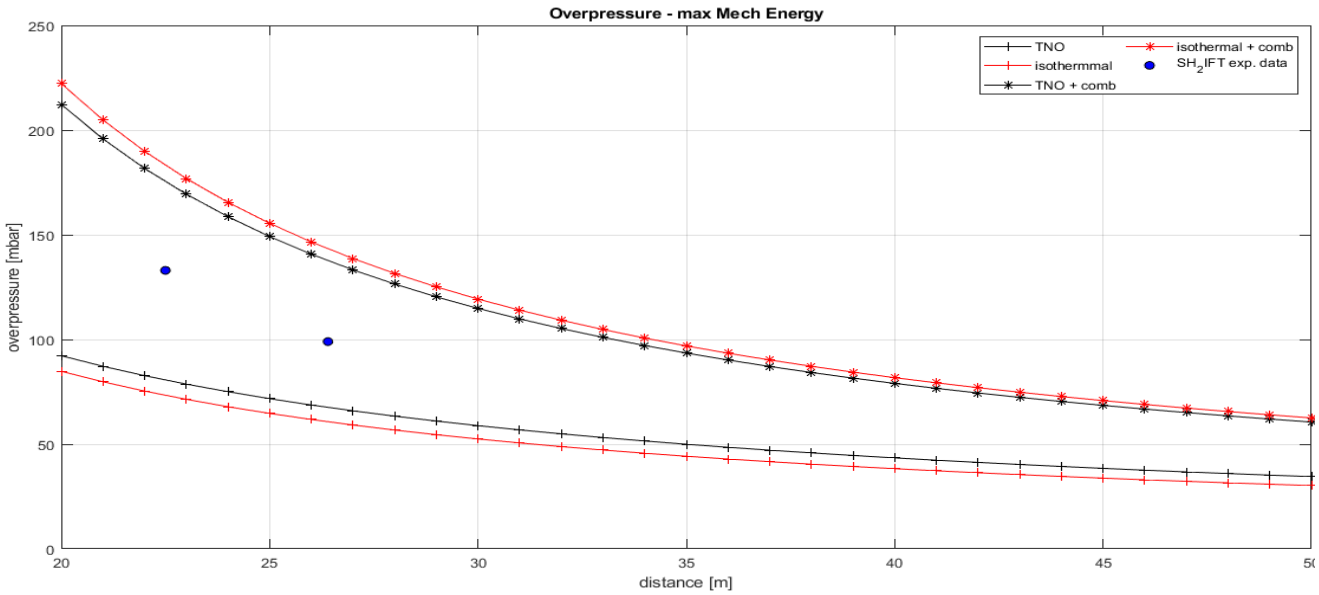

Figure 4.12: Overpressure with and without combustion at different distances by simulating the SH_2IFT Project experiment

Figure 4.12 shows a general overestimation of the experimental data when combustion is taken into account. This over-prediction was expected, since the same result was obtained for the experiments conducted by BMW for seven out of the eight analysed *BLEVEs*. It may be speculated that the coefficient β - which identifies the fraction of the hydrogen lower heat value that takes part to the shock-wave generation - needs to be tuned through more experimental observations. Furthermore, the para to ortho transition was neglected up to this point. The results obtained when considering this transition to participate in the over-pressure generation are shown in the next subsection.
It is relevant to highlight that the Sachs scaled distance is once again calculated for each case. In this way, the accuracy of the TNT equivalent mass method can be questioned if this parameter identifies the region of space in which the calculations are carried out as *near field*. Table 4.8 collects the values of the Sachs scaled distances calculated considering the different distances and the combustion process.

Table 4.8: Sachs scaled distances at different distances (Abbreviations: Mech. = Mechanical, Ch. = Chemical, En. = Energy, d = distance from the explosion)

Model	Sachs scaled distances [−] - d = 22.5 m	
	Mech. energy only	Mech. energy + Ch. En.
TNO	4.76	1.88
Isothermal	3.56	1.83
	Sachs scaled distances [−] - d = 26.4 m	
Model	Mech. energy only	Mech. energy + Ch. En.
TNO	5.58	2.21
Isothermal	4.17	2.15

Table 4.8 shows values of Sachs scaled distances minors of two at 22.5 meters from the explosion when combustion is considered. It may be speculated that this result could explain the over-estimation provided by the TNT equivalent mass method. However, an over-prediction of the results is obtained also in the *far-field* - i.e., $R_{Sachs} > 2$ - at 26.4 meters when hydrogen combustion is added to the models. Therefore, it is necessary to show the estimations obtained with the Baker method to understand if an agreement between the two methods on the generated overpressure can be found. Table 4.9 collects the overpressure estimations obtained with the Baker method in comparison to the ones provided by the TNT equivalent mass method.

Table 4.9: SH_2IFT Project - overpressure estimations considering hydrogen combustion. (Abbrevations: RGB real gas behavior, IGB = ideal gas behavior)

Method	Overpressure at 22.5 m from the explosion [mbar]		
	RGB - TNO	IGB -Isothermal	Exp data
TNT	176	183	133
Baker	172	162	133
Method	Overpressure at 26.4 m from the explosion [mbar]		
	RGB - TNO	IGB -Isothermal	Exp data
TNT	138	143	99
Baker	142	142	99

As shown in table 4.9, the TNT equivalent mass method provides more conservative estimations with respect to the Baker method at 22.5 meters from the explosion - i.e. in the *near field*. Nevertheless, a good agreement between the different calculations can be found at 22.6 m from the explosion - i.e. in the *far field*. In particular, both the methods provide an overestimation of the experimental data.
Hence, it is not unreasonable to address the over-prediction with a different phenomenon, which could be the para to ortho transition. More precisely, it may be speculated that the energy absorption associated with this chemical reaction could affect the magnitude of the shock-wave pressure. As explained in the previous chapter, the difference between the experimental data and the estimations is used to define the enthaply difference associated with the para to ortho transition. Along with the endothermic nature of the reaction, the necessary time for the reaction to occur is estimated. The obtained results are collected in the following subsection, in which an extensive discussion of the phenomenon is proposed.

4.2.4 Para to ortho transition: results

As explained above, this subsection focuses on the results obtained considering the para to ortho transition to describe the overpressure generated during the SH_2IFT Project *BLEVE*. Previously, in section 3.4 an adaptation of the TNT equivalent mass method and the Baker one was shown. This adaptation aims to take this chemical reaction into account to estimate the generated overpressure. More precisely, the gap between the experimental data and the estimations presented in table 4.9 is used to trace back the energy which could be associated with the reaction. Moreover, the estimations on the time requested by the reaction to occur are presented in this subsection.

It is critical to explain that the first step to take the para to ortho transition into account is the definition of the kinetic constants. The following table collects the estimations of the kinetic constant of the ortho to para reaction and the kinetic constant of the para to ortho reaction. As explained in the previous chapter (section 3.4), these constants are calculated in function of hydrogen temperature after the explosion. Along with the kinetic constants, table 4.9 also collects the reaction time of a "complete transition" - i.e. the time to reach a near normal-hydrogen concentration of ortho-isomer starting from a 0.2% ortho-concentration.

Table 4.10: Kinetic constants and reaction time (Abbreviations: T_{H_2} = hydrogen temperature, $\Delta\, t$ = reaction time)

$T_{H_2}\,[K]$	$k\,[10^{-3^{-1}}]$	$k'\,[10^{-3^{-1}}]$	$\Delta\, t\,[ms]$
800	23.7	57.6	650
950	21.9	55.1	630
1100	20.6	52.9	640
1250	19.4	50.9	660
1400	18.4	49.1	670
1550	17.6	47.5	690
1700	16.9	46.0	710
1850	16.3	44.7	720
2000	15.8	43.5	740
2150	15.3	42.4	760

Table 4.9 shows how a transition from a concentration of 0.2% ortho-hydrogen to 70% ortho-hydrogen can happen in around 600-700 ms. The exact reaction time is a function of the hydrogen temperature after the *BLEVE*, which is currently unknown. As explained in the previous chapter, considering the immediate ignition of the fuel inside the vessel, it is not unreasonable to set this temperature to values above the room temperature. In particular, values between 800 K and 2150 K are considered to calculate the reaction time with the empirical correlation proposed by Milenko [46].
The following step of the analysis of this transition's role into the overpressure generation is the estimation of the energy absorbed by the reaction. Following the considerations and the equations collected in the previous chapter, the enthalpy difference which can be asso-

ciated with the reaction is calculated as 330 $kJ\,kg^{-1}$. This enthalpy difference is estimated considering the specific enthalpies of para-hydrogen and ortho-hydrogen calculated with the Cool-Prop package [48]. Furthermore, this hentalphy diffierence is associated with a reaction from a 0.2% ortho-hydrogen to 75% ortho-hydrogen. Hence, is the maximum enthaply which could be absorbed to reach the equilibrium concentration at non-cryogenic temperatures. Furthermore, this value agrees with the ones found in literature [4].

As explained above, the coefficient γ identifies the fraction of this enthalpy difference which may be involved in the shock-wave generation. The following table collects the estimations of this coefficient, in function of the model used to describe the overpressure generated by the *BLEVE*.

Table 4.11: Enthaply fractions (γ) associated with the gap between experimental data and estimations (Abbreviations: d = distance from the explosion)

Method	Enthalpy fractions: γ [−] - d = 22.5 m	
	RGB - TNO	IGB -Isothermal
TNT	119%	189%
Baker	53%	60%
Method	Enthalpy fractions: γ [−] - d = 26.4 m	
	RGB - TNO	IGB -Isothermal
TNT	92%	134%
Baker	27%	71%

Table 4.11 collects the estimations of the coefficient γ. As expected, these fractions are above 100% is some cases. These cases are the most conservative overpressure estimations: the highest obtained fraction is 189% for the isothermal model at 22.5 m from the explosion using the TNT method. It is relevant to highlight that this case is identified with the smallest Sachs scaled distance: $R_{Sachs} = 1.83$. Hence, it is not unreasonable to consider this result as a consequence of the conservative results provided by the TNT equivalent mass method in the *near field* region. Furthermore, there is only one case in which γ results greater than 100% in the *far field* region: the case of the isothermal model applied at 26.4 m from the explosion using the TNT equivalent mass method. All the other cases provide γ estimations under 100%, which are results compatible with the model proposed in the previous chapter.

These enthaply fractions can be used to calculate the ortho-hydrogen concentration after the explosion. More precisely, these new final concentrations may be associated with the fraction of the enthaply gap previously calculated, therefore they may explain the gap between the experimental data and the model estimations. The following table shows the ortho-hydrogen final concentrations calculated in function of the distance from the explosion and the implemented models.

Table 4.12: $o - H_2$ concentrations associated with the gap between experimental data and estimations (Abbreviations: d = distance from the explosion)

Method	$o - H_2$ *ratio* [−] - d = 22.5 m	
	RGB - TNO	IGB - Isothermal
TNT	-	-
Baker	40%	45%
Method	$o - H_2$ *ratio* [−] - d = 26.4 m	
	RGB - TNO	IGB -Isothermal
TNT	69%	-
Baker	21%	53%

The $o - H_2$ concentrations shown in table 4.12 refer to para to ortho transitions which start at an ortho-isomer concentration equal to 0.2% and end at the indicated final percentage. It can be noted how these results indicate $o - H_2$ concentrations under the equilibrium concentration in normal-hydrogen - i.e. 75% $o - H_2$ in hydrogen at normal conditions. Table 4.10 shows the reaction time necessary to reach an almost normal-hydrogen concentration of the para-hydrogen (precisely 70%). Therefore, it is reasonable to expect a lower reaction time to reach the concentrations indicated in the table above. Hence, this new reaction time is estimated following the model explained in the previous chapter and collected in the following table.

Table 4.13: Reaction time to reach specific concentrations of $o - H_2$ in function of hydrogen temperature (Abbreviations: T_{H_2} = hydrogen temperature, c_{o-H_2} = ortho-idrogen final concentration, $\Delta\, t$ = reaction time)

$T_{H_2}\,[K]$	$c_{o-H_2} = 40\%$	$c_{o-H_2} = 45\%$	$c_{o-H_2} = 69\%$	$c_{o-H_2} = 21\%$	$c_{o-H_2} = 53\%$
800	380	400	597	310	437
950	400	418	603	324	455
1100	415	439	616	338	473
1250	431	451	632	351	491
1400	446	467	649	363	508
1550	461	482	667	376	524
1700	475	497	684	387	540
1850	489	512	701	399	556
2000	503	527	718	410	571
2150	515	540	735	420	585

As shown in the table above, the minimum estimated reaction time in function of the hydrogen temperature after the explosion is 310 ms. This time is the minimum time during which a para to ortho transition could take place and justify an energy absorption that may explain the difference between the estimated overpressure and the experimental data. It should be noted that this time is around one order of magnitude greater than the estimated duration of the *BLEVE*. In fact, the mechanical explosion lasted around 30 - 40 ms according with the experimental data. Hence, it is not clear how the chemical transition may affect the overpressure generation. This discrepancy could suggest that the para to ortho transition does not affect the shock-wave, but more experimental data are required to investigate the phenomenon. Furthermore, the fireball generated by the explosion, which lifted many meters above the ground, lasted seconds. This scenario also presented itself during the "Bursting tank scenario" [5]. In the first chapter of this work it is possible to notice one the "Bursting tank scenario" fireballs: figure 2.5. In that figure the generated fireball lifted above the ground 1800 ms after the ignition. Hence, it reasonable not to exclude the involvement of the transition into the generation of the fireball. It is also relevant to point that, according with literature, fireballs can often impose damaging thermal loads at greater

distances than blast waves. Hence, the role of the $p-H_2$ to $o-H_2$ transition in fireball generation could be an important topic to investigate and discuss with respect to hydrogen safety.

Another aspect which may need some more discussion is the combustion process and its involvement in the shock-wave generation. In this work, the model proposed by Molkov and Kashkarov [11] was adopted to modify the Baker method and a similar approach was taken for the TNT equivalent mass method. Following the model proposed by Molkov and Kashkarov, the fraction of the hydrogen LHV taken into account (β) was set at 0.054. This value was proposed thanks to the analysing of experiments conducted on gaseous hydrogen tanks [11]. Therefore, it is not unreasonable to consider that this coefficient may need to be tuned through the analysis of more experiments conducted on liquid hydrogen tanks. Furthermore, the experiments analysed to find the value of β [11] were focused on high pressure vessels. Hence, the effect of the different pressure level between those experiments and the ones analysed in this work may affect this energy fraction.

Chapter 5

Conclusions

The transition towards a sustainable energy production is a huge challenge which is going to be faced during the following years and it will probably characterize the XXI century. The implementation of renewable and clean unconventional fuels will be crucial to assist the energy industry in its process of abandonment of conventional fossil fuels. On one hand, the low carbon footprint of these solutions makes them appealing and mostly suitable for new applications. On the other hand, the majority of these unconventional fuels is stored in its gaseous phase. This particular storage technique is not fully efficient in terms of transportability and sustainability. Increasing the storage pressure could be a solution to obtain a higher density and therefore minimizing the volume to transport.

Cryogenic fuels like liquid hydrogen are produced to reach this target density without the necessity of an immense storage pressure. To reach a condition of an appealing transportability from an industrial point of view, the liquefaction process is a valid alternative to the high-pressure gaseous vessels. Hence, the implementation of liquid hydrogen fueled solutions, with the purpose to replace conventional fuels, can be a challenging yet extremely valid option in the energy transition scenario. To reach a valid shared knowledge on the applicability of these still mostly unconventional fuels, the investigation of their safety during production processes, transportation and final use is of overriding importance.
Liquid hydrogen experiments concerning simulated accidents are still rare and expensive, but they represent a huge source of essential data, fundamental to build a well established state of the art concerning hazardeous scenarios. Hydrogen unique thermo-physical properties make the adaptation of already existing models a vital task. Such models are suitable for the description of hazardeous scenarios related to conventional fuels and they need to be adapted and validated to obtain a target reliability when applied to liquid hydrogen.

In this work, models often applied to hazardous scenario concerning conventional fuels (e.g. propane, liquefied petroleum gas) were applied to LH_2 simulated accidents with the purpose to describe the aftermath of a liquid hydrogen *Boiling Liquid Expanding Vapor Explosion*.
The "bursting case scenario" experiments conducted in the 1990s by BMW and the more

recent SH_2IFT Project provided essential data to investigate the reliability of such models. In particular, these experiments were conducted on liquid hydrogen inducted "fired" and "un-fired" (*BLEVEs*). The simulation of the accidents was necessary to collect crucial experimental data concerning the overpressure caused by the shock-wave generated with the explosions.

The results of the experiments analysis showed how conventional models often provide underestimations of the pressure waves magnitude. According with previous studies, the conventional models, classified as "real gas behavior" (RGB) and "ideal gas behavior" (IGB), were implemented to describe the mechanical energy liberated with the explosions. Hence, a new model to take hydrogen combustion into account was proposed [65]. Following this new model, a good agreement between the experimental data and the estimations was found for one of the "bursting tank scenario" experiments. This agreement may suggest that hydrogen combustion could affect the generation of the shock-wave, which results in a higher overpressure than the one estimated with the conventional models.
As it concerns the SH_2IFT Project *BLEVE*, an overestimation of the experimental data was obtained by adding the effect of hydrogen combustion to the model. It may be speculated that the coefficients which take into account the reflection of the shock-wave on the ground and the fraction of the hydrogen lower heat value which converts into the blast wave pressure may need to be more accurately tuned to provide a more precise overpressure estimation. However, it was decided to propose a new model considering the transition between the two spin isomers of hydrogen. The reverse problem was solved to investigate if this endothermic reaction could explain, or partially explain, the difference in terms of overpressure between the estimations and the measures. More precisely, the enthaply difference associated with the reaction was calculated and an estimation of the time requested by the reaction to take place was proposed. The obtained results showed how it may be reasonable not to neglect the involvement of the transition in the generation of the shock-wave without consulting further experimental data. In particular, it is not unlikely that this endothermic reaction might affect the development of the fireball after the catastrophic liquid hdrogen release. Therefore, a more accurate model considering mechanical energy, combustion energy, and para-isomer to ortho-isomer transition may be useful to provide a better description of the consequences of a liquid hydrogen *Boiling Liquid Expanding Vapor Explosion*. An accurate description of this hazardeous scenario could be a vital step in the process of liquid hydrogen deployment as a common fuel.

To sum up, the analysis of experimental data allowed the building of a useful, yet still incomplete, model which has the purpose to describe the overpressure generated by a liquid hydrogen *Boiling Liquid Expanding Vapor Explosion*. Moreover, the role of hydrogen combustion and the para to ortho transition in the generation of the shock-wave are still not fully understood.

In conclusion, future experiments aimed to the description of these processes will hopefully provide new crucial data. With the goal of a clean and sustainable energy production industry, it is then reasonable to put effort in LH_2 studies in order to, slowly but surely, stimulate its widespread roll-out.

Appendix A

BMW - Safety tests: Ideal Gas Behavior script

```
%% ASPECTS OF SAFETY AND ACCEPTANCE OF LH, TANK SYSTEMS IN PASSENGER CARS

                                %% K. PEHR

                            %% IDEAL GAS BEHAVIOR

clear;

                    %Definition of the termophisycal constants
                                %TANK CONSTANTS
%Total mass of the tank in each case[kg]
liquidM_0 = [1.8,5.4];

%Total volume of the tank [m^3]
V_T = 0.12;

                                    %PRESSURE
%Ambient pressure [Pa]
P_atm = 101325;

%Critic pressure
P_c = % CoolProp Data %

%Ambient pressure [MPa]
P_a = 0.101325;

%Pressure of the tank before explosion: 2 bar to 16 bar [Pa]
P_exp = linspace(200000,1100000,10);

                                  %TEMPERATURE
%Saturated liquid temperature at P_atm [K]
```

```
32 T_LH2_0 = % CoolProp Data %;
33
34 %Critic temperature
35 T_c = % CoolProp Data %
36
37                                    %HENTALPY
38 %Hentalpy of the saturated liquid [kJ/kg]
39 HL_sat = % CoolProp Data %;
40 HV_sat = % CoolProp Data %
41
42                              %DENSITY and SPECIFIC VOLUME
43 %Liquid density at T_sat and P_atm [kg/m^3]
44 D_LH2 = liquidM_0 / V_T;
45
46 %Specific volume of the liquid phase at boiling point [m^3/kg]
47 v_l_0 = % CoolProp Data %
48
49 v_v_0 = % CoolProp Data %
50
51                                  %INTERNAL ENERGY
52 %Internal energy of the liquid phase at boiling point [kJ/kg]
53 u_l_0 = % CoolProp Data %
54
55 %Internal energy of the liquid phase at boiling point [kJ/kg]
56 u_v_0 = % CoolProp Data %
57
58                                  %SPECIFIC ENTROPY
59 %Entropy of the liquid phase at boiling point [kJ/kgK]
60 s_l_0 = % CoolProp Data %;
61
62 %Entropy of the vapour phase at boiling point [kJ/kgK]
63 s_v_0 = % CoolProp Data %;
64
65                                  %OTHER CONSTANTS
66 %Latent heat of vaporization [kJ/kg]
67 Δ_H_vap = (HV_sat - HL_sat);
68
69 %Specific heat of the liquid at boiling temeprature [J/kgK]
70 C_p_L = % CoolProp Data %
71
72 %Specific heat ratio: gamma = 1.4 for H2
73 gamma = 1.4;
74
75 %Specific heat ratio: gamma = 1.4 for air
76 gamma0 = 1.4;
77
78 %Co-volume constant [m^3/kg]
79 b = 7.69*10^-3;
80
81                              %EXPLODING TANK PARAMETERS
```

```
82
83
84  for i = 1:1:10
85
86      %The liquid and vapour densities are taken from NIST at given
87      %condition of P_sat = P_exp [kg/m^3]
88      liquidD(i) = %%%%%%%%%%%%%%%%%%%%%%
89      gaseousD(i) = %%%%%%%%%%%%%%%%%%%%%%%%%%%%%%%%%%
90      for k = 1:1:2
91          liquidV(k,i) = liquidM_0(k) / liquidD(i);
92          gaseousV(k,i) = V_T - liquidV(k,i);
93
94          %therefore the mass of the vapour phase is: [kg]
95          gaseousM(k,i) = gaseousD(i)*gaseousV(k,i);
96
97          %and the total mass of hydrogen is: [kg]
98          M_T(k,i) = liquidM_0(k) + gaseousM(k,i);
99      end
100 end
101
102
103 %At the saturated conditions the temperature of the liquid and the vapour
104 %phase is the same
105 for i = 1:1:10
106     %GH2 temperature [K]
107     T_GH2(i) = % CoolProp Data %
108     %LH2 temperature [K]
109     T_LH2(i) = % CoolProp Data %
110 end
111
112
113                             %% IDEAL GAS BEHAVIOR MODELS
114
115 for i = 1:1:10
116
117     f(i) = %%%%%%%%%%%%%%%%%%%%%%%%%%%%%%%%%%%%%%%%%%%%%%%%
118
119     for k =1:1:2
120
121         %Expanding volume: total volume of hydrogen that contributes to the
122         %mechanical energy release. [m^3]
123         V_exp(k,i) = %%%%%%%%%%%%%%%%%%%%%%%%%%%%%%%%%%%%%%%%%%%%%%%%%%%%%%%%
124
125         %Isocoric process: E_Brode [MJ]
126         E_Brode(k,i) = %%%%%%%%%%%%%%%%%%%%%%%%%%%%%%%%%%%%%%%%%%%%%%%%%%%%%%
127
128         %Isotermal process: E_ie [MJ]
129         E_ie(k,i) = ...
              %%%%%%%%%%%%%%%%%%%%%%%%%%%%%%%%%%%%%%%%%%%%%%%%%%%%%%%%%%%%%%%%%%%%
130
```

```
131         %Thermodinamic Availability: E_ta [MJ]
132         E_ta(k,i) = ...
                %%%%%%%%%%%%%%%%%%%%%%%%%%%%%%%%%%%%%%%%%%%%%%%%%%%%%%%%%%%%%%%%
133
134         %Adiabatic process: E_Prough [MJ]
135         E_Prough(k,i) = ...
                %%%%%%%%%%%%%%%%%%%%%%%%%%%%%%%%%%%%%%%%%%%%%%%%%%%%%%%%%%%%%%%%
136     end
137 end
138
139                 %% OVERPRESSURE WITH TNT METHOD - NO COMBUSTION
140
141 %Defining an array for the distance from the explosion [m]
142 d = linspace(3,102,100);
143
144 %Defining the fraction of energy that partecipates at the overpressure [-]
145 beta = 1;
146 for k = 1:1:2
147
148     %TNT equivalent masses [kg]
149     TNT_Brode_id(k) = max(E_Brode(k,:)) / 4.68;
150     TNT_ie_id(k) = max(E_ie(k,:)) / 4.68;
151     TNT_ta_id(k) = max(E_ta(k,:)) / 4.68;
152     TNT_Prough_id(k) = max(E_Prough(k,:))/ 4.68;
153
154     %Sachs scaled distances [-]
155     %NB: at R>2 the far field can be found, therefore, the equation
156     %proposed by Kinney and Graham (1985) can be employed to estimate the
157     %overpressure from the TNT scaled distance
158     R_Brode_id(k) = min(d) * (P_atm / (beta*max(E_Brode(k,:)*1000000)))^(1/3);
159     R_ie_id(k) = min(d) * (P_atm / (beta*max(E_ie(k,:)*1000000)))^(1/3);
160     R_ta_id(k) = min(d) * (P_atm / (beta*max(E_ta(k,:)*1000000)))^(1/3);
161     R_Prough_id(k) = min(d) * (P_atm / (beta*max(E_Prough(k,:)*1000000)))^(1/3);
162
163     for i = 1:1:100
164
165         %TNT scaled distances [m * kg^1/3]
166         Z_1_id(k,i) = %%%%%%%%%%%%%%%%%%%%%%%%%%%%%%%%;
167
168         %Defining the elements of the equation for the overpressure
169         %calculated with the isothermal model
170         A_2_id(k,i) = 808*(1+(Z_2_id(k,i)/4.5)^2);
171         B_2_id(k,i) = (1 + (Z_2_id(k,i)/0.048)^2)^0.5;
172         C_2_id(k,i) = (1 + (Z_2_id(k,i)/0.32)^2)^0.5;
173         D_2_id(k,i) = (1 + (Z_2_id(k,i)/1.35)^2)^0.5;
174         P_S_2_id(k,i) = P_atm * A_2_id(k,i) / ( B_2_id(k,i) * C_2_id(k,i) * ...
                D_2_id(k,i)); %[Pa]
175         overpressure_2_id(k,i) = P_S_2_id(k,i)*0.01; %[mbar]
176
177
```

```
178
179
180
181         %Defining the equation for the impulse for each applied method [Pa*s]
182         impulse_ie_id(k,i) = %%%%%%%%%%%%%%%%%%%%%%%%%%%%%%%%%%%%%%%%%%%%
183     end
184 end
185
186 %1) 1.8 kg oh LH2
187 for i = 1:1:10
188     %TNT equivalent mass [kg]
189     TNT_ie_surf_1_8(i) = %%%%%%%%%%%%%%%%%%%%%%%%
190
191     for k = 1:1:100
192         %TNT scaled distance [m * kg^1/3]
193         Z_surf_1_8(k,i) = %%%%%%%%%%%%%%%%%%%%%%%%%%;
194
195         %Defining the terms of the equation for the overpressure calculated ...
                with the
196         %isotermal model
197         A_surf_1_8(k,i) = 808*(1+(Z_surf_1_8(k,i)/4.5)^2);
198         B_surf_1_8(k,i) = (1 + (Z_surf_1_8(k,i)/0.048)^2)^0.5;
199         C_surf_1_8(k,i) = (1 + (Z_surf_1_8(k,i)/0.32)^2)^0.5;
200         D_surf_1_8(k,i) = (1 + (Z_surf_1_8(k,i)/1.35)^2)^0.5;
201         P_S_surf_1_8(k,i) = P_atm * A_surf_1_8(k,i) / ( B_surf_1_8(k,i) * ...
                C_surf_1_8(k,i) * D_surf_1_8(k,i)); %[Pa]
202         overpressure_surf_1_8(k,i) = P_S_surf_1_8(k,i)*0.01; %[mbar]
203     end
204 end
205
206 %2) 5.4 kg oh LH2
207 for i = 1:1:10
208     %TNT equivalent mass [kg]
209     TNT_ie_surf_5_4(i) = %%%%%%%%%%%%%%%%%%%%%%%%%%
210
211     for k = 1:1:100
212         %TNT scaled distance [m * kg^1/3]
213         Z_surf_5_4(k,i) = %%%%%%%%%%%%%%%%%%%%%%%%%%%%%%
214
215         %Defining the terms of the equation for the overpressure calculated ...
                with the
216         %isotermal model
217         A_surf_5_4(k,i) = 808*(1+(Z_surf_5_4(k,i)/4.5)^2);
218         B_surf_5_4(k,i) = (1 + (Z_surf_5_4(k,i)/0.048)^2)^0.5;
219         C_surf_5_4(k,i) = (1 + (Z_surf_5_4(k,i)/0.32)^2)^0.5;
220         D_surf_5_4(k,i) = (1 + (Z_surf_5_4(k,i)/1.35)^2)^0.5;
221         P_S_surf_5_4(k,i) = P_atm * A_surf_5_4(k,i) / ( B_surf_5_4(k,i) * ...
                C_surf_5_4(k,i) * D_surf_5_4(k,i)); %[Pa]
222         overpressure_surf_5_4(k,i) = P_S_surf_5_4(k,i)*0.01; %[mbar]
223     end
```

```
224 end
225
226
227                                 %NO COMBUSTION
228 %Tank radius [m]
229 r_T = (3*V_T/(4*pi))^(1/3);
230
231 %Defining the parameters for the experimental data from BMW
232 d_BMW = 3; %[m]
233 p_rupture_BMW = [4,11]; %[bar]
234 op_BMW = [100,150,450];
235
236                       % 1) mass of liquid hydrogen 1.8 kg
237
238 %Calculating the adimensional distance for the experimental data
239 ad_R_BMW_1_8 = zeros(4,10);
240
241 Mech_en_1_8 = [E_Brode(1,:);E_ie(1,:);E_ta(1,:);E_Prough(1,:)]; %[MJ]
242
243 for k = 1:1:4
244     for i = 1:1:10
245         ad_R_BMW_1_8(k,i) = d_BMW*(P_a)^(1/3)/ ((Mech_en_1_8(k,i))^(1/3));
246     end
247 end
248 disp('R (3m) with BMW exp data: 1.8 kg of LH2 NO COMB');
249 disp(min(ad_R_BMW_1_8(1,:)));
250 disp(min(ad_R_BMW_1_8(2,:)));
251 disp(min(ad_R_BMW_1_8(3,:)));
252 disp(min(ad_R_BMW_1_8(4,:)));
253 %ad_R_BMW_1_8 = [ 2.0925 , 2.0583 , 2.4148 , 2.0449 ]
254
255 %the adimensional pressure ratio is:
256 P_1_8 = [0.15 , 0.15 , 0.12 , 0.15 ];
257
258 %The dimensional ovepressure is:
259 op_BMW_1_8 = ((P_1_8 +1) * P_atm - P_atm)*0.01; %[mbar]
260
261 disp('op (3m) with BMW exp data: 1.8 kg of LH2 NO COMB');
262 disp(op_BMW_1_8);
263
264 %2) mass of liquid hydrogen 5.4 kg
265
266 %Calculating the adimensional distance for the experimental data
267 ad_R_BMW_5_4 = zeros(4,10);
268
269 Mech_en_5_4 = [E_Brode(2,:);E_ie(2,:);E_ta(2,:);E_Prough(2,:)]; %[MJ]
270
271 for k = 1:1:4
272     for i = 1:1:10
273         ad_R_BMW_5_4(k,i) = d_BMW*(P_a)^(1/3)/ ((Mech_en_5_4(k,i))^(1/3));
```

```
    end
end

disp('R (3m) with BMW exp data: 5.4 kg of LH2 NO COMB');
disp(min(ad_R_BMW_5_4(1,:)));
disp(min(ad_R_BMW_5_4(2,:)));
disp(min(ad_R_BMW_5_4(3,:)));
disp(min(ad_R_BMW_5_4(4,:)));

%ad_R_BMW_5_4 = [ 2.0936 , 2.0629 , 2.4202 , 2.0410 ]

%the adimensional pressure ratio is:
P_5_4 = [0.15 , 0.15 , 0.12 , 0.15 ];

%The dimensional ovepressure is:
op_BMW_5_4 = ((P_5_4 + 1) * P_atm - P_atm)*0.01; %[mbar]

disp('op (3m) with BMW exp data: 5.4 kg of LH2 NO COMB');
disp(op_BMW_5_4);

                                %COMBUSTION

%molar mass of H2 [kg/mol]
mmH2 = 2.013*10^-3;

%mol of hydrogen fo each case (mass of LH2 and GH2) [mol]
mol_H2 = zeros(2,10);
for k = 1:1:2
    for i = 1:1:10
        mol_H2(k,i) = (liquidM_0(k) + gaseousM(k,i))/mmH2;
    end
end

%Occupied volume in normal conditions: 22.4 [L/mol]
%Total volume of hydrogen in normal conditions
VU_H2 = zeros(2,10);
for k = 1:1:2
    for i =1:1:10
        VU_H2(k,i) = mol_H2(k,i) * 22.4 / 1000;
    end
end

%Using the reaction 2H2 + (O2 + 3.76N2) -> 2H2O + 3.76N2 is possible to
%calculate the total volume occupied by the products of complete
%combustion. 1 mole of H2 consumes 2.38 mol of air: (1+3.76)/2

for k = 1:1:2
    for i = 1:1:10
        mol_air(k,i) = %%%%%%%%%;
        VU_air(k,i) = %%%%%%%%%;
```

```
324
325         %Total volume of the sphere with stoichiometric hydrogen-air mixture
326         VU(k,i) = %%%%%%%%%%%
327     end
328 end
329
330 %Combustion products expansion coefficient of stoichiometric hydrogene-air ...
       mixture
331 Ei = 6.85;
332
333 %Volume of the sphere occupied by the combustion products
334 Vb = zeros(2,10);
335 for k = 1:1:2
336     for i =1:1:10
337         Vb(k,i) = VU(k,i) * Ei;
338     end
339 end
340
341 %Radius of the sphere occupied by the combustion products
342 for i = 1:1:10
343     r_b_1_8(i) = (3*Vb(1,i) / (2*pi))^(1/3);
344     r_b_5_4(i) = (3*Vb(2,i) / (2*pi))^(1/3);
345 end
346 r_b = [r_b_1_8 ; r_b_5_4];
347
348 %Lower heat value of hydrogen [J/kg]
349 LHV_H2 = 1.1993*10^8;
350
351 %Total chemical energy inside the hydrogen [J]
352 E_ch = zeros(2,10);
353 for k = 1:1:2
354     for i = 1:1:10
355         E_ch(k,i) = (liquidM_0(k)+gaseousM(k,i)) * LHV_H2;
356     end
357 end
358
359 %Defining the parameter beta as in the stand alone tank experiment from
360 %Molkov et al.
361 beta_ch = 0.054; %[-]
362
363 %1) mass of liquid hydrogen: 1.8 kg
364
365 for i = 1:1:10
366     for k = 1:1:4
367 rp_1_8(k,i) = %%%%%%%%%%%%%%%%%%%%%%%%%
368     end
369 end
370
371           %% TNT EQUIVALENT MASS AND OVEPRESSURE WITH COMBUSTION
372
```

```
373
374 %Lower heat value of hydrogen [J/kg]
375 LHV_H2 = 1.1993*10^8;
376
377 %Defining the parameter beta as in the stand alone tank experiment from
378 %Molkov et al.
379 beta_ch = 0.054; %[-]
380
381 %1) Tank filled with 1.8 kg of liquid hydrogen
382
383 rad_1_8 = zeros(1,100);
384 for k = 1:1:4
385
386     %Sachs scaled distances [m]
387     R_Sachs_1_8(k) = min(d) * (P_a / (beta*max(Mech_en_1_8(k)) + ...
        beta_ch*(min(d)/max(r_b(1,:)))^3*max(E_ch(1,:)/1000000)))^(1/3);
388
389     for i = 1:1:100
390
391         rad_1_8(i) = (d(i)/max(r_b(1,:)))^3;
392         if rad_1_8(i) < 1
393         %TNT equivalent masses [kg]
394         TNTmass_1_8(k,i) = %%%%%%%%%%%%%%%%%%%%%%
395         else
396         TNTmass_1_8(k,i) = %%%%%%%%%%%%%%%%%%%%%%
397         end
398         %TNT scaled distances [m * kg^1/3]
399         Z_1_8(k,i) = %%%%%%%%%%%%%%%%%%%%
400
401         %Defining the terms of the equation for the overpressure for each
402         %method
403         A_1_8(k,i) = 808*(1+(Z_1_8(k,i)/4.5)^2);
404         B_1_8(k,i) = (1 + (Z_1_8(k,i)/0.048)^2)^0.5;
405         C_1_8(k,i) = (1 + (Z_1_8(k,i)/0.32)^2)^0.5;
406         D_1_8(k,i) = (1 + (Z_1_8(k,i)/1.35)^2)^0.5;
407         P_S_ch_1_8(k,i) = P_atm * A_1_8(k,i) / ( B_1_8(k,i) * C_1_8(k,i) * ...
            D_1_8(k,i)); %[Pa]
408         overpressure_ch_1_8(k,i) = P_S_ch_1_8(k,i)*0.01; %[mbar]
409
410         %Defining the equation for the impulse for each applied method
411         impulse_ch_1_8(k,i) = %%%%%%%%%%%%%%%%%%%%%%%%%%%%%%%%%%%%%%%%%%%%%%%%
412     end
413 end
414
415 %2) Tank filled with 5.4 kg of liquid hydrogen
416 rad_5_4 = zeros(1,100);
417
418 for k = 1:1:4
419     %Sachs scaled distances [m]
```

```
420     R_Sachs_5_4(k) = min(d)*(P_a / (beta*max(Mech_en_5_4(k,:))+ ...
            beta_ch*((min(d)/(max(r_b(2,:))))^3)*max(E_ch(2,:))/1000000))^(1/3);
421
422     for     i = 1:1:100
423
424         rad_5_4(i) = (d(i)/max(r_b(2,:)))^3;
425         %TNT equivalent masses [kg]
426         if rad_5_4(i) < 1
427         TNTmass_5_4(k,i) = %%%%%%%%%%%%%%%%%%%%%%
428         else
429         TNTmass_5_4(k,i) = %%%%%%%%%%%%%%%%%%%%%%
430         end
431         %TNT scaled distances [m * kg^1/3]
432         Z_5_4(k,i) = %%%%%%%%%%%%%%%%%%%%%%
433
434         %Defining the terms of the equation for the overpressure for each
435         %method
436         A_5_4(k,i) = 808*(1+(Z_5_4(k,i)/4.5)^2);
437         B_5_4(k,i) = (1 + (Z_5_4(k,i)/0.048)^2)^0.5;
438         C_5_4(k,i) = (1 + (Z_5_4(k,i)/0.32)^2)^0.5;
439         D_5_4(k,i) = (1 + (Z_5_4(k,i)/1.35)^2)^0.5;
440         P_S_ch_5_4(k,i) = P_atm * A_5_4(k,i) / ( B_5_4(k,i) * C_5_4(k,i) * ...
                D_5_4(k,i)); %[Pa]
441         overpressure_ch_5_4(k,i) = P_S_ch_5_4(k,i)*0.01; %[mbar]
442
443         %Defining the equation for the impulse for each applied method
444         impulse_ch_5_4(k,i) = ((6.7 * (1 + (Z_5_4(k,i) / 0.23)^4)^0.5) / ...
                (Z_5_4(k,i)^2 * (1 + ...
                (Z_5_4(k,i)/1.55)^3)^(1/3)))*(TNTmass_5_4(k))^(1/3);
445
446     end
447 end
```

Appendix B

BMW - Safety tests: Real Gas Behavior script

```
%% ASPECTS OF SAFETY AND ACCEPTANCE OF LH, TANK SYSTEMS IN PASSENGER CARS

                                %% K. PEHR

                            %% REAL GAS BEHAVIOR


                                %INTERNAL ENERGY
%Internal energy of the liquid phase at boiling point [kJ/kg]
u_l_0 = % CoolProp Data %

%Internal energy of the vapour phase at boiling point [kJ/kg]
u_v_0 = % CoolProp Data %


                                %SPECIFIC ENTROPY
%Entropy of the liquid phase at boiling point [kJ/kgK]
s_l_0 = % CoolProp Data %;

%Entropy of the vapour phase at boiling point [kJ/kgK]
s_v_0 = % CoolProp Data %;


                                %OTHER

%fraction of energy converted in overpressure [-]
%K_TNO = [-]
%K_Planas = [-]
K_Se = 0.14;
K_Genova = 0.05;
%K_Birk = [-]
```

```
32
33 %Defining the fraction of energy that partecipates to the overpressure [-]
34 beta_TNO = 2;
35 beta_Planas = 0.4;
36 beta_Se = 1;
37 beta_Genova = 1;
38 beta_Birk = 2;
39
40 %amount of energy which participate in the generation of the pressure wave ...
       (Genova model) [-]
41 psi = 0.07;
42
43 %Constant of hydrogen gas [J/kgK]
44 R = 4125.5;
45
46                              %EXPLODING TANK PARAMETERS
47
48 for i = 1:1:10
49
50     %The liquid and vapour densities are taken from NIST at given
51     %condition of P_sat = P_exp [kg/m^3]
52     liquidD(i) = % CoolProp Data %
53     gaseousD(i) = % CoolProp Data %
54
55     for k = 1:1:2
56         liquidV(k,i) = liquidM_0(k) / liquidD(i);
57         gaseousV(k,i) = V_T - liquidV(k,i);
58
59         %therefore the mass of the vapour phase is: [kg]
60         gaseousM(k,i) = gaseousD(i)*gaseousV(k,i);
61
62         %and the total mass of hydrogen is: [kg]
63         M_T(k,i) = liquidM_0(k) + gaseousM(k,i);
64     end
65 end
66
67 %At the saturated conditions the temperature of the liquid and the vapour
68 %phase is the same
69 for i = 1:1:10
70     %GH2 temperature [K]
71     T_GH2(i) = % CoolProp Data %
72     %LH2 temperature [K]
73     T_LH2(i) = % CoolProp Data %
74
75 end
76
77                         %% REAL GAS BEHAVIOR MODELS
78
79 for i = 1:1:10
80
```

```
81      %Specific entropy of liquid hydrogen at different pressures and
82      %temperatures[kJ/kgK]
83      s_l(i) = %%%%%%%%%%%%%%%%%%%%
84
85      %Specific entropy of the vapour phase before the explosion [kJ/kgK]
86      s_v(i) = %%%%%%%%%%%%%%%%%%%%%%%
87
88      %Specific entropy fraction of the liquid phase [-]
89      X_l(i) = %%%%%%%%%%%%%%%%%%%%%%
90
91      %Specific entropy fraction of the vapor phase [-]
92      X_v(i) = %%%%%%%%%%%%%%%%%%%%%%
93
94      %Specific energy of the liquid phase after the isoentropic expansion [kJ/kg]
95      u_l_is(i) = %%%%%%%%%%%%%%%%%%%%%%
96
97      %Specific energy of the vapour phase after the isoentropic expansion [kJ/kg]
98      u_v_is(i) = %%%%%%%%%%%%%%%%%%%%%%
99
100     %Specific energy of the liquid phase before the explosion [kJ/kg]
101     u_l(i) = %%%%%%%%%%%%%%%%%%%%
102
103     %Specific energy of the vapour phase before the explosion [kJ/kg]
104     u_v(i) = %%%%%%%%%%%%%%%%%%%%%%
105
106     %Specific hentalpy of the liquid phase before the explosion [kJ/kg]
107     h_l(i) = %%%%%%%%%%%%%%%%%%%%%%
108
109     %Specific heat at constant pressure of the liquid phase between the
110     %initial and final states [kJ/kgK]
111     cpl(i) = %%%%%%%%%%%%%%%%%%%%%%
112
113     %Average specific heat at constant pressure of the liquid phase between the
114     %initial and final states [kJ/kgK]
115     cplm = (mean(cpl));
116
117     for k =1:1:2
118         %Overall energy of the system [kJ]
119         Ui(k,i) = u_l(i)*liquidM_0(k) + u_v(i)*gaseousM(k,i);
120
121         %Vapour fraction after the irreversible expansion [-]
122         X(k,i) = %%%%%%%%%%%%%%%%%%%%%%%%%%%%%%%%%%%%%%%%%%%%%%%%
123
124         %Mechanical energy for each method [MJ]
125         E_TNO(k,i) = (liquidM_0(k)*(u_l(i)-u_l_is(i))+ gaseousM(k,i)*(u_v(i) ...
                - u_v_is(i)))/1000;
126         E_Planas(k,i) = (((u_l_0-u_v_0)*M_T(k)*X(k,i) - M_T(k)*u_l_0 + ...
                Ui(k,i)))/1000;
127         E_Se(k,i) = K_Se*(liquidM_0(k)*(h_l(i) - HL_sat))/1000;
128         E_Genova(k,i) = psi*liquidM_0(k)*cplm*(T_LH2(i)- T_LH2_0)/1000;
```

```
129          E_Birk(k,i) = (gaseousM(k,i)*(u_v(i) - u_v_is(i)))/1000;
130      end
131  end
```

Appendix C

SH_2IFT Project: Ideal Gas Behavior script

```
                    %% SH2IFT PROJECT - IDEAL GAS BEHAVIOR

clear;

               %Definition of the termophisycal constants

%Pressure of the tank before explosion:50 bar [Pa]
P_exp = 5000000;
                       %% INITIAL MASSES AND VOLUMES

%Pressure in the tank before starting the fire [Pa]
P_1 = 950000;

%Gas saturated temperature at 9.5 bar [K]
T_GH2_1 = % CoolProp Data %

%Gas density at T_GH2_1 and 9.5 bar [kg/m^3]
D_GH2_1 = % CoolProp Data %

%Liquid density at T_sat and 9.5 bar [kg/m^3]
D_L_1 = % CoolProp Data %

%Now it is possible to calculate the volume and the mass of the liquid and ...
    the gaseous phase
M_LH2_ft = 5; %first try liquid mass
err = 1; %initialization of the err variable

    while  err > 0.00001
        V_LH2_ft = M_LH2_ft / D_L_1; %first try liquid Volume

        V_GH2_ft = V_T - V_LH2_ft; %first try supercritc Volume
```

```
31
32          M_GH2_ft = V_GH2_ft * D_GH2_1; %first try supercritic mass
33
34          M_LH2_st = M_LH2_ft; %re definition of the first try liquid mass
35
36          M_LH2_ft = M_T - M_GH2_ft; %initialization of the variable second try ...
                liquid mass
37
38          err = abs(M_LH2_st - M_LH2_ft); %definition of the error
39      end
40  M_LH2 = M_LH2_st;
41  M_GH2 = M_GH2_ft;
42
43
44
45                          %% EXPLODING TANK PARAMETERS
46
47  %Defining an array for different liquid temperatures [K]
48  T_liquid = linspace(T_LH2,T_c,10)';
49
50  M_LH2_max = M_LH2;
51  M_LH2_min = 0;
52
53  %Defining an array containing different masses from the minimum to the maximum
54  liquidM = linspace(M_LH2_min,M_LH2_max,10);
55
56                            %% IDEAL GAS BEHAVIOR
57
58  for k = 1:1:10
59
60      %Density of the liquid at 50 bar and T_liquid [kg/m^3]
61      D_LH2(k) = %%%%%%%%%%%%%%%%%%%%%%%
62
63      %Definition of f, flashing fraction
64      f(k) = %%%%%%%%%%%%%%%%%%%%%%%%%%%%
65
66      for i = 1:1:10
67          liquidV(k,i) = %%%%%%%%%%%%%%%%
68          gaseousV(k,i)= V_T - liquidV(k,i); %[m^3]
69          gaseousM(i) = M_T - liquidM(i); %[kg]
70          gaseousD(k,i) = gaseousM(i) / gaseousV(k,i); %[kg/m^3]
71          V_exp(k,i) = V_T + liquidM(i)*(f(k)/gaseousD(k,i) - 1/D_LH2(k)); %[m^3]
72          E_Brode(k,i) = %%%%%%%%%%%%%%%
73          E_ie(k,i) = %%%%%%%%%%%%%%%%%
74          E_ta(k,i) = %%%%%%%%%%%%%%%%%%%
75          E_Prough(k,i) = %%%%%%%%%%%%%%%%%%%%%%
76      end
77
78
79  end
```

```
80
81              %% OVERPRESSURE WITH TNT METHOD - NO COMBUSTION
82
83  %Defining an array for the distance
84  d = linspace(10,109,100);
85
86  %Defining the fraction of energy that partecipates at the overpressure
87  beta = 1;
88
89  %Sachs scaled distances [m]
90  R_ie = min(d) * (P_atm / (beta*max(max(E_ie))*1000000))^(1/3);
91  R_Brode = min(d) * (P_atm / (beta*max(max(E_Brode))*1000000))^(1/3);
92  R_ta = min(d) * (P_atm / (beta*max(max(E_ta))*1000000))^(1/3);
93  R_Prough = min(d) * (P_atm / (beta*max(max(E_Prough))*1000000))^(1/3);
94
95  %TNT equivalent masses [kg]
96  TNT_ie = %%%%%%%%%%%%%%
97  TNT_Brode = %%%%%%%%%%%%%%
98  TNT_ta = %%%%%%%%%%%%%%
99  TNT_Prough = %%%%%%%%%%%%%%
100
101 %TNT scaled distances [m * kg^1/3]
102 Z_1 = d / ((beta * TNT_ie)^(1/3));
103 Z_2 = d / ((beta * TNT_Brode)^(1/3));
104 Z_3 = d / ((beta * TNT_ta)^(1/3));
105 Z_4 = d / ((beta * TNT_Prough)^(1/3));
106
107 for i = 1:1:100
108
109     %Defining the terms of the equation for the overpressure calculation
110     %with isothermal process model
111     A_1(i) = 808*(1+(Z_1(i)/4.5)^2);
112     B_1(i) = (1 + (Z_1(i)/0.048)^2)^0.5;
113     C_1(i) = (1 + (Z_1(i)/0.32)^2)^0.5;
114     D_1(i) = (1 + (Z_1(i)/1.35)^2)^0.5;
115     P_S_1(i) = P_atm * A_1(i) / ( B_1(i) * C_1(i) * D_1(i)); %[Pa]
116     overpressure_1(i) = P_S_1(i)*0.01; %[mbar];
117
118     %Defining the equation for the impulse for each applied model
119     impulse_ie(i) = %%%%%%%%%%%%%%%%%%%%%%%%%%%%%%
120
121 end
122
123   %% Overpressure with and without combustion using Baker method
124
125 d_probe = 22.5; %m
126 op_probe = 133; %mbar
127 d_probe_1 = 26.4;
128 op_probe_1 = 99;
129                                 %NO COMBUSTION
```

```
130 Rr_ie = d_probe*(P_atm/(beta*max(max(E_ie*1000000))))^(1/3);
131 Rr_Brode = d_probe*(P_atm/(beta*max(max(E_Brode*1000000))))^(1/3);
132 Rr_ta = d_probe*(P_atm/(beta*max(max(E_ta*1000000))))^(1/3);
133 Rr_Prough = d_probe*(P_atm/(beta*max(max(E_Prough*1000000))))^(1/3);
134
135 Rr_ie_1 = d_probe_1*(P_atm/(beta*max(max(E_ie*1000000))))^(1/3);
136 Rr_Brode_1 = d_probe_1*(P_atm/(beta*max(max(E_Brode*1000000))))^(1/3);
137 Rr_ta_1 = d_probe_1*(P_atm/(beta*max(max(E_ta*1000000))))^(1/3);
138 Rr_Prough_1 = d_probe_1*(P_atm/(beta*max(max(E_Prough*1000000))))^(1/3);
139
140 R = [Rr_ie,Rr_Brode,Rr_ta,Rr_Prough];
141 disp('R (22.5m) with SH2IFT exp data');
142 disp(R);
143
144 %R =  [ 3.5602    4.1913    3.9207    4.1710 ]
145
146 %the adimensional pressure ratio is:
147 P_nocomb = [0.08 , 0.06 , 0.07 , 0.08 ];
148
149 %The dimensional ovepressure is:
150 op_nocomb = ((P_nocomb + 1) * P_atm - P_atm)*0.01; %[mbar]
151
152 disp('op (22.5m) with SH2IFT exp data');
153 disp(op_nocomb);
154
155 R_1 = [Rr_ie_1,Rr_Brode_1,Rr_ta_1,Rr_Prough_1];
156 disp('R (26.4m) with SH2IFT exp data');
157 disp(R_1);
158
159 %R =  [ 4.1773    4.9177    4.6003    4.8940 ]
160
161 %the adimensional pressure ratio is:
162 P_nocomb_1 = [0.055 , 0.045 , 0.05 , 0.045 ];
163
164 %The dimensional ovepressure is:
165 op_nocomb_1 = ((P_nocomb_1 + 1) * P_atm - P_atm)*0.01; %[mbar]
166
167 disp('op (26.4m) with SH2IFT exp data');
168 disp(op_nocomb_1);
169                                  %COMBUSTION
170
171 rp_ie = %%%%%%%%%%%%%%%%%%%%
172 rp_Brode = %%%%%%%%%%%%%%%%%%
173 rp_ta = %%%%%%%%%%%%%%%%%%%%
174 rp_Prough = %%%%%%%%%%%%%%%%
175
176 rp_ie_1 = %%%%%%%%%%%%%%%%%%%%
177 rp_Brode_1 = %%%%%%%%%%%%%%%%%%%%
178 rp_ta_1 = %%%%%%%%%%%%%%%%%%
179 rp_Prough_1 = %%%%%%%%%%%%%%%%%%%%
```

```
180
181 rp = [rp_ie,rp_Brode,rp_ta,rp_Prough];
182 disp('R (22.5m) with SH2IFT exp data and comb');
183 disp(rp);
184
185 %rp =  [  1.8327    1.8662    1.8542    1.8654 ]
186
187 %the adimensional pressure ratio is:
188 P_comb = [0.16 , 0.15 , 0.15 , 0.14 ];
189
190 %The dimensional ovepressure is:
191 op_comb = ((P_comb + 1) * P_atm - P_atm)*0.01; %[mbar]
192
193 disp('op (22.5m) with SH2IFT exp data and comb');
194 disp(op_comb);
195
196 rp_1 = [rp_ie_1,rp_Brode_1,rp_ta_1,rp_Prough_1];
197 disp('R (26.4m) with SH2IFT exp data and comb');
198 disp(rp_1);
199
200 %rp =  [  2.1504    2.1897    2.1756    2.1887 ]
201
202 %the adimensional pressure ratio is:
203 P_comb_1 = [0.14 , 0.13 , 0.135 , 0.13 ];
204
205 %The dimensional ovepressure is:
206 op_comb_1 = ((P_comb_1 + 1) * P_atm - P_atm)*0.01; %[mbar]
207
208 disp('op (26.4m) with SH2IFT exp data and comb');
209 disp(op_comb_1);
210
211
212             %% TNT EQUIVALENT MASS AND OVEPRESSURE WITH COMBUSTION
213 %The mechanical energy considered for the ovepressure is [J]
214 mech_en = ...
    [max(max(E_ie*1000000)),max(max(E_Brode*1000000)),max(max(E_ta*1000000)),max(max(E_Prough*1
215
216 for k = 1:1:4
217
218     %Sachs scaled distances [m]
219     R_Sachs(k) = 22.5 * (P_atm / (beta*mech_en(k)+beta_ch*E_ch))^(1/3);
220     R_Sachs_1(k) = 26.4 * (P_atm / (beta*mech_en(k)+beta_ch*E_ch))^(1/3);
221
222     for i = 1:1:100
223
224         radio(i) = %%%%%%%%%%%%%%%%%%%
225         if radio(i) < 1
226         TNTmass(k,i) = %%%%%%%%%%%%%%%%%%%%%
227         else
228         TNTmass(k,i) = %%%%%%%%%%%%%%%%%%%%%%%%
```

```
229         end
230         %TNT scaled distances [m * kg^1/3]
231         Z(k,i) = %%%%%%%%%%%%%%%%%%%%%%
232
233         %Defining the terms of the equation for the overpressure for each
234         %model
235         A(k,i) = 808*(1+(Z(k,i)/4.5)^2);
236         B(k,i) = (1 + (Z(k,i)/0.048)^2)^0.5;
237         C(k,i) = (1 + (Z(k,i)/0.32)^2)^0.5;
238         D(k,i) = (1 + (Z(k,i)/1.35)^2)^0.5;
239         P_S_ch(k,i) = P_atm * A(k,i) / ( B(k,i) * C(k,i) * D(k,i)); %[Pa]
240         overpressure_ch(k,i) = P_S_ch(k,i)*0.01; %[mbar]
241
242         %Defining the equation for the impulse for each applied model
243         impulse_ch(k,i) = %%%%%%%%%%%%%%%%%%%%%%%%%%%%%%%%
244     end
245 end
246
247             %% ORTHO - PARA - TNT method - reverse problem
248 %Defining the difference between the measured overpressure and the
249 %calculated one
250
251 %Measured op at 22.5 m [mbar]
252 meas_1 = 133;
253
254 %Measured op at 26.4 m [mbar]
255 meas_2 = 99;
256
257 %Calculated op at 22.5 m [mbar] - Isoermal Model
258 calc_1 = (overpressure_ch(1,13) + overpressure_ch(1,14))/2;
259
260 %Calculated op at 26.4 m [mbar] - Isotermal Model
261 dist = 26.4;
262 interp_a = 17;
263 interp_b = 18;
264 dis_a = d(interp_a);
265 dis_b = d(interp_b);
266 op_calc_a = overpressure_ch(1,interp_a);
267 op_calc_b = overpressure_ch(1,interp_b);
268 calc_2 = op_calc_a + (op_calc_b - op_calc_a)/((dis_b-dis_a)/(dist-dis_a));
269
270 %overpressure error at 22.5 m [mbar]
271 p_err_1 = abs(calc_1-meas_1);
272
273 %overpressure error at 26.4 m [mbar]
274 p_err_2 = abs(calc_2-meas_2);
275
276 %overpressure error array;
277 p_err = [p_err_1 p_err_2];
278
```

```
%TNT scaled distance difference [m * kg^1/3]
syms z

res1 = (808*(1+(z/4.5)^2) / ((1 + (z/0.048)^2)^0.5*(1 + (z/0.32)^2)^0.5*(1 + ...
    (z/1.35)^2)^0.5)) == p_err(1)/(P_atm/100);
z1 = abs(vpasolve(res1,z));

res2 = (808*(1+(z/4.5)^2) / ((1 + (z/0.048)^2)^0.5*(1 + (z/0.32)^2)^0.5*(1 + ...
    (z/1.35)^2)^0.5)) == p_err(2)/(P_atm/100);
z2 = abs(vpasolve(res2,z));

zz = [z1 z2];

%Now It is possible to calculate the difference in the TNT mass [kg]
TNTerr1 = double((dist / z1)^3);
TNTerr2 = double((dist / z2)^3);
TNT_err = [TNTerr1 TNTerr2];

%NB: The difference is thought to be the energy absorbed by the ortho - para
%reaction
%Now It is possible to calculate the coefficient gamma to take into account
%the para-ortho energy absorption

%Definition of the entalpy of the complete reaction

%parahydrogen initial concentration [-]
c0p = 99.8;

%parahydrogen final concentration [-]
c1p = 25;

%parahydrogen initial enthalpy (immediatly after the explosion) [kJ/kg]
%It is considered the hydrogen to be instantaneously saturated gas at P_atm
h0p = (py.CoolProp.CoolProp.PropsSI('H','P',P_atm,'Q',1,'Parahydrogen'))/1000;

%parahydrogen final enthalpy [kJ/kg]
%The transition is considered to happen at constant temperature
h1p = (py.CoolProp.CoolProp.PropsSI('H','P',P_atm,'Q',1,'Parahydrogen'))/1000;

%orthohydrogen initial concentration [-]
c0o = 0.2;
%orthohydrogen final concentration [-]
c1o = 75;

%parahydrogen enthalpy (immediatly after the explosion) [kJ/kg]
%It is considered the hydrogen to be instantaneously saturated gas at P_atm
h0o = (py.CoolProp.CoolProp.PropsSI('H','P',P_atm,'Q',1,'Orthohydrogen'))/1000;

%parahydrogen final enthalpy [kJ/kg]
%The transition is considered to happen at constant temperature
```

```
327 h1o = (py.CoolProp.CoolProp.PropsSI('H','P',P_atm,'Q',1,'Orthohydrogen'))/1000;
328
329 %Enthaply of the transition [kJ/kg]
330 Delta_h_po = (c1p*h1p + c1o*h1o) - (c0p*h0p + c0o*h0o);
331
332 %Total enthaply of the transition [kJ]
333 Delta_H_po = Delta_h_po * M_T;
334
335 %Now It is possible to calculate the coefficient gamma using TNT =
336 %gamma*Δh_para_ortho/4680
337 g_p_o = (TNT_err * 4680 / Delta_H_po);
338
339 %% ORTHO - PARA - Baker method - reverse problem
340
341 %Measured op at 22.5 m [mbar]
342 meas_1 = 133;
343
344 %Measured op at 26.4 m [mbar]
345 meas_2 = 99;
346
347 meas = [meas_1 meas_2];
348
349 %Defining the ad overpressure for the measured overpressure
350 %0.1313    0.0977
351 Ps_meas = (meas + P_atm/100)/(P_atm/100) -1;
352
353 %Using the Baker graphics to find the adimentional distance
354 R_meas = [1.77 2.08];
355
356 %It is now possible to redefine R to calculate coefficient of
357 %the para-ortho enthalpy
358 %R = r(p0 / alphaE + betaEch -gammaDeltaHpo)^(1/3)
359 gamma_po_1 = (alpha(1)*max(max(E_ie*1000))+beta_ch*E_ch/1000 - ...
       22.5^3*P_atm/1000/R_meas(1)^3)/Delta_H_po;
360 gamma_po_2 = (alpha(1)*max(max(E_ie*1000))+beta_ch*E_ch/1000 - ...
       26.4^3*P_atm/1000/R_meas(2)^3)/Delta_H_po;
361
362 g_p_o_B = [gamma_po_1 gamma_po_2];
363
364 %It is also possbile to consider the reaction as not completed, thus
365 %avoiding the definition of the coefficient gamma
366 D_H_nc = [g_p_o ; g_p_o_B]*Delta_H_po;
367
368 %Using the definition of the enthalpy difference It is possible to
369 %calculate the final ortho-hydrogen concentration
370 c1o_nc = (D_H_nc/M_T + c0p/100*h0p + c0o/100*h0o - h1p)/(h1o-h1p);
```

Appendix D

SH_2IFT Project: Real Gas Behavior script

```
                    %% SH2IFT PROJECT - REAL GAS BEHAVIOR
                            %% REAL GAS BEHAVIOR

for i = 1:1:10

    %Density of the liquid at 50 bar and T_liquid [kg/m^3]
    D_LH2(i) = %%%%%%%%%%%%%%%%%%%%%%%%%%%%%%%%

    %Specific entropy of the liquid at 50 bar and T_liquid [kJ/kgK]
    s_l(i) = %%%%%%%%%%%%%%%%%%%%%%%%%%%%

    %Specific entropy fraction of the liquid phase [-]
    X_l(i) = %%%%%%%%%%%%%%%%%%%%%%%%

    %Specific energy of the liquid phase after the isoentropic expansion [kJ/kg]
    u_l_is(i) = %%%%%%%%%%%%%%%%%%%%%%

    %Specific energy of the liquid phase before the explosion [kJ/kg]
    u_l(i) = %%%%%%%%%%%%%%%%%%%%%%

    %Specific hentalpy of the liquid phase before the explosion [kJ/kg]
    h_l(i) = %%%%%%%%%%%%%%%%%%%%%%

    %Specific heat at constant pressure of the liquid phase between the
    %initial and final states [kJ/kgK]
    cpl(i) = % CoolProp Data %

    %Average specific heat at constant pressure of the liquid phase between the
    %initial and final states [kJ/kgK]
    cplm = mean(cpl);

```

```
32          for j = 1:1:10
33          liquidV(i,j) = liquidM(j)/D_LH2(i);
34          gaseousV(i,j)= V_T - liquidV(i,j);
35          gaseousM(j) = M_T - liquidM(j);
36          gaseousD(i,j) = gaseousM(j) / gaseousV(i,j);
37
38          %Gaseous Hydrogen speed of sound [m/s]
39          gas_H2_ss(i,j) = ((gamma*P_exp)/((gaseousD(i,j))))^0.5;
40
41          %Gas temperature [K]
42          T_gas(i,j) = % CoolProp Data %
43
44          %Specific energy of the vapour phase before the explosion [kJ/kg]
45          u_v(i,j) = % CoolProp Data %
46
47          %Specific entropy of the vapour at 50 bar and T_liquid [kJ/kgK]
48          s_v(i,j) = % CoolProp Data %
49
50          %Specific entropy fraction of the vapor phase [-]
51          X_v(i,j) = %%%%%%%%%%%%%%%%%%%%%%%%%%%%
52
53          %Specific energy of the vapour phase after the isoentropic expansion
54          u_v_is(i,j) = %%%%%%%%%%%%%%%%%%%%%%%%%%%%
55
56          %Overall energy of the system [kJ]
57          Ui(i,j) = %%%%%%%%%%%%%%%%%%%%%%%%
58
59          %Vapour fraction after the irreversible expansion [-]
60          X(i,j) = %%%%%%%%%%%%%%%%%%%%%%%%%%%%
61
62          %Mechanical energy for each method [MJ]
63          E_TNO(i,j) = %%%%%%%%%%%%%%%%%%
64          E_Planas(i,j) = %%%%%%%%%%%%%%%%%%
65          E_Se(i,j) = %%%%%%%%%%%%%%%%%%%%
66          E_Genova(i,j) = %%%%%%%%%%%%%%%%%%%%%%
67          E_Birk(i,j) = %%%%%%%%%%%%%%%%%%%%%%
68          end
69  end
```

Appendix E

para-hydrogen to ortho-hydrogen reaction: script

```
                          %% MILENKO CORRELATION
for k = 1:1:10
    A(k) = 18.2 * T_end(k)^0.56 * D_OH2(k);
    B(k) = 5*10^4*(0.77 + 921*T_end(k)^(-2.5))*(D_OH2(k))^3.6;

    K(k) = A(k) + B(k);
end

for i = 1:1:10

    Kr(i) = K(i)* exp(-DeltaG(i) / (R * T_end(i)));
end
%%                          TRANSITION TIME

%Concentration of orthohydrogen before the explosion: [-]
c0 = 0.002;

%Concentration of orthohydrogen after the explosion: [-]
c1 = 0.70;

%Time for the transition: BMW safety test [10^3 h]

for i = 1:1:10

    Δt(i) = ...
        (1/Kr(i))*(log(c1/c0)-log((K(i)*c1+Kr(i)*(c1-1))/(K(i)*c0+Kr(i)*(c0-1))));

end
t_hours = Δt * 10^(-3);
t_sec = t_hours * 3600;
t_min = min(min(t_sec));
```

```
31
32 %% Reaction time for incomplete reactions calculated in SH2IFT_rgb_3 and ...
       SH2IFT_igb_3
33
34 %Final concentrations of ortho-hydrogen to match the overpressure results
35
36 c_final_r = [cr_22_5_TNT cr_26_4_TNT cr_22_5_B cr_26_4_B]*100;
37 c_final_i = [ci_22_5_TNT ci_26_4_TNT ci_22_5_B ci_26_4_B]*100;
38 c_final = [c_final_r c_final_i]/100;
39
40 for k = 1:1:8
41     c1 = c_final(k);
42
43     for i = 1:1:10
44         num1(i) = K(i) * c1;
45         num2(i) = Kr(i)*(c1-1);
46         den1(i) = K(i)*c0;
47         den2(i) = Kr(i)*(c0-1);
48         log2(i) = log((num1(i)+num2(i))/(den1(i)+den2(i)));
49         log1 = log(c1/c0);
50         par_tot(i) = log1 - log2(i);
51         Δt(i) = Kr(i)^-1 * par_tot(i);
52
53     end
54 t_hours = Δt * 10^(-3);
55 t_sec = t_hours * 3600;
```

Bibliography

[1] The International Energy Agency. *The future of hydrogen*. 2019. URL: https://iea.blob.core.windows.net/assets/9e3a3493-b9a6-4b7d-b499-7ca48e357561/The_Future_of_Hydrogen.pdf.

[2] R. Ono, M. Nifuku, and S. Fujiwara. "Minimum ignition energy of hydrogen–air mixture: Effects of humidity and spark duration". In: *Journal of electrostatics* 65 (2007), pp. 87–93. DOI: 10.1016/j.elstat.2006.07.004.

[3] National Institute of Science and Technology. *NIST*. 2021. URL: https://www.nist.gov/.

[4] G. Pepitpas and S.M. Aceves. "PARA-H2 TO ORTHO-H2 CONVERSION IN A FULL-SCALE AUTOMOTIVE CRYOGENIC PRESSURIZED HYDROGEN STORAGE UP TO 345 BAR". In: *International Journal of Hydrogen Energy* 39 (2014), pp. 6533–6547. DOI: 10.1016/j.ijhydene.2014.01.205.

[5] K. Pehr. "ASPECTS OF SAFETY AND ACCEPTANCE OF LH, TANK SYSTEMS IN PASSENGER CARS". In: *Int. J. Hydrogen Energy* 21 (1996), pp. 387–395. DOI: 0360-3199/96.

[6] F. Ustolin, N. Paltrinieri, and G. Landucci. "An innovative and comprehensive approach for the consequence analysis of liquid hydrogen vessel explosions". In: *Journal of Loss Prevention in the Process Industries* 68 (2020). DOI: 10.1016/j.jlp.2020.104323.

[7] F. Ustolin and N. Paltrinieri. "Hydrogen Fireball Consequence Analysis". In: *CHEMICAL ENGINEERING TRANSACTIONS* 82 (2020), pp. 211–216. DOI: 10.3303/CET2082036.

[8] V. Villa et al. "Towards dynamic risk analysis: A review of the risk assessment approach and its limitations in the chemical process industry". In: *Safety Science* 89 (2016), pp. 77–93. DOI: 10.1016/j.ssci.2016.06.002.

[9] N. Paltrinieri, N. Dechy, and E. Salzano. "Lessons Learned from Toulouse and Buncefield Disasters: From Risk Analysis Failures to the Identification of Atypical Scenarios Through a Better Knowledge Management". In: *Risk Analysis* 32 (2012), pp. 1404–1420. DOI: 10.1111/j.1539-6924.2011.01749.x.

[10] E. Salzano, M. Carboni, and G. Pio. "The effects of low-temperature phenomena on rapid phase transition of liquid hydrogen". In: *International Journal of hydrogen energy* (2020). DOI: doi.org/10.1016/j.ijhydene.2020.08.140.

[11] S. Molkov and S. Kashkarov. "Blast wave from a high-pressure gas tank rupture in a fire: Stand-alone and under-vehicle hydrogen tanks". In: *international journal of hydrogen energy* 40 (2015), pp. 12581–12603. DOI: 10.1016/j.ijhydene.2015.07.001.

[12] C. Sinigaglia and F. Lewiski. "Production, storage, fuel stations of hydrogen and its utilization in automotive applications-a review". In: *international journal of hydrogen energy* 42 (2017), pp. 24597–24611. DOI: 10.1016/j.ijhydene.2017.08.063.

[13] A. Antzaras and A. Leminidou. "Recent advances on materials and processes for intensified production of blue hydrogen". In: *Renewable and Sustainable Energy Reviews* (2021). DOI: 10.1016/j.rser.2021.111917.

[14] J. Manna and P. Jha. "Opportunities for green hydrogen production in petroleum refining and ammonia synthesis industries in India". In: *international journal of hydrogen energy* 46 (2021), pp. 38212–38231. DOI: 10.1016/j.ijhydene.2021.09.064.

[15] S. van Rennsen. "The hydrogen solution?" In: *Nature Climate Change* 10 (2020), pp. 799–801. DOI: 10.1038/s41558-020-0891-0.

[16] NationalGrid. *The hydrogen colour spectrum*. URL: https://www.nationalgrid.com/stories/energy-explained/hydrogen-colour-spectrum.

[17] A. Naquash and M. Qyyum. "Renewable LNG production: Biogas upgrading through CO2 solidification integrated with single-loop mixed refrigerant biomethane liquefaction process". In: *Energy Conversion and Management* 243 (2021). DOI: 10.1016/J.ENCONMAN.2021.114363.

[18] J. Xu and W. Lin. "Integrated hydrogen liquefaction processes with LNG production by two-stage helium reverse Brayton cycles taking industrial by-products as feedstock gas". In: *Energy* 227 (2021). DOI: 10.1016/j.energy.2021.120443.

[19] Y. Bi. "Optimization and analysis of a novel hydrogen liquefaction process for circulating hydrogen refrigeration". In: *international journal of hydrogen energy* (2021). DOI: 10.1016/j.ijhydene.2021.10.012.

[20] A. Campari. "DESIGN AND OPTIMIZATION OF AN AUTO-THERMAL EMERGENCY SYSTEM FOR CRYOGENIC FUELS". Alma MAter Studiorum - University of Bologna, 2021.

[21] N.T. Stetson, S. McWhorter, and C.C. Ahn. *Introduction to hydrogen storage*. Compendium of Hydrogen Energy - Hydrogen Storage, Distribution and Infrastructure. Woodhead Publishing, 2016. ISBN: 978-1-78242-362-1.

[22] F. Ustolin. "Modelling of Accident Scenarios from Liquid Hydrogen transport and Use". PhD thesis. 2021. ISBN: 978-82-326-5575-5.

[23] EN 14398-1. *Cryogenic vessels — Large transportable non-vacuum insulated vessels.*

[24] A. Barletta. *Introduzione matematica alla TRASMISSIONE DEL CALORE.* Pitagora Editrice Bologna, 2005. ISBN: 88-371-1568-7.

[25] G.G. Ihas. *Cryogenic refrigeration and Liquid Hydrogen Storage.* Handbook of Hydrogen Energy. CRC Press, 2014. ISBN: 978-1-4200-5450-7.

[26] CCPS. *Guidelines for Vapor Cloud Explosion, Pressure Vessel Burst, BLEVE, and Flash Fire Hazards.* Center for Chemical Process Safety. Wiley, 2010. ISBN: 978-0-470-25147-8.

[27] T. Abbasi and S.A. Abbasi. "The boiling liquid expanding vapour explosion (BLEVE): Mechanism, consequence assessment, management". In: *Journal of Hazardous Materials* 141 (2007), pp. 489–519. DOI: 10.1016/j.jhazmat.2006.09.056.

[28] R. Reid. "Possible mechanism for pressurized-liquid tank explosions or BLEVE's". In: *Science* 203 (1979), pp. 1263–1265. DOI: 10.1126/science.203.4386.1263.

[29] J.M. Salla, M. Demichela, and J. Casal. "A new approach to the superheat limit temperature". In: *Journal of loss prevention in the process industries* 19 (2006), pp. 670–700. DOI: 10.1016/j.jlp.2006.04.004.

[30] J. Casal. *Evaluation of the Effects and Consequences of Major Accidents in Industrial Plants.* Elesevier, 2008. ISBN: 978-0-444-63883-0.

[31] F. Ustolin, L. Odsaeter, and G. Reigstad. "Theories and Mechanism of Rapid Phase Transition". In: *CHEMICAL ENGINEERING TRANSACTIONS* 82 (2020), pp. 253–258. DOI: 10.3303/CET2082043.

[32] S. Mokhatab and J. Mak. *Handbook of Liquefied Natural Gas.* Elsevier, 2014. ISBN: 978-0-12-404585-9.

[33] J. Liu, Y. Fan, and K. Zou. "Prediction of flame length of horizontal hydrogen jet-fire during high-pressure leakage process". In: *Procedia Engineering* 211 (2018), pp. 471–478. DOI: 10.1016/j.proeng.2017.12.038.

[34] T. Blanchat. "Summary of the Phoenix Series Large Scale LNG Pool Fire Experiments". In: 23rd International Colloquium on the Dynamics of Explosions and Reactive Systems (ICDERS) July 24-29, 2011 Irvine, CA.

[35] F. Ustolin and N. Paltrinieri. "Hydrogen Fireball Consequence Analysis". In: *CHEMICAL ENGINEERING TRANSACTIONS* 82 (2020), pp. 211–216. DOI: 10.3303/CET2082036.

[36] C.L. Beyler. *Fire Hazard Calculations for Large, Open Hydrocarbon Fires.* Hurley M.J. et al. (eds) SFPE Handbook of Fire Protection Engineering. Springer, New York, NY, 2016. ISBN: 978-1-4939-2564-3.

[37] J. B. Gayle and J. W. Bransford. *Size and Duration of Fireballs from Propellant Explosions.* NASA TM X-53314Y, 1965.

[38] R.W. High. "The Saturn Fireball". In: *Annals of the New York Academy of Sciences* 152 (1968), pp. 441–451.

[39] J. Hord. "Explosion criteria for liquid hydrogen test facilities". In: *NBS Report* (1972).

[40] J.A. Fay and D.H. Lewis. "Unsteady burning of unconfined fuel vapor clouds". In: *Symposium (International) on Combustion* (1977). DOI: 10.1016/S0082-0784(77)80424-4.

[41] C.J.H. Bosh and R.A.P.M. Waterings. *Methods for the calculation of physical effects.* Committee for the Prevention of Disasters. PUBLICATIEREEKS GEVAARLIJKE STOFFEN, 1996.

[42] A. Carbone and F. Ferrari. *Corso di Fisica Moderna Ingegneria Elettrica, Energetica e dell'Ambiente.* University of Bologna, 2019.

[43] L. Pauling. *Introduction to Quantum Mechanics with Applications to Chemistry.* Dover Publications, 1985. ISBN: 978-0-486-64871-2.

[44] P.C. Souers. *Hydrogen Properties for Fusion Energy.* University of California press, 1986. DOI: 10.1525/9780520338401.

[45] L. Chen and R. Xiao. "Thermodynamic analysis of the para-to-ortho hydrogen conversion in cryo-compressed hydrogen vessels for automotive applications". In: *international journal o f hydrogen energy* 45 (2020), pp. 24928–24937. DOI: 10.1016/j.ijhydene.2020.05.252.

[46] Y. Y. Milenko, R. M. Sibileva, and M. A. Strzhemechny. "Natural Ortho-Para Conversion Rate in Liquid and Gaseous Hydrogen". In: *Journal of Low Temperature Physics* 107 (1997), pp. 77–92. DOI: 012.

[47] W.E. Baker and P.A. Cox. *Explosion hazards and evaluation.* Fundamental studies in engineering 5. Elsevier, 1983. ISBN: 0-444-420940.

[48] I. Bell and J. Wronski. "Pure and Pseudo-Pure Fluid Thermophysical Property Evaluation and the Open-Source Thermophysical Property Library CoolProp". In: *Industrial & Engineering Chemistry Research* 53 (2014), pp. 2498–2508. DOI: 10.1021/ie4033999.

[49] B. Hemmatian and J. Casal. "A new procedure to estimate BLEVE overpressure". In: *Process Safety and Environmental Protection* 111 (2017), pp. 320–325. DOI: 10.1016/j.psep.2017.07.016.

[50] R.W. Prugh. "Possible mechanism for pressurized-liquid tank explosions or BLEVE's". In: *Science* 80 (1991), pp. 1263–1265. DOI: 10.1177/104239159100300102.

[51] H.L. Brode. "Blast wave from a spherical charge". In: *Physics of Fluids* 2 (1959), pp. 217–229. DOI: 10.1063/1.1705911.

[52] J.M. Smith and H.C. Van Ness. "Introduction to chemical engineering thermodynamics". In: *JOURNAL OF CHEMICAL EDUCATION* (1996), pp. 584–585. DOI: 10.1021/ed027p584.3.

[53] D.A. Crowl. "Using thermodynamic availability to determine the energy of explosion". In: *Plant/operations progress* 10 (1991), pp. 136–142. DOI: 10.1002/prsb.720100306.

[54] D.A. Crowl. "Calculating the energy of explosion using thermodynamic availability". In: *Journal of Loss Prevention in the Process Industries* 5 (1992), pp. 109–118. DOI: 10.1016/0950-4230(92)80007-U.

[55] E. Planas-Cuchi, J.M. Salla, and J. Casal. "Calculating overpressure fromBLEVE explosions". In: *Journal of Loss Prevention in the Process Industries* 17 (2004), pp. 431–436. DOI: 10.1016/j.jlp.2004.08.002.

[56] J. Casal and J.M. Salla. "Using liquid superheating energy for a quick estimation of overpressure in BLEVEs and similar explosions". In: *Journal of Hazardeous Materials* A137 (2006), pp. 1321–1327. DOI: 10.1016/j.jhazmat.2006.05.001.

[57] B. Genova and M. Silvestrini. "Evaluation of the blast-wave overpressure and fragments initial velocity for a BLEVE event via empirical correlations derived by a simplified model of released energy". In: *Journal of Loss Prevention in the Process Industries* 21 (2008), pp. 110–117. DOI: 10.1016/j.jlp.2007.11.004.

[58] A.M. Birk and C. Davison. "Blast overpressures from medium scale BLEVE tests". In: *Journal of Applied Physics* 26 (1955), pp. 766–775. DOI: 10.1063/1.1722085.

[59] J. Casal and J. Arnaldos. *Modelling and understanding Bleves*. Handbook of Hazardous Materials Spills Technology. McGraw-Hill, New York., 2001.

[60] G.F. Kinney and K. J. Graham. *Explosive shocks in air*. Springer Science, 1985. ISBN: 978-3-642-86684-5.

[61] H.L. Brode. "Numerical Solutions of Spherical Blast Waves". In: *Journal of Loss Prevention in the Process Industries* 20 (2007), pp. 194–206. DOI: 10.1016/j.jlp.2007.03.0014.

[62] H.W. Liepmann and A. Roshko. *Elements of gasdynamics*. New York: John Wiley Sons, Inc., 1967.

[63] Matlab R2021b. *vpa-solve*. 2021. URL: https://it.mathworks.com/help/symbolic/sym.vpasolve.html.

[64] Vladimir Molkov. *Fundamentals of hydrogensafety engineering II*. 2019.

[65] F. Ustolin et al. "On the Mechanical Energy Involved in the Catastrophic Rupture of Liquid Hydrogen Tanks". In: *CHEMICAL ENGINEERING TRANSACTIONS* 91 (2022).

Acknowledgements